2011-12-09

Reduction in Wick Drain Effectiveness in Typical Utah Clays

Gabriel M. Smith
Brigham Young University - Provo

Reduction in Wick Drain Effectiveness

in Typical Utah Clays

Gabriel M. Smith

A thesis submitted to the faculty of
Brigham Young University
in partial fulfillment of the requirements for the degree of

Master of Science

Kyle M. Rollins, Chair
W. Spencer Guthrie
Norman L. Jones

Department of Civil and Environmental Engineering

Brigham Young University

December 2011

ABSTRACT

Reduction in Wick Drain Effectiveness
in Typical Utah Clays

Gabriel M. Smith
Department of Civil and Environmental Engineering, BYU
Master of Science

Consolidation theory states that decreasing the spacing of prefabricated vertical drains will decrease the time required to achieve primary consolidation. Previous field tests have shown that there exists a "critical" drain spacing, which is the point at which further spacing decrease does not decrease the time of primary consolidation. This "critical" spacing is thought to be due to disturbance effects from installation of the drains. Previous studies have found that the "critical" drain spacing may be dependent upon soil layering and drain and mandrel dimensions. Thin, interbedded clay layers have been found to be affected greatly due to the smear zone, while few tests have been conducted to determine the validity for thick bedded clays. Currently two design and analysis methods are in existence, neither of which is standardized. The two methods are the modeling of the smear zone, which requires knowledge of soil parameters within that zone, and the modeling using a back-calculated C_h/C_v ratio.

In order to evaluate the validity of these design methods and to obtain more data that can be used in determining the relationship between anchor type, drain spacing, and soil profile, full-scale field tests were conducted at Mountain View Corridor in Lehi, Utah. These field tests were performed along a test section that was divided into sections containing 5.8, 5.0, 4.0 and 3.0 ft triangular spacings and rebar or plate anchors. By using the smear zone model, with a C_h/C_v ratio of 1.25 and d_s of 3.07 times d_m, the time rate of settlement was able to be predicted reasonably well, while using the back-calculated C_h/C_v ratio, with no smear zone, also predicted the time rate reasonably well.

From the testing, it was found that the thick clay profile can facilitate closer spacings than a thin clay profile. Also, it was found that the rebar anchor type causes about twice the disturbance of the plate anchor. The results helped validate the existing models and show that the effectiveness of the drains is dependent upon drain spacing, soil profile, and anchor type

Keywords: wick drain, radial consolidation, soft clay, mandrel

ACKNOWLEDGMENTS

I thank my advisor, Dr. Kyle M. Rollins, for his guidance and mentoring through my research and graduate studies. I also thank the members of my graduate committee, Drs. Norman L. Jones and W. Spencer Guthrie, for their time and effort. I especially thank my wife, Leslie, for her love, support, and encouragement throughout my education and especially throughout my thesis and graduate work.

Financial support for this study was provided by the Utah Department of Transportation through Contract No. 08.07-2. This support is gratefully acknowledged. The author alone is responsible for the preparation and accuracy of the information, data, analysis, discussions, recommendations, and conclusions presented herein. The contents do not necessarily reflect the views, opinions, endorsements, or policies of the Utah Department of Transportation. The Utah Department of Transportation makes no representation or warranty of any kind, and assumes no liability therefore.

The geotechnical investigation data and settlement monitoring was provided by RB&G Engineering, Inc. The additional PV drains and the analysis program were provided by HB Wick Drains, a division of Hayward Baker, Inc., formerly Nilex, Inc.

TABLE OF CONTENTS

LIST OF TABLES

LIST OF FIGURES

1 INTRODUCTION

One major concern during construction of highway embankments and bridge approach fills is the rate of primary consolidation settlement of the underlying clay layers. Paving operations and construction of the bridge structure must be delayed until the consolidation settlement has been completed. Therefore, efforts to accelerate this process are highly desirable both in terms of construction time and cost. To accelerate the consolidation of the soft clay at the San Francisco-Oakland Bay Bridge, for example, vertical sand drains were installed in 1925 and were patented in the United States the following year. The sand drains were the predecessor to prefabricated vertical (PV) drains, which were patented in Sweden during the late 1930s. The PV drains of the 1940s consisted of wood and cardboard, but, since then, the materials have evolved to consist of plastic corrugated cores enclosed by a geotextile filter fabric. These modern PV drains, also referred to as wick drains or band drains, are widely used on construction projects where embankments are underlain by thick clay deposits (Bo et al. 2003).

The vertical drains are installed through the clay layer on a triangular or rectangular grid pattern, as shown in Figure 1-1, and allow water in the clay to drain horizontally to the drain rather than only vertically to horizontal sand layers, as illustrated in Figure 1-2. Because the time for consolidation is proportional to the square of the drainage path distance, reducing this distance can substantially reduce the time for consolidation of a thick clay layer. The drains are installed into the soil profile by pushing a steel mandrel into the ground and the drains are held in place at the bottom with an anchor plate or steel rebar, as the mandrel is retracted.

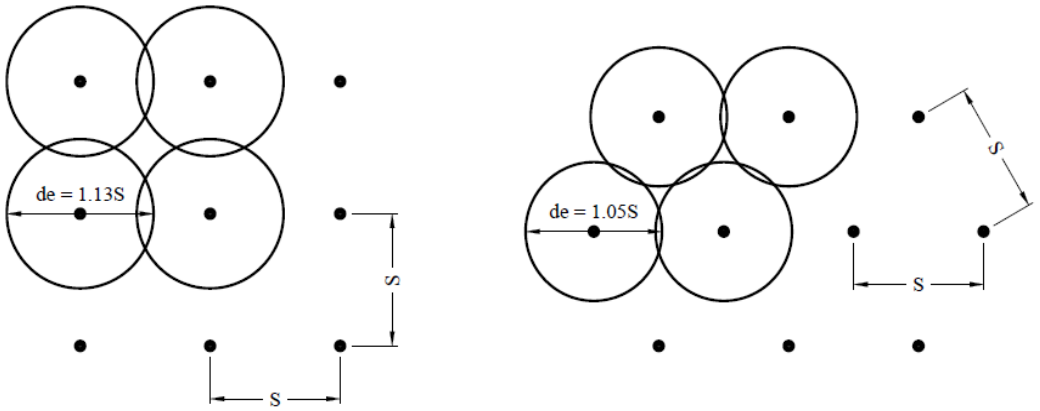

Figure 1-1. Plan View Showing Layout of PV Drains with a) Square Spacing, b) Triangular Spacing

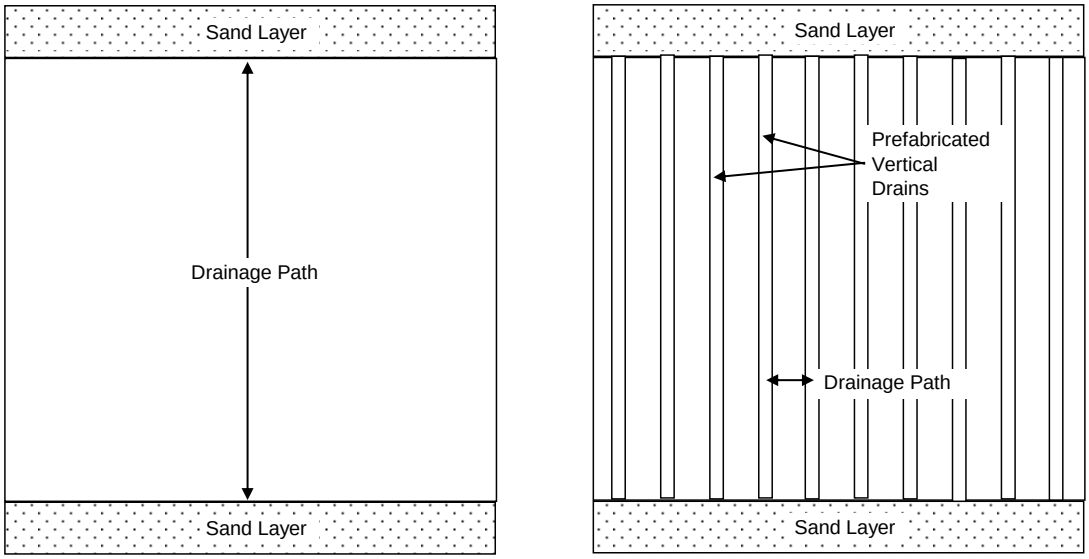

Figure 1-2. Drainage Path Lengths without and with PV Drains Installed (Smith and Rollins 2007)

Although consolidation theory indicates that clay layers will consolidate faster as vertical drain spacing decreases, investigators have noted the detrimental effects of installation disturbance for many years (Barron 1948, Hansbo 1979). Smearing during drain insertion can reduce the effective permeability of higher permeability layers, by smearing low permeability clays and silts across high permeability sand layers. The permeability in the smear zone is a

function of the radial distance from the edge of the drain to the extent of the disturbed zone and magnitudes of the permeability of the layers through which the pore water must travel.

During the Interstate 15 (I-15) design-build project in Salt Lake Valley, field tests indicated that prefabricated vertical (PV) drain spacings closer than about 1.75 m did not provide any additional benefit (Saye et al. 2001). Apparently, disturbance of the sensitive clay due to installation of the drains reduced the permeability in the smear zone around the drains sufficiently to overcome any benefit from the closer spacing. However, this minimum effective spacing or "critical drain spacing" is related to soil sensitivity and soil layering as well as the geometry of the anchor and mandrel. For smaller anchor/mandrel geometries and more uniform soil profiles, the drain spacing could potentially be decreased with corresponding benefits.

As expansion of I-15 and other roadways continues on soft clays in Utah, reliance on the 1.75 m minimum spacing criteria could lead to unnecessarily long construction times and, therefore, higher construction costs. Similar concerns are important at many other locations where construction occurs over compressible clay layers. This research study was aimed at developing improved models to account for the effect of smear zones on the performance of PV drains in soft clays.

1.1 Objectives

This report will present the findings of a full-scale field test of various PV drain spacings along the Mountain View Corridor (MVC) project, located in Lehi, Utah. The data collected from the field test will be used to analyze whether decreasing the spacing of the PV drains will decrease the time required to obtain 95% consolidation (t_{95}). The research objectives to be considered are:

1. Quantify the rate of settlement associated with variations in PV drain spacing and anchor types.
2. Determine whether decreased PV drain spacing yields a decreased t_{95} or if a "critical drain spacing" exists beyond which closer spacing is ineffective.
3. Compare field results with generalized design equations for predicting time rate of settlement that account for "smear effects" from PV drain installation and make recommendations for design practice.

1.2 Scope

By installing PV drains at various spacings across a full scale test site, and by using the observed time-settlement data at the test site, a computer model will be developed that will calculate the predicted time-settlement relationship along the test site. By using this model, relationships between spacing, anchor type, and drain effectiveness can be identified and quantified.

The test section will be divided into segments of the various spacings and anchor types and will be instrumented with settlement monitoring systems. The drains will be installed using two different anchor types, rebar and plate, and at four different spacings, 5.8, 5.0, 4.0 and 3.0 ft.

The relationship between the drain spacing and drain effectiveness, as well as between anchor type and drain effectiveness, will be determined by comparing the t_{95} for each. Along with comparing the t_{95}, the ratio of soil parameters measured in the disturbed soil to the same parameters measured in the undisturbed soil will also be defined.

The test results will be used to evaluate two design models that are often used in engineering practice. This first model employs a smear zone with a specified radius and soil

properties to compute the time rate of settlement. The second model employs an effective ratio of the horizontal to vertical coefficients of consolidation (C_h/C_v) defined as a function of the normalized drain spacing.

2 LITERATURE REVIEW

This chapter includes a review and summary of articles in the technical literature that are relevant to the issues involved in this research. The articles present the current understanding of procedures for accounting for the zone of soil disturbance, or smear zone, associated with the installation of PV drains. The articles also summarize case histories where the analysis procedures have been compared with field performance.

2.1 Consolidation Theory

Consolidation settlement of a clay layer is caused by additional load being placed on the soil due to an embankment or structure. This additional load causes excess pore pressure to develop in the clay layer, which slowly dissipates with time. As the pore pressures dissipate, the effective stress increases on the soil particles, and the void ratio begins to decrease. This change in void ratio leads to settlement of the underlying clay. This type of settlement is referred to as primary consolidation (Das 2011).

There are two issues associated with primary consolidation. First, the magnitude of settlement must be computed, and, second, the time rate of settlement must be determined. Both issues are of concern to the construction of a project. The magnitude of settlement determines whether settlement is important to consider, while the settlement rate determines how much time must be allowed for consolidation to take place. Both parts need to be considered in order to minimize construction delays and reduce the overall cost of the construction project.

2.1.1 Primary Consolidation Settlement Magnitude

Based on consolidation theory, the magnitude of settlement for a single clay layer system can be determined by one of the following three equations (Das 2011), depending on whether the soil is normally or overconsolidated. Equation

Equation 2-1 is used when the clay is normally consolidated (i.e. $\sigma'_0 = \sigma'_c$). Equation 2-2 is used for the case where the clay is overconsolidated, even with the addition of induced stress (i.e. $\sigma'_0 + \Delta\sigma' \leq \sigma'_c$). Equation 2-3 is used for the final case where the clay is overconsolidated prior to the addition of the induced stress and normally consolidated following the induced stress addition (i.e. $\sigma'_0 \leq \sigma'_c \leq \sigma'_0 + \Delta\sigma'$). The total settlement for all the clay layers in the profile is then obtained by summing the settlement for all the individual layers.

$$S_c = \frac{C_c H}{1 + e_0} \log\left(\frac{\sigma'_0 + \Delta\sigma'}{\sigma'_0}\right) \quad \textbf{(2-1)}$$

$$S_c = \frac{C_r H}{1 + e_0} \log\left(\frac{\sigma'_0 + \Delta\sigma'}{\sigma'_0}\right) \quad \textbf{(2-2)}$$

$$S_c = \frac{C_r H}{1 + e_0} \log\left(\frac{\sigma'_c}{\sigma'_0}\right) + \frac{C_c H}{1 + e_0} \log\left(\frac{\sigma'_0 + \Delta\sigma'}{\sigma'_c}\right) \quad \textbf{(2-3)}$$

where

C_c = compression index

C_r = recompression index

σ'_0 = initial effective vertical pressure

σ'_c = preconsolidation pressure

$\Delta\sigma'$ = induced pressure produced by the surface load

H = total thickness of the clay layer or sublayer

2.1.2 Time Rate of Vertical Consolidation

The time rate of vertical consolidation is governed by the rate of pore pressure dissipation. The degree of consolidation is the consolidation settlement at any time divided by the maximum consolidation settlement that occurs due to the increase in effective stress caused by the application of additional loads. This rate of consolidation is governed by the coefficient of vertical consolidation (C_v), which is calculated from laboratory consolidation testing of the clay. The average degree of vertical consolidation ($\bar{U}_v$) is found by Equation 2-4.

$$\bar{U}_v = 1 - \frac{u}{u_0} \quad \textbf{(2-4)}$$

For a single clay layer with a constant C_v value, Equations 2-5 and 2-6 can be used to solve for the average degree of consolidation rather than using an explicit or implicit finite difference approach. Equation 2-5 is applicable for cases when $\bar{U}_v$ is less than or equal to 60%, and Equation 2-6 is for when $\bar{U}_v$ is greater than 60% (Das 2011).

$$U\% = 100\sqrt{\frac{4T_v}{\pi}} \quad \textbf{(2-5)}$$

$$U\% = 100 - 10^{\left[{(1.781 - T_v)}/{0.933}\right]} \quad \textbf{(2-6)}$$

where

$$T_v = \frac{C_v t}{{H_{dr}}^2} \quad \textbf{(2-7)}$$

C_v = coefficient of vertical consolidation

t = time

H_{dr} = the drainage path length (longest path for water in clay layer to drain)

Because the rate of consolidation is inversely proportional to drainage path length squared, the time for consolidation increases by a factor of four as the thickness of a clay layer doubles. Therefore, for thick clay layers, the time for an average degree of consolidation of 95% (t_{95}) can be many tens of years. As a result, it is generally not practical to pre-load a clay layer and wait for vertical consolidation to occur prior to construction if the layer is more than about 20 ft. thick.

For most transportation construction projects, it is desirable to complete primary consolidation settlement in less than 90 days. Due to the construction time constraint, it is desirable to accelerate the rate of settlement by installing PV drains. The PV drains allow for the pore water to drain both vertically and horizontally.

2.1.3 Time Rate of Radial Consolidation

As indicated previously, installation of PV drains reduces the drainage path thickness and dramatically reduces the time to consolidation. The radial drainage equations are more complex than the vertical drainage equations due to the presence of the smear zone. The presence of the smear zone leads to the introduction of new soil parameters required to utilize the equations for the time rate of radial consolidation.

The Barron (1948) equal-strain equation to calculate the average degree of radial consolidation ($\bar{U}_r$ or $\bar{U}_h$) (Das 2011) is defined by Equation 2-8, which is a function of the PV drain spacing, the smear zone diameter, the ratio of the in-situ horizontal permeability to the horizontal permeability in the smear zone, and the horizontal coefficient of consolidation.

$$\bar{U}_r = 1 - e^{-\frac{8T_r'}{\alpha'}} \quad \textbf{(2-8)}$$

$$T_r' = \frac{C_h t}{d_w^2} \quad \textbf{(2-9)}$$

$$\alpha' = \frac{n^4}{n^2 - m^2} ln\left(\frac{n}{m}\right) - \frac{3n^2 - m^2}{4} + \frac{k_h}{k_s}(n^2 - m^2)\ln(m) \quad \textbf{(2-10)}$$

$$m = \frac{d_s}{d_w} \quad \textbf{(2-11)}$$

$$n = \frac{d_e}{d_w} \quad \textbf{(2-12)}$$

$$d_w = \frac{2(b_w + t_w)}{\pi} \quad \textbf{(2-13)}$$

where

C_h = coefficient of horizontal consolidation

t = time

k_h = the in-situ horizontal permeability

k_s = the horizontal permeability of the clay in the smear zone

d_s = diameter of the smear zone

d_w = the equivalent diameter of the wick

b_w = wick drain width

t_w = wick drain thickness

d_e = the equivalent cell diameter

Triangular Spacing: $d_e = 1.05S$

Square Spacing: $d_e = 1.13S$

S = drain spacing

Since the smear zone diameter and the horizontal permeability in the smear zone are difficult to define without full scale tests or case histories, the ratio of the smear zone diameter to the wick or drain diameter is often assumed to be 1.0 for design purposes and a lower effective C_h value is used. With these simplifying assumptions, Equation 2-10 reduces down to Equation 2-14, which is a function of the PV drain spacing, and the horizontal coefficient of consolidation.

$$\alpha' = \frac{n^4}{n^2 - 1} ln(n) - \frac{3n^2 - 1}{4} \quad \textbf{(2-14)}$$

2.1.1 Time Rate of Combined Consolidation

After calculating the average degree of vertical and radial consolidation independently, the combined average degree of consolidation, $\bar{U}$, can be found by using Carrillo's relationship (1942). Carrillo's relationship is defined by Equation 2-15.

$$\bar{U} = 1 - (1 - \bar{U}_r)(1 - \bar{U}_v) \quad \textbf{(2-15)}$$

where

$\bar{U}_r$ = radial average degree of consolidation

$\bar{U}_v$ = vertical average degree of consolidation

2.2 Smear Zone Theories

The PV drains are installed by a steel mandrel that is pushed, and sometimes vibrated, into the soft soil. The mandrel is advanced until the proper installation depth is reached. Once the depth is reached, the mandrel is then retracted and the drain is held in place by the anchor. The advancing and retracting mandrel will remold the soft soils and causes a decreased permeability zone. This area of decreased permeability is the smear zone and is shown in Figure 2-1. Within this zone, the soil properties are not the same as in the undisturbed zone. The

difference in properties causes problems to arise when implementing radial drainage consolidation theory. Numerous studies have been completed in an attempt to develop better understanding of the soil properties within the smear zone and to develop accurate predictions of the effects of radial drainage during consolidation.

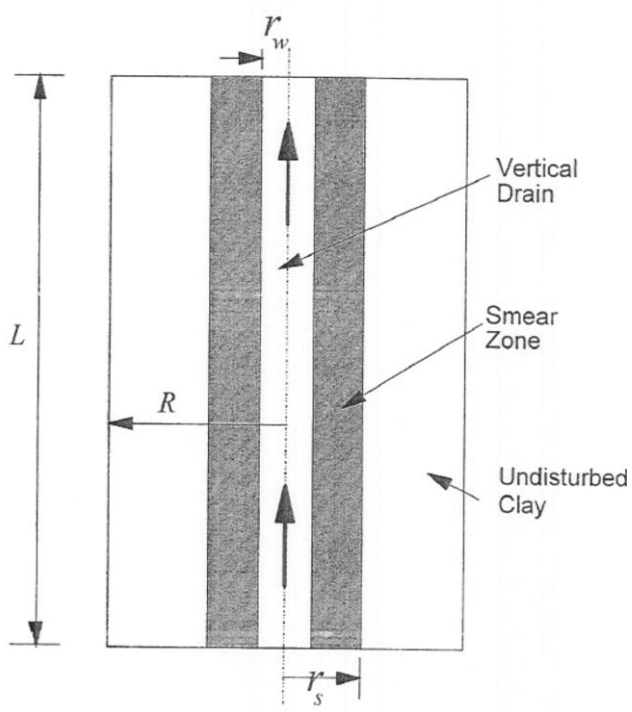

Figure 2-1. Cross Section of PV Drain and Smear Zone (Sharma and Xiao 2000)

Hansbo (1979, 1981) recommended that modifications be made to the Barron (1948) solution. The Hansbo modifications allowed the Barron solution to handle the physical dimensions and characteristics of PV drains, and effects of PV drain installation (Bergado 1999). Hansbo (1987) proposed a model in which the smear zone radius is two times the equivalent radius of the mandrel. Hansbo also proposed the use of a constant horizontal permeability in the smear zone that is equal to the vertical permeability. The horizontal permeability in the smear zone was lower than the horizontal permeability outside the smear zone and approached that of

the vertical permeability. The smear zone radius and permeability ratio was verified by Bergado et al. (1991, 1999) through analyzing full-scale embankment and laboratory model testing.

Sathananthan and Indraratna (2006) performed laboratory tests to evaluate the radius of the smear zone and the permeability in that zone. The tests were performed by using a large-scale radial drainage consolidometer. The consolidometer was 650 mm internal diameter and 1,040 mm in height. Due to the large size of the consolidometer, undisturbed samples were unable to be used; therefore, the tests were performed in reconstituted alluvial Moruya clay. In order to quantify disturbance effects, PV drains were installed in the reconstituted clay volume, and, following the installation, 32 soil samples were collected at various horizontal and vertical locations relative to the drain. These samples were then tested using standard oedometer tests. The large scale tests provided the data to produce Figure 2-2.

From the data collected during the laboratory testing and based upon the conclusions of Sathananthan and Indraratna (2006), the smear zone was found to be approximately 2.5 times the equivalent mandrel radius. Although the k_h/k_v ratio was between 1.8 and 2 in the undisturbed zone, the permeability ratio decreased almost linearly with normalized distance to a value of about 1.0 near the edge of the PV drain, which represents a decrease of about 50%. The laboratory testing also showed the vertical permeability relatively constant with respect to normalized distance from the edge of the PV drain while the horizontal permeability remained relatively constant outside the smear zone and decreased linearly inside the smear zone.

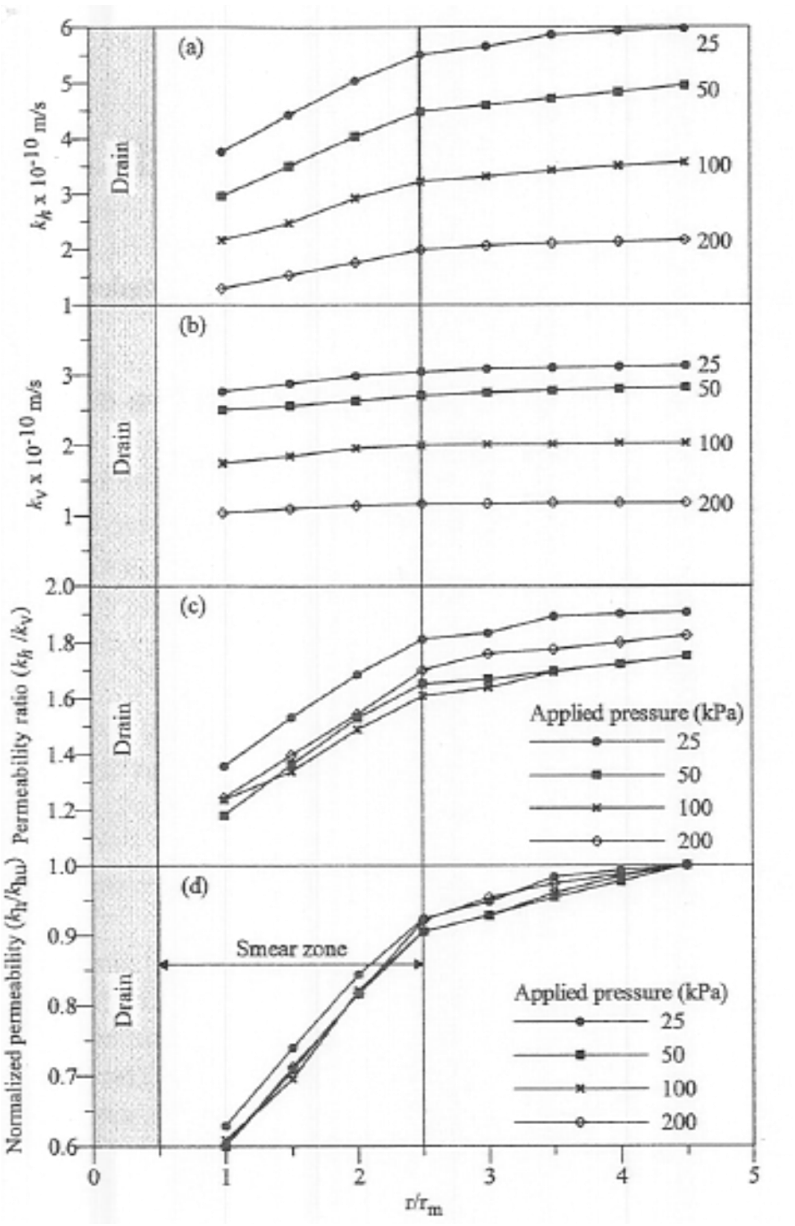

Figure 2-2. (a) Horizontal Permeability, (b) Vertical Permeability, (c) Permeability Ratio, (d) Normalized Lateral Permeability, Versus Radial Distance (Sathananthan and Indraratna 2006)

Walker and Indraratna (2006) realized that the constant horizontal permeability assumption used by Hansbo did not accurately portray the conditions after drain installation. To better match actual field conditions, Walker and Indraratna developed a method based on an assumption that the permeability exhibits a parabolic decay towards the drain, as illustrated in

Figure 2-3. This parabolic permeability decrease is in reasonable agreement with the laboratory measurements made by Sathananthan and Indraratna (2006) and field measurements made by Bergado et al. (1991, 1999).

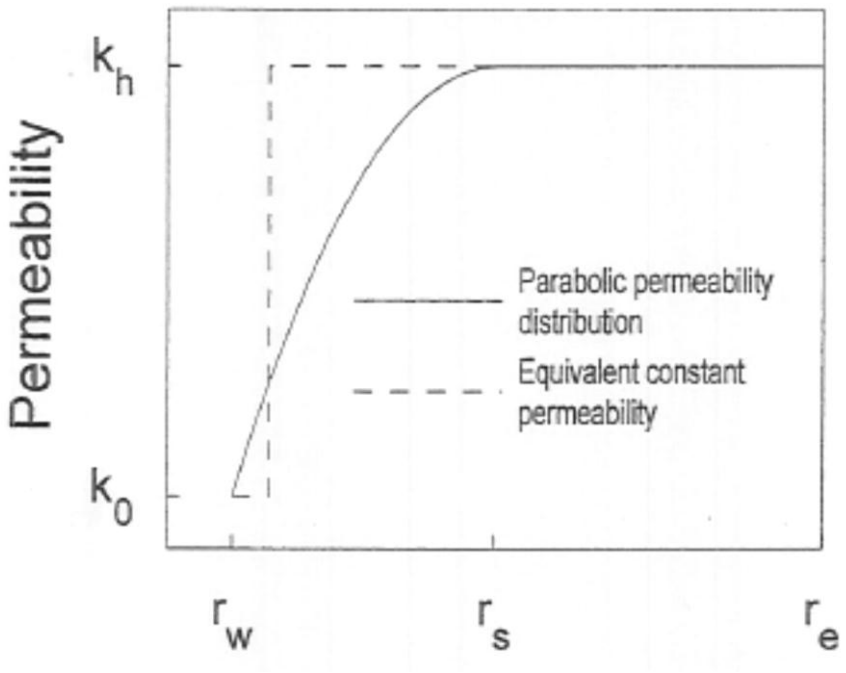

Figure 2-3. Parabolic Permeability Distribution (Walker and Indraratna 2006)

Walker and Indraratna compared the results of the modified Hansbo equations, as well as their parabolic decay equations, to laboratory test results. The comparison of the predicted and measured settlement curve is shown in Figure 2-4.

As can be seen in Figure 2-4, the agreement between the measured and computed curves for Hansbo's constant permeability case is dependent upon the r_s/r_w ratio. The Hansbo solution, which assumed a constant permeability that was lower in the smear zone than outside the smear zone, fits the data when the r_s/r_w ratio falls between one and six. The parabolic permeability case, developed by Walker and Indraratna (2006), provides modifications for Hansbo's (1981)

solution. The modifications allow for better performance predictions to be made by basing the radial drainage equations on a measured permeability distribution instead of using an estimation of the smear zone radius with a constant permeability.

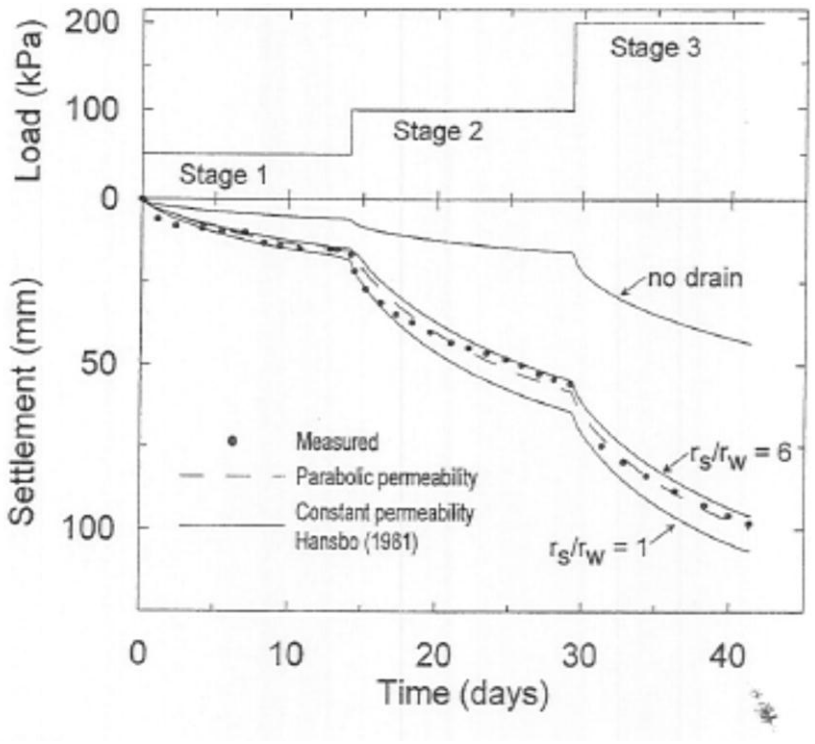

Figure 2-4. Comparison of Predicted and Measured Settlements for Constant Permeability and Parabolic Permeability Distributions (Walker and Indraratna 2006)

Ghandeharioon et al. (2010) performed testing and utilized critical state soil mechanics (CSSM) to define more accurately the smear zone and the associated permeability decrease within the zone. To define the smear zone, they utilized the elliptical cavity expansion theory along with CSSM. From these two theories and their testing, they found that the smear zone diameter is 3.07 times the equivalent mandrel diameter. The testing also resulted in the development of a relationship between permeability, plastic shear strain, and the radial distance normalized by the equivalent elliptical mandrel radius, as shown in Figure 2-5.

With Figure 2-5, the smear zone diameter and permeability ratio can be more accurately chosen. These values can then be entered into the PV drain design equations to obtain more accurate results.

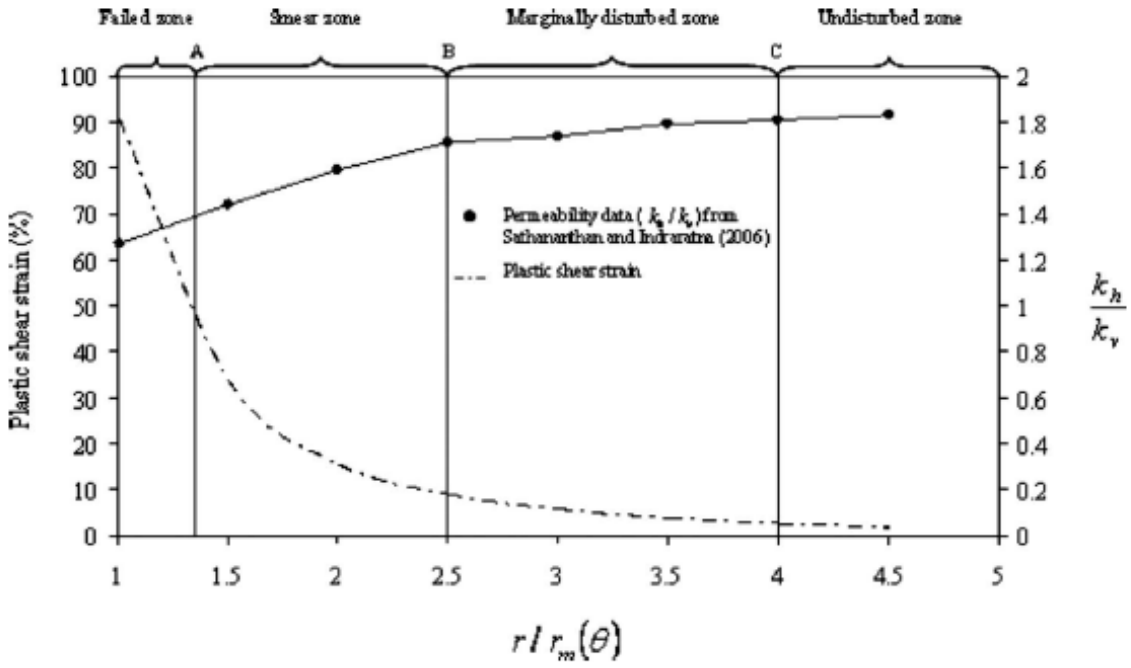

Figure 2-5. Horizontal to Vertical Permeability and Plastic Shear Strain Related to the Radial Distance Normalized by the Equivalent Elliptical Mandrel Radius (Ghandeharioon et al. 2010)

In addition to the work of Sathananthan and Indraratna (2006), Bergado et al. (1991, 1999), and Ghandeharioon (2010), a number of other investigators have studied this problem and made recommendations regarding the smear radius and permeability reduction. A summary of previous researchers' recommended values for the smear zone radii and the ratios of the horizontal permeability to the vertical permeability are summarized in

Table 2-1. Rixner et al. (1986) defined possible ranges of the horizontal to smear zone permeability ratios for soft clays based on the layered structure of the soil, as shown in Table 2-2.

Table 2-1. Various Studies' Recommendations for Smear Zone Radii and Ratios of Horizontal Permeabilities to Vertical Permeabilities

Study	Smear Zone Radius	Horizontal to Vertical Permeability Ratio
Indraratna and Redana (1998)[1,2]	4 to 5 times r_w	~1.0
Hird and Moseley (2000)[2]	3 times r_w	-
Sharma and Xiao (2000)[2]	~4 times r_w	-
Zhu and Yin (2000)[2]	~5 times r_w	-
Hansbo (1987)[3]	2 times r_m	-
Sathananthan and Indraratna (2006)[1]	2.5 times r_m	1.1 to 1.8
Rixner et al.[4]	2.5 to 3 times r_m	See Table 2-2
Bergado (1991)[3]	2.5 times r_m	1.5 to 2.0
Chai and Miura[4]	2 to 3 times r_m	-
Ghandeharioon et al. (2010)[2]	3.07 times r_m	1.4 to 1.7

[1] (Sathananthan and Indraratna 2006)

[2] (Ghandeharioon et al. 2010)

[3] (Bergado et al. 1991)

[4] (Bergado 1999)

Table 2-2. Ratios of Horizontal Permeability to Vertical Permeability for Soft Clays Based on Clay Layering (Rixner et al. 1986)

Clay Layering	k_h/k_v
No evidence of layering	1.2 ± 0.2
No or only slightly developed macrofabric	1 to 1.5
Slight layering	2 to 5
Fairly to well-developed macrofabric	2 to 4
Varved clays in northeastern U.S.	10 ± 5
Varved clays and other deposits containing embedded and more or less continuous permeable layers	3 to 15

2.3 Previous Field Studies

Prior to the 2002 Winter Olympics, which were held in Salt Lake City, Utah, a major reconstruction of I-15 occurred. During the reconstruction, PV drains were installed to facilitate the accelerated settlement of the underlying soft cohesive soils. The pre-bid design for PV drain spacing of 1.5 m, which yielded a 90-day minimum consolidation period, was questioned by the contractors and subcontractors. In response to the questioning, a test site in the area of North Temple Street and 600 South in Salt Lake City, Utah, was established to evaluate the rate of settlement as a function of drain spacing under full-scale conditions. The field tests, analysis of the results, and, the conclusions of the field testing during the reconstruction have been presented in at least three published articles (Saye et al. 2001, Saye 2002, Saye and Ladd 2004)

Along the established test section, three triangular drain spacings (2.0 m, 1.5 m, and 1.0 m) were used and each cluster was instrumented to facilitate the calculation and analysis of the settlement. Figure 2-6 shows the test site layout with the PV drain spacing, and instrument types. In addition, the effect of a larger anchor with the same spacing was investigated. The ultimate goal of the testing was to quantify the disturbance effect based on drain spacing.

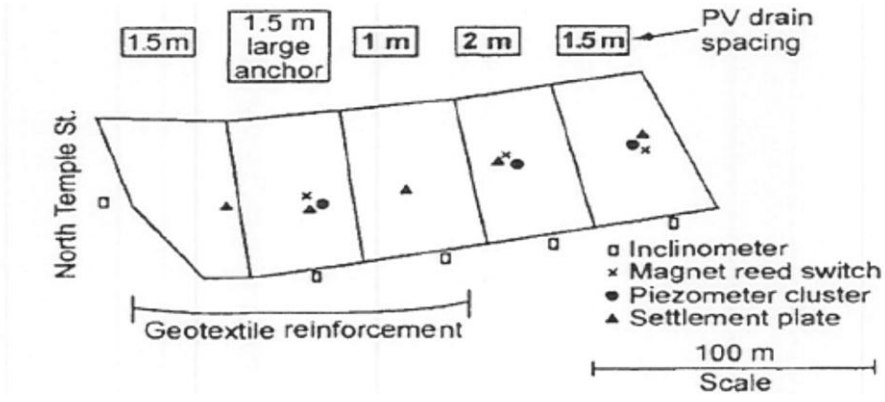

Figure 2-6. North Temple Street Layout (Saye and Ladd 2004)

Based on the measured settlement from settlement plates and embedded sensors (magnet reed switch) and piezometer data, the horizontal coefficient of consolidation (C_h) was back-calculated for each drain spacing as shown in Table 2-3. The results in Table 2-3 show that the C_h values decreased significantly as the spacing decreased, presumably owing to increased soil disturbance at closer spacings. Saye and Ladd found that, due to the large decrease of the C_h value, the rate of consolidation did not increase below a spacing of about 1.5 m (2004).

Table 2-3. Summary of C_h Values Back-Calculated from Full-Scale Consolidation Tests in Connection with the I-15 Reconstruction in Salt Lake Valley (Saye And Ladd 2004)

Drain Spacing	Back Calculated c_h (ft^2/yr)		
	Settlement Plate	Magnet Reed Switch	Piezometer
6.6 ft (2 m)	141.0	150.7 ± 2.3 std. dev. 5 layers	173.3 ± 3.1 std. dev. 3 piezometers
4.9 ft (1.5 m)	102.3	117.3 ± 2.2 std. dev. 5 layers	111.9 ± 5.6 std. dev. 4 piezometers
3.3 ft (1.0 m)	33.4	-	61.4 ± 1.8 std. dev. 2 piezometers

From the data collected at the test section, the t_{95} times (time for 95% degree of consolidation) for various spacings were calculated using a constant C_h value that assumed no smear effects. This constant C_h value was selected based on the back-calculated value at a spacing of 2.0 m. Figure 2-7 shows the t_{95} values from field observations compared to the calculated values calculated using the constant C_h value. The calculated values represent the theoretical scenario while the observed values represent the real-life field scenario. The figure illustrates the importance in accounting for disturbance effects due to installation; by neglecting any disturbance effects the design and analysis can be non-conservative.

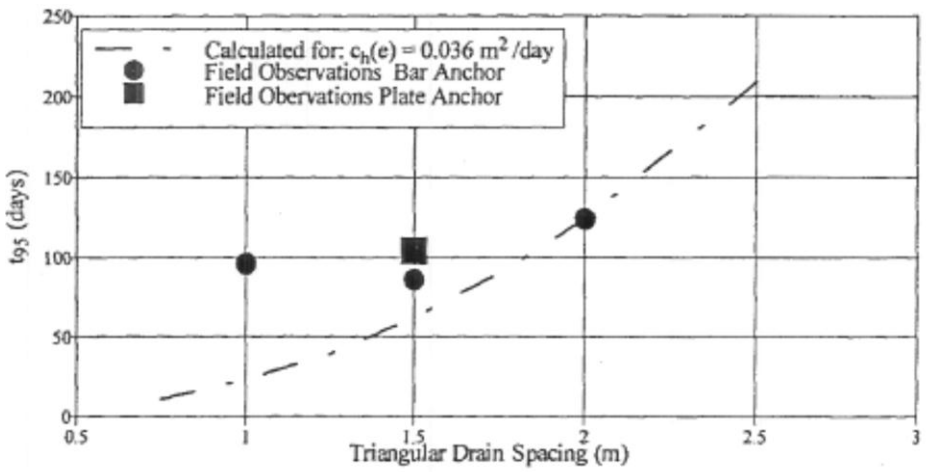

Figure 2-7. Effect of Spacing on Consolidation Times (Saye et al. 2001, Saye 2002)

As spacing decreases, the measured t_{95} values diverge from the calculated curve and do not continue to decrease as predicted. From the comparison, it was determined by Saye et al. that the minimum t_{95} occurs between 1.5 and 1.75 m spacing, which verified the pre-bid spacing and minimum consolidation time period. Based upon the results, the spacing was changed from 1.5 m during the first phase to 1.75 m during the second phase of construction (Saye et al. 2001, Saye 2002).

Saye (2002) furthered his work by using case histories along with his own research along I-15 to propose that disturbance by the installation of PV drains was similar, if not greater, than the disturbance by the installation of displacement sand drains. Saye developed Figure 2-8, which combined his research on thin clay beds typical of the I-15 site with other case histories, involving PV drains as well as full-displacement sand drains, to illustrate his proposal of disturbance effects.

In the figure, the equivalent cell diameter (d_e) was normalized by the equivalent mandrel diameter (d_m) and is plotted on the abscissa, while the back-calculated C_h/C_v ratio is plotted on

the ordinate. The equivalent mandrel diameter was found by calculating the perimeter of the mandrel/anchor combination and converting it into an equivalent circular diameter.

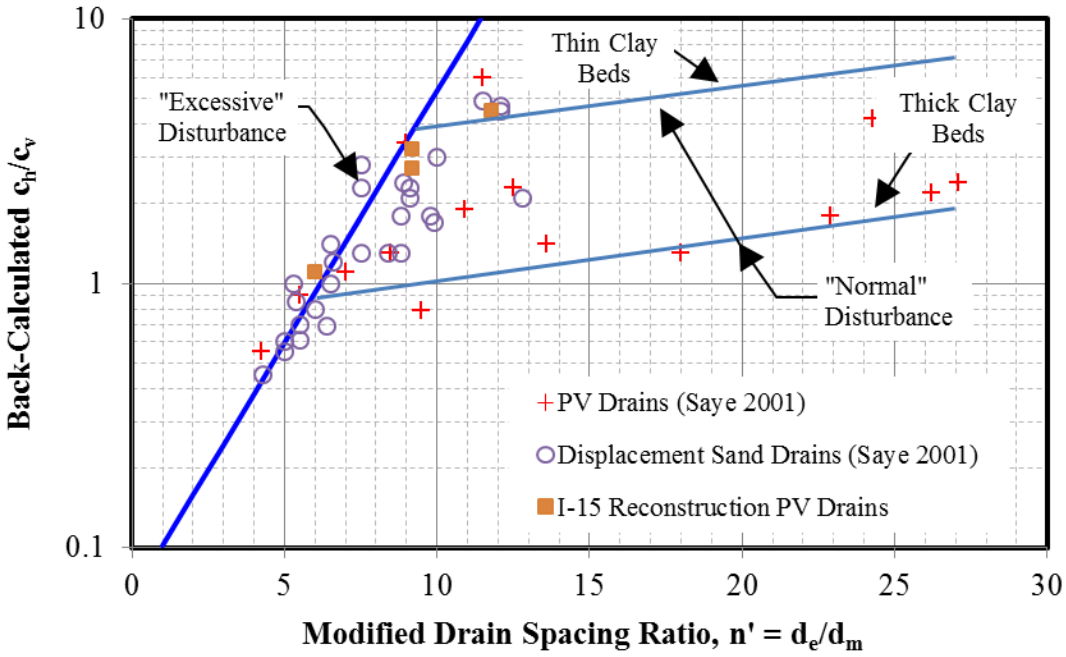

Figure 2-8. Back-Calculated C_h/C_v Ratios for Various Field Test Sites (Saye 2002)

The figure represents a potential design or analysis model to account for disturbance effects. The steep slope represents the line of "excessive" disturbance, while the flatter slopes represent "normal," or minimal disturbance. Various "normal" disturbance lines exist based on the undisturbed, in-situ horizontal to vertical permeability or coefficient of consolidation ratio. A smaller undisturbed in-situ permeability ratio is shown by the lower slope, which represents thick uniform clay beds, while a high ratio is shown as the upper slope and represents soil such as varved clays, which consist of interbedded layers of silts and clays.

Figure 2-8 shows that, at high drain spacing ratios (e.g. greater than 9), disturbance from drain installation is relatively minor and the C_h/C_v ratio decreases relatively little as the drain spacing ratio decreases. However, the data appear to suggest that when the drain spacing ratio

decreases below some critical value (e.g. 6 to 9), the drain installation begins to produce excessive soil disturbance and the C_h/C_v value decreases substantially. If the spacing to diameter ratio is too small, the smear zone will cause a significant reduction in C_h, and t_{95} will increase substantially. Based on the data collected by Saye (2002), the critical drain spacing ratio, where the change in slope occurs, is dependent on the layering of the soil profile. For thinly bedded profiles, the critical drain spacing ratio is around 9, whereas for thickly bedded profiles the critical drain spacing could be as low as 6. This indicates that closer drain spacing could be used in thickly bedded profiles in comparison to thinly bedded profiles without the risk of excessive disturbance.

To further the work by Saye et al. and investigate the effect of anchor size on the minimum effective spacing, Smith and Rollins (2007, 2009) conducted field tests on PV drains with various spacing at the Salt Lake International Airport in Utah, which contained thinly bedded clay deposits as shown from the CPT logs in Figure 2-9.

The tests were conducted at drain spacings of 6 ft, 5 ft, 4 ft, and 3 ft in test areas that were approximately 50 ft square. The field tests utilized a smaller mandrel/anchor combination compared to that used by Saye (2002). With the use of the smaller mandrel and anchor, the results yielded a smaller minimum effective spacing based on the measured t_{95} values as shown in Figure 2-10.

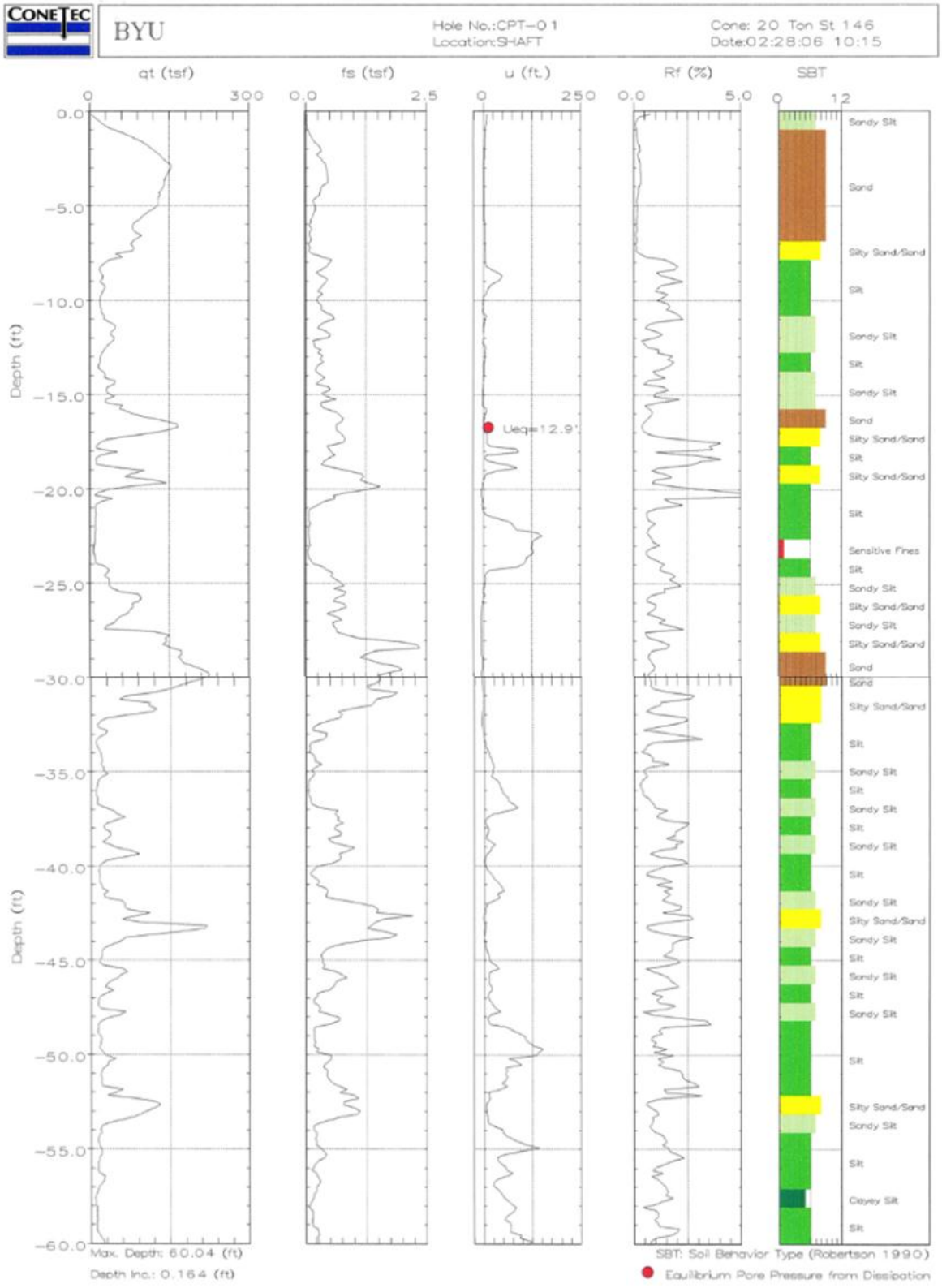

Figure 2-9. SLC Airport CPT Log

Smith and Rollins concluded that the smaller minimum effective drain spacing (0.9 m to 1.22 m), compared to previous work by Saye et al., was most likely attributable to the use of the smaller mandrel/anchor combination.

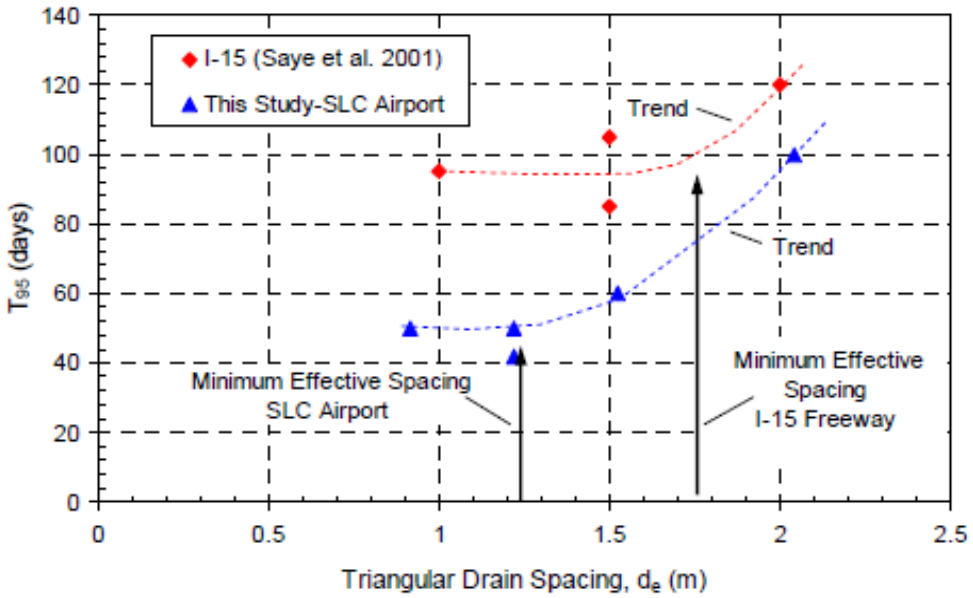

Figure 2-10. Effect of PV Drain Spacing on Consolidation Times for I-15 and SLC Airport Studies (Smith and Rollins 2009)

Back-calculated C_h/C_v ratios obtained by Smith and Rollins are plotted along with the data collected by Saye in Figure 2-11. The data from the SLC airport test generally confirm the trend lines proposed by Saye (2002) for the thinly bedded clay.

Smith and Rollins also concluded that, by using the ratio of drain spacing to equivalent diameter, the effects of mandrel disturbance could be predicted reasonably well. Unfortunately, the time-settlement data reported by Smith and Rollins were not collected as frequently as might be desired and there were some questions regarding the elevations of the recording units. As a result, there is some uncertainty in the back-calculated C_h/C_v ratios as indicated by the uncertainty bars shown in Figure 2-11.

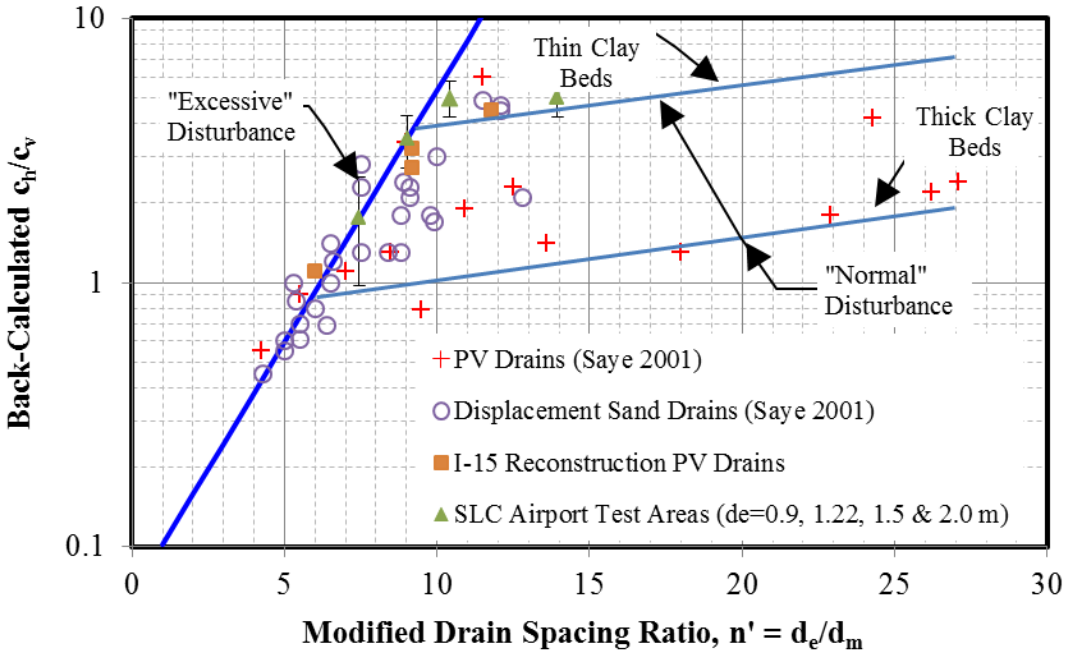

Figure 2-11. Additional Back-Calculated C_h/C_v Ratios from Various Field Test Locations Using Various PV Drain Spacings (Smith and Rollins 2009)

2.4 Limitations of Previous Work

Based on the research performed by others, there have been attempts made to better understand and model consolidation due to radial drainage. The previous research and conclusions made have a few limitations that lead to a lack of standardized design of PV drains. These limitations are as follows:

1. The properties that define the smear zone (i.e. smear diameter, variation of permeability, etc.) have been quite variable from study to study. Uncertainty in the permeability distribution has also been shown by previous research. Without a standardized definition of the smear zone, the consolidation due to radial drainage will vary greatly due to these parameters being present in the design equations.

2. Based upon laboratory testing, the assumption of a constant permeability in the smear zone appears to be unrealistic; however, limited data are available to better define the distribution of permeability within the smear zone.
3. Only very limited full-scale field test data are available for evaluating the effect of PV drain spacing on drain effectiveness. Previous testing suggests that the drain effectiveness and "critical" drain spacing may be dependent on in-situ soil layering, but there are very few tests that validate this suggestion.

3 TESTING PROCEDURES

The full-scale field testing program conducted in this research was accomplished with the aid of RB&G engineering, the Utah Department of Transportation (UDOT), and HB Wick Drains, a division of Hayward Baker (formerly Nilex, Inc.). RB&G was the design engineer for the project and made routine measurements of the settlement instrumentation during construction. UDOT, the owner of the project, oversaw construction and was responsible for surveying the elevations of the settlement monitoring stations. HB Wick Drains provided the additional PV drains necessary for the study, along with the personnel and equipment to install them.

3.1 Test Site

The field test was located along the UDOT MVC project site, which connects Redwood Road to I-15 along 2100 North in Lehi, Utah. The test areas are located on the relatively flat flood plain just west of the Jordan River. A total of 10 test areas with four different drain spacings and two anchor types were located between station 95+00 and 105+00 on the west bound lanes and between station 285+00 and 295+00 of the east bound lanes, as shown in Figure 3-1. Each of the different spacings and anchor types in these areas were compared to one another in order to develop relationships between anchor type, spacing, and drain effectiveness.

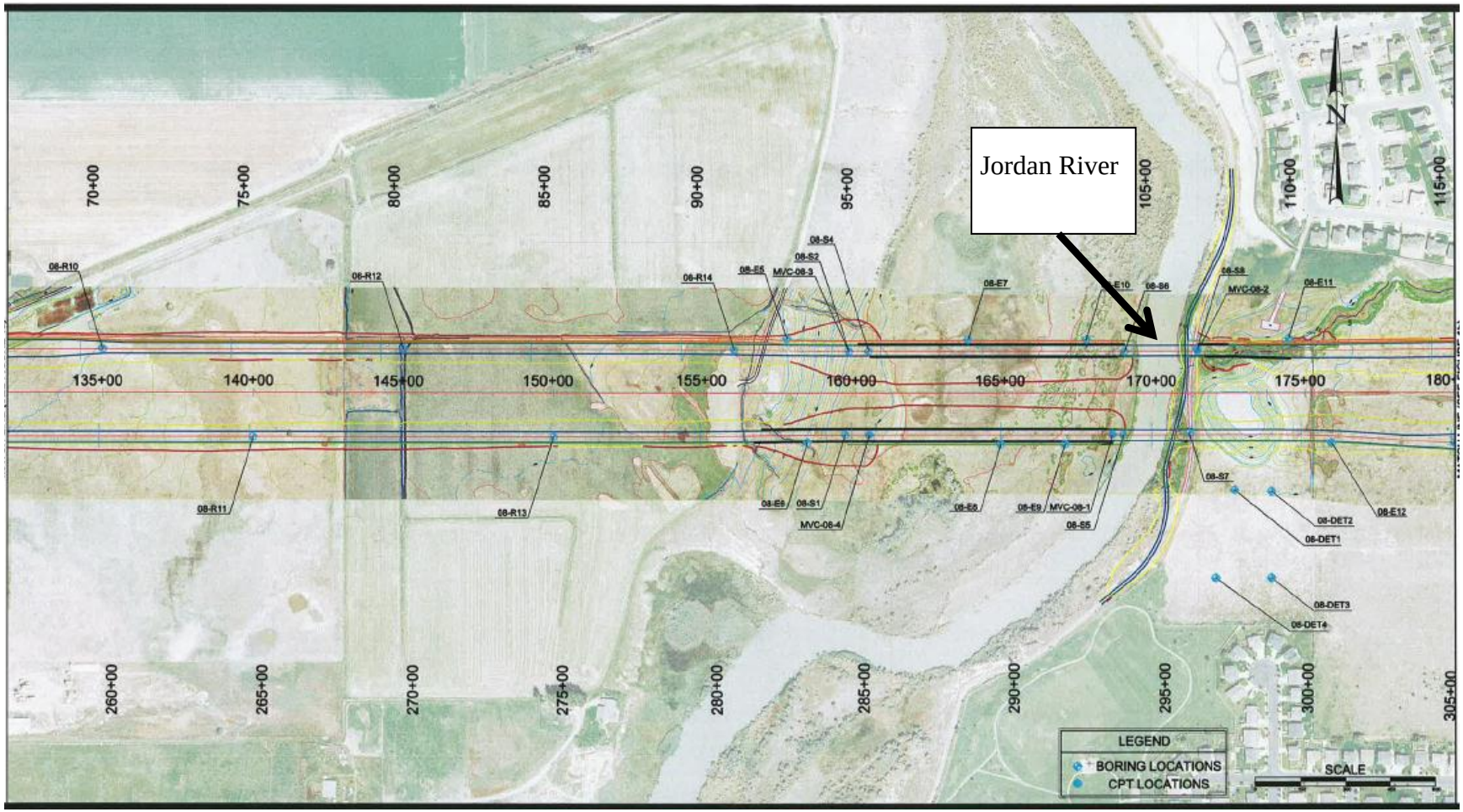

Figure 3-1. MVC Test Section (RB&G Engineering, Inc. 2009)

Figure 3-2 provides an elevation view showing the typical geometry for the embankment and surcharge placed along the MVC test site. The fill section consists of a lower layer with MSE walls supporting a vertical face with a sloped fill above the top of the wall. The fill was placed according to the contractor's schedule; therefore, the fill varied in height across the test section. Fill heights ranged from 26 to 33.5 ft within the test area, with the MSE wall heights ranging from 17.1 to 24.6 ft. Figure 3-3 shows the close-up of the test area detailing the drain spacing, anchor type, and settlement monitoring instruments throughout the test section.

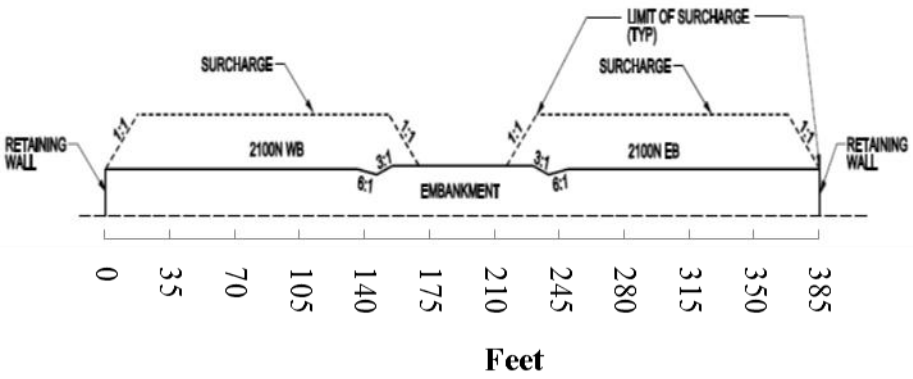

Figure 3-2. Typical Embankment Geometry

3.1 Instrumentation

In order to monitor the settlement, each test section, as shown in Figure 3-3, had monitoring instruments installed. The instrumentation included manometer settlement systems and vibrating wire settlement systems, which are denoted as S-# and VWS-#, respectively, in Figure 3-3. Each test area was instrumented with at least one of the above instruments. A total of 12 instruments were employed in the test section, which required four additional instruments beyond what was originally planned for the construction when no variation in spacing was anticipated.

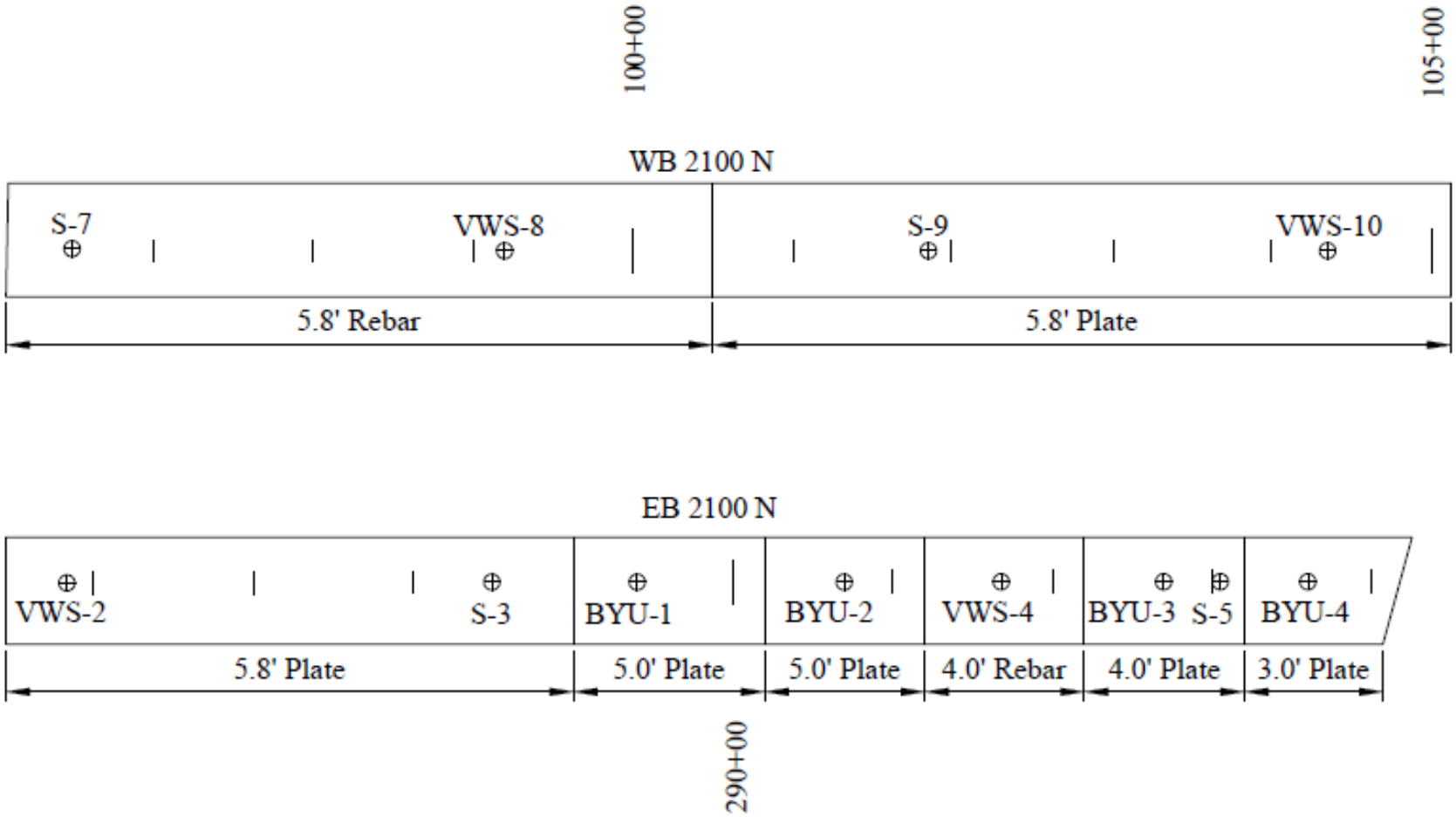

Figure 3-3. MVC Test Site Location with Spacings and Instrumentation

3.1.1 Manometer Settlement Systems

The manometer settlement system was installed as shown in Figure 3-4 and consisted of two flexible tubes that extend from a settlement platform, shown in Figure 3-5, to a gauge box, shown in Figure 3-6. The two tubes provide redundancy in readings in case one tube malfunctions. Prior to fill placement, the tubes are flushed with a mixture of 50% water and 50% antifreeze, which flows out the open end at the platform. The height of the fluid is then measured at the gauge box to establish the initial elevation of the platform. As the soil under the embankment settles, the elevation of the platform decreases relative to the initial value. To make a measurement, fluid is again added to the tubes, and the height of water at the platform is measured after allowing the fluid level to stabilize as a function of time. The settlement is the difference between any elevation and the initial elevation. Ideally, the gauge box would be located far enough from the embankment that it would not settle due to fill placement. However, in many cases this is not practical, and the gauge box also settles with time. Therefore, it is necessary to survey the elevation of the measurement box when a reading is made to correct for the change in elevation of the gauge box.

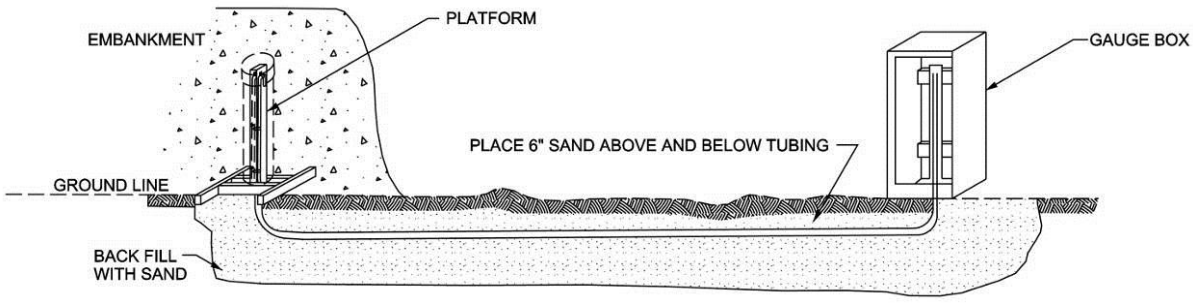

Figure 3-4. Settlement Platform Installation Detail

Figure 3-5. Manometer Settlement Platform

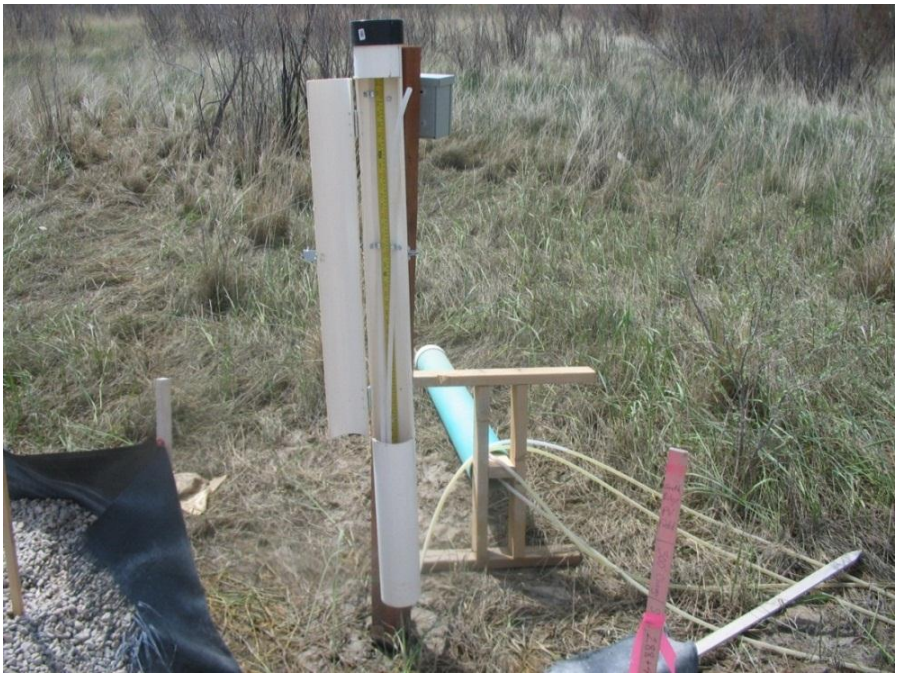

Figure 3-6. Manometer Gauge Box

Occasionally the manometer tubes need to be flushed with new fluid. When the tubes are flushed, a volume of new fluid equal to one and a half to two times the tube's capacity is added to the tubes, which is allowed to spill out the open ends. The new fluid displaces the old fluid and a new initial reading is taken as the initial elevation.

3.1.2 Vibrating Wire Settlement Systems

The Geokon vibrating wire settlement system (VWS) was installed as illustrated in Figure 3-7. The VWS contained two liquid-filled tubes that extend from the sensor at the settlement location to the reservoir at the readout enclosure, shown in Figure 3-8, which should be at a location that does not experience any settlement. Usually the instrument readout boxes are placed close to the construction area, due to space limitations of the construction site. Since the readout boxes are placed close to the location where the settlement is being monitored, the readout boxes will settle with time and results in the need for the elevation of the instrument readout to be surveyed.

After installation and prior to fill placement, an initial reading is taken to define the starting pressure corresponding to the starting elevation. As a result of settlement, the pressure changes at the sensor and causes a change in the frequency of the vibrating wire. The difference between any given reading and the initial reading, after accounting for temperature effects, is multiplied by a calibration factor to calculate the settlement at that time. Since the enclosure box may actually settle along with the sensor, the calculated settlement must be adjusted by the change in the elevation of the instrument readout box to account for differential settlement between the readout box and settlement platform.

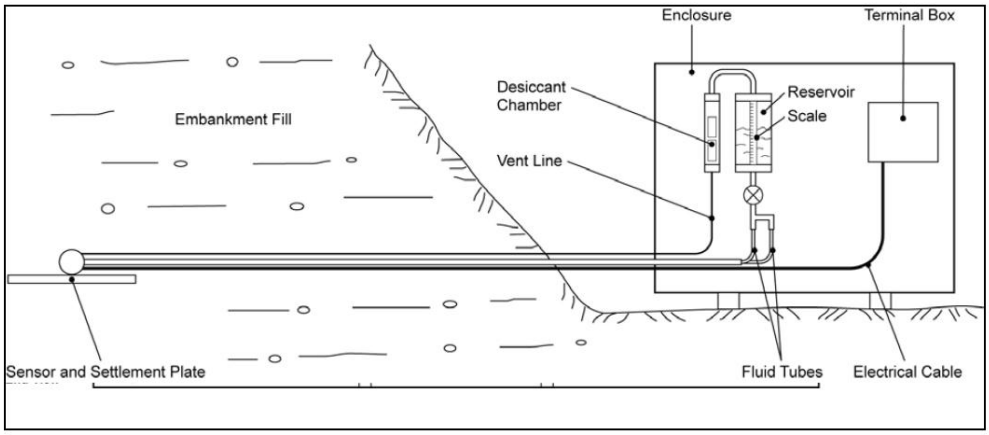

Figure 3-7. Vibrating Wire Settlement System Installation Detail (Geokon, Inc. 2010)

Figure 3-8. Vibrating Wire Readout Box

3.2 Drain Specifications

3.2.1 Mandrel Dimension

Two different mandrel/anchor combinations were used along the MVC test site, as shown in Figure 3-9. The first combination used a 3.9 in. by 7.1 in. plate anchor with the standard mandrel. The second combination used the same standard mandrel along with a 10 in. length of #4 rebar.

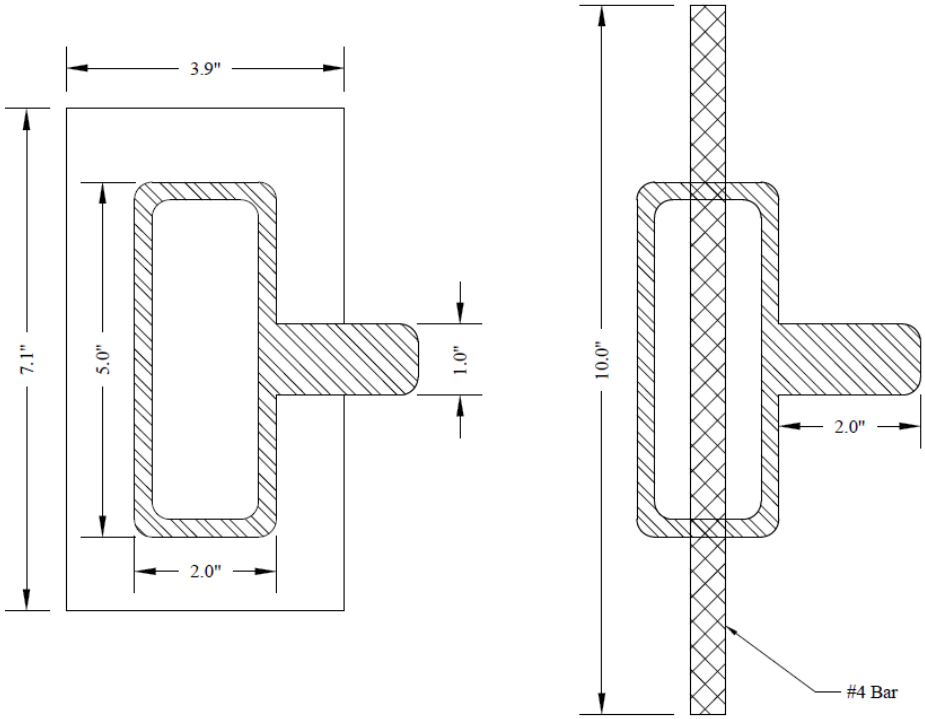

Figure 3-9. Mandrel and Anchor Dimensions

Figure 3-10. Mandrel with PV Drain and Rebar Anchor Prior to Installation

Figure 3-11. Mandrel with PV Drain and Plate Anchor Prior to Installation

3.2.2 PV Drain Dimensions

The PV drains used at the MVC test site were Mebra-Drain 7407. The drain consists of a corrugated polypropylene core surrounded by a non-woven polypropylene filter fabric, which has an apparent opening size equal to a US #70 sieve, or 0.0083 in. The drain is 4 in. wide and 0.142 in. thick, which gives an equivalent wick diameter (d_w) of 0.22 in. based on Equation 2-13. Figure 3-12 provides an illustration of the drain.

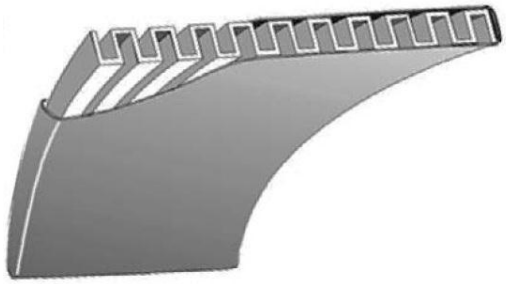

Figure 3-12. PV Drain Drawing

4 GEOTECHNICAL SITE CHARACTERIZATION

The subsurface exploration results were provided in the soil report prepared by RB&G Engineering. A total of nine bore holes (labeled 08-S/E#) and three CPTs (labeled MVC-08-#) were used to characterize the soil profile along the test section, as shown in Figure 4-1.

Some typical bore hole and CPT logs are presented in Figure 4-2 and Figure 4-3. The profile typically consists of alternating layers of clay and silty sand (SM) to a depth of about 10 ft, which are underlain by a clay layer to a depth of about 85 to 90 ft where a sand drainage layer is encountered. The clay layer is predominantly lean clay (CL) but contains a layer of fat clay (CH) between depths of about 60 to 78 ft. The CPT soundings indicate that the clay is thickly bedded with remarkably uniform tip resistance and side friction values.

The CPT log shows a very consistent tip stress throughout the entire depth of the profile. Beginning at a depth of 7 ft, until a depth of 80 ft, the average tip stress is approximately 10 tsf, with about 2 tsf variation. This low tip stress is consistent with a soil profile that contains no sand or gravel layers intermixed with the clay. A soil profile without any sands or gravels present, the ratio of horizontal to vertical permeability should be closer to unity than a profile with interbedded sands and gravels with clay.

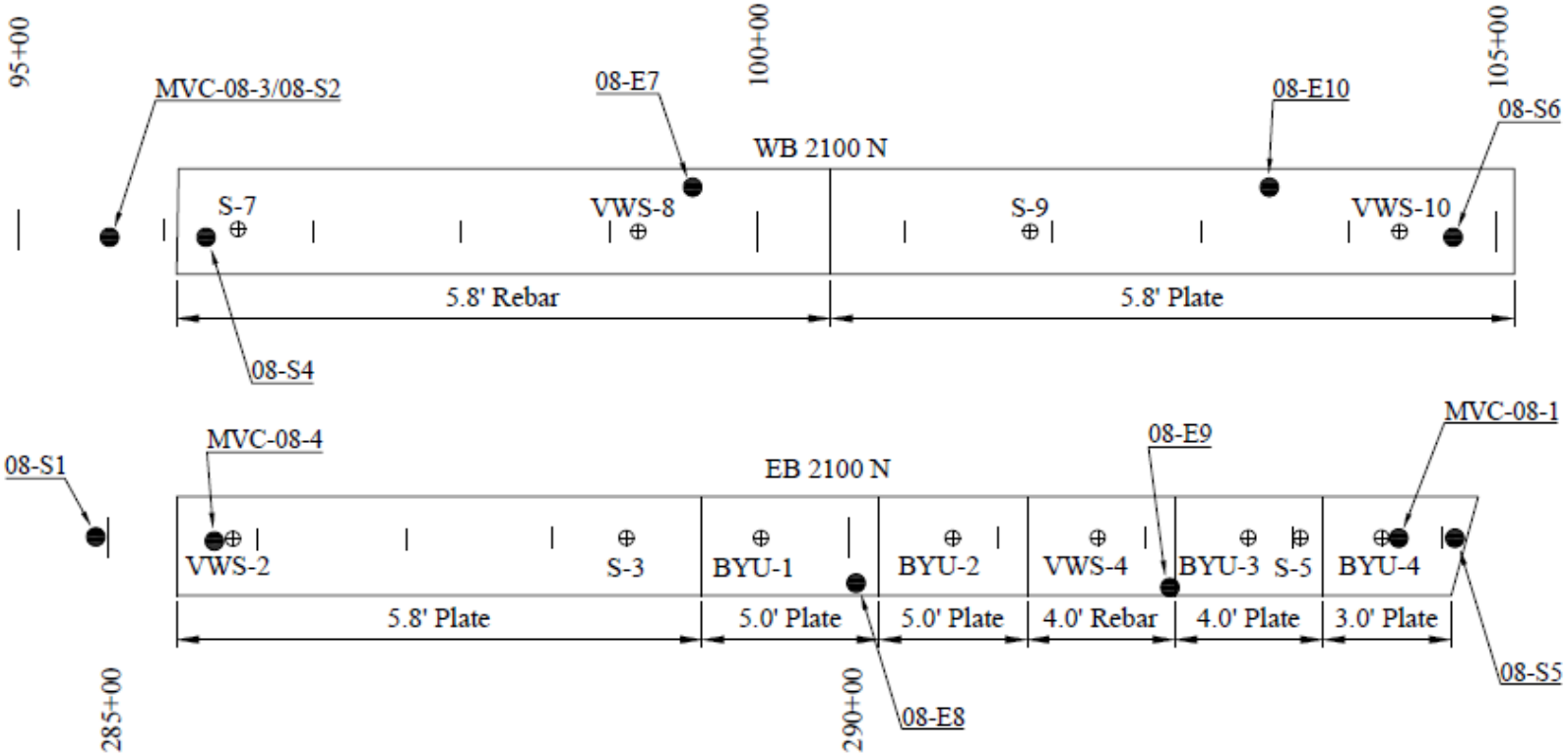

Figure 4-1. MVC Test Site with CPT and Bore Hole Locations

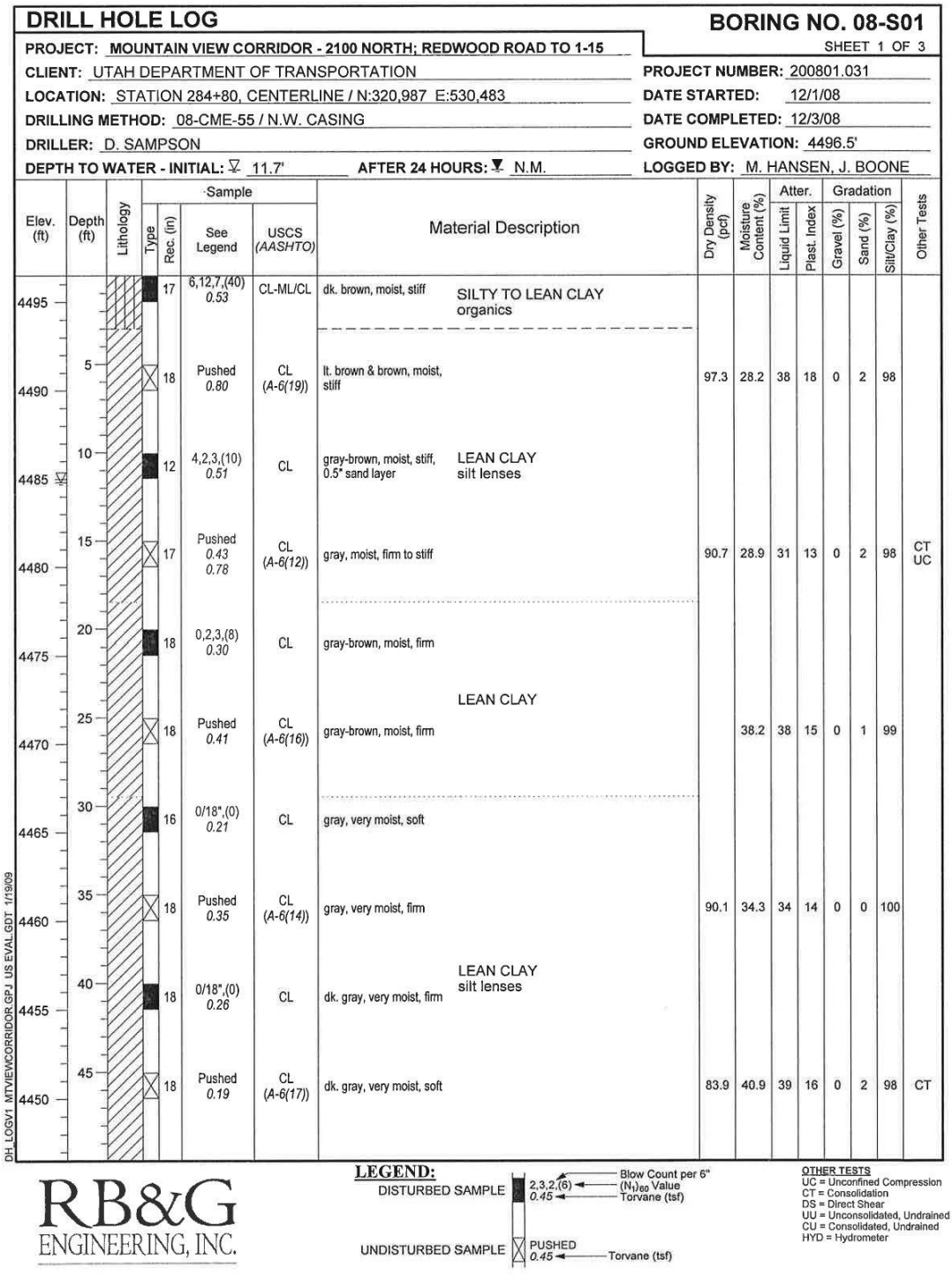

Figure 4-2. Typical Bore Log for the MVC Test Site

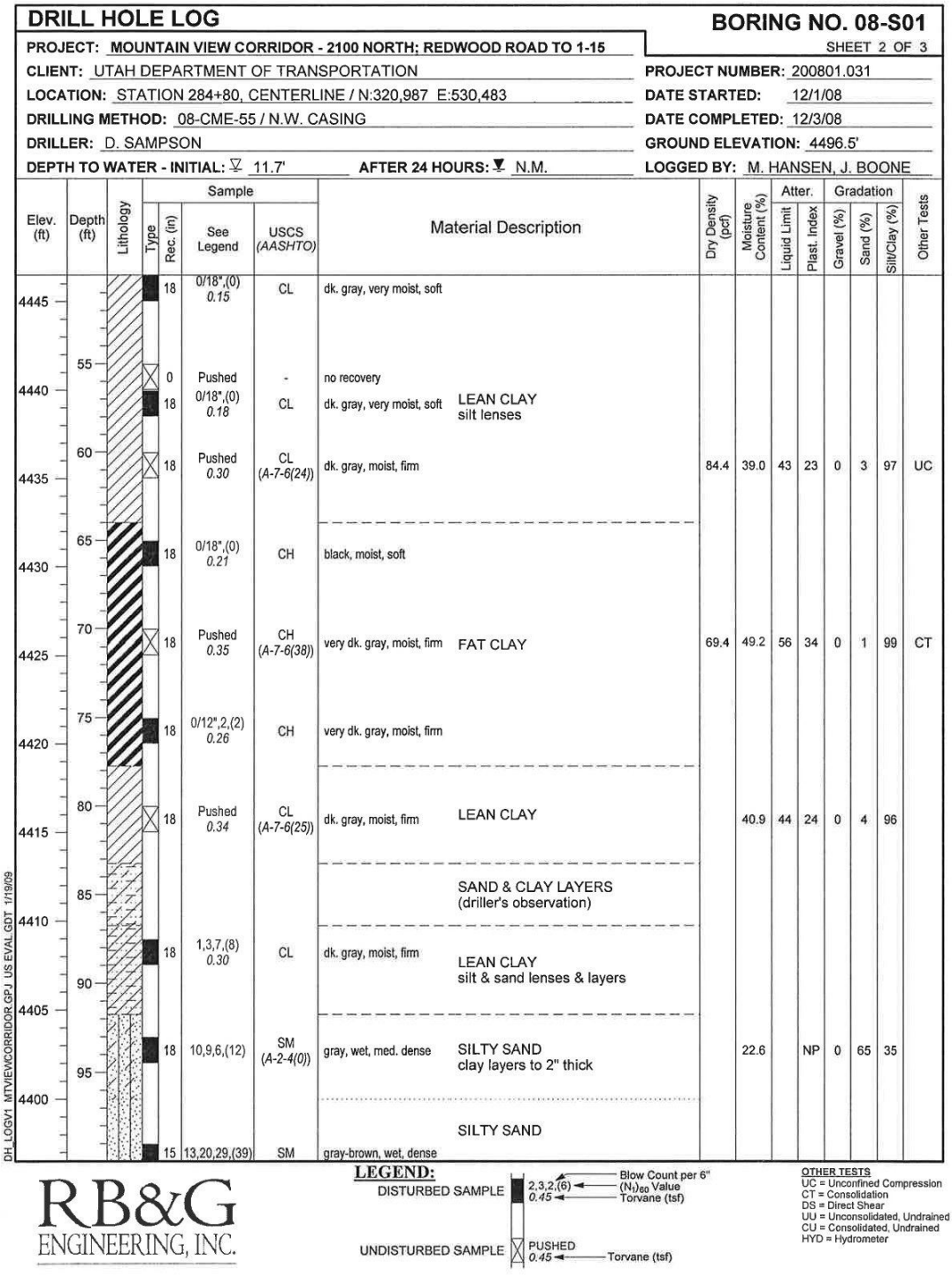

Figure 4-2 continued

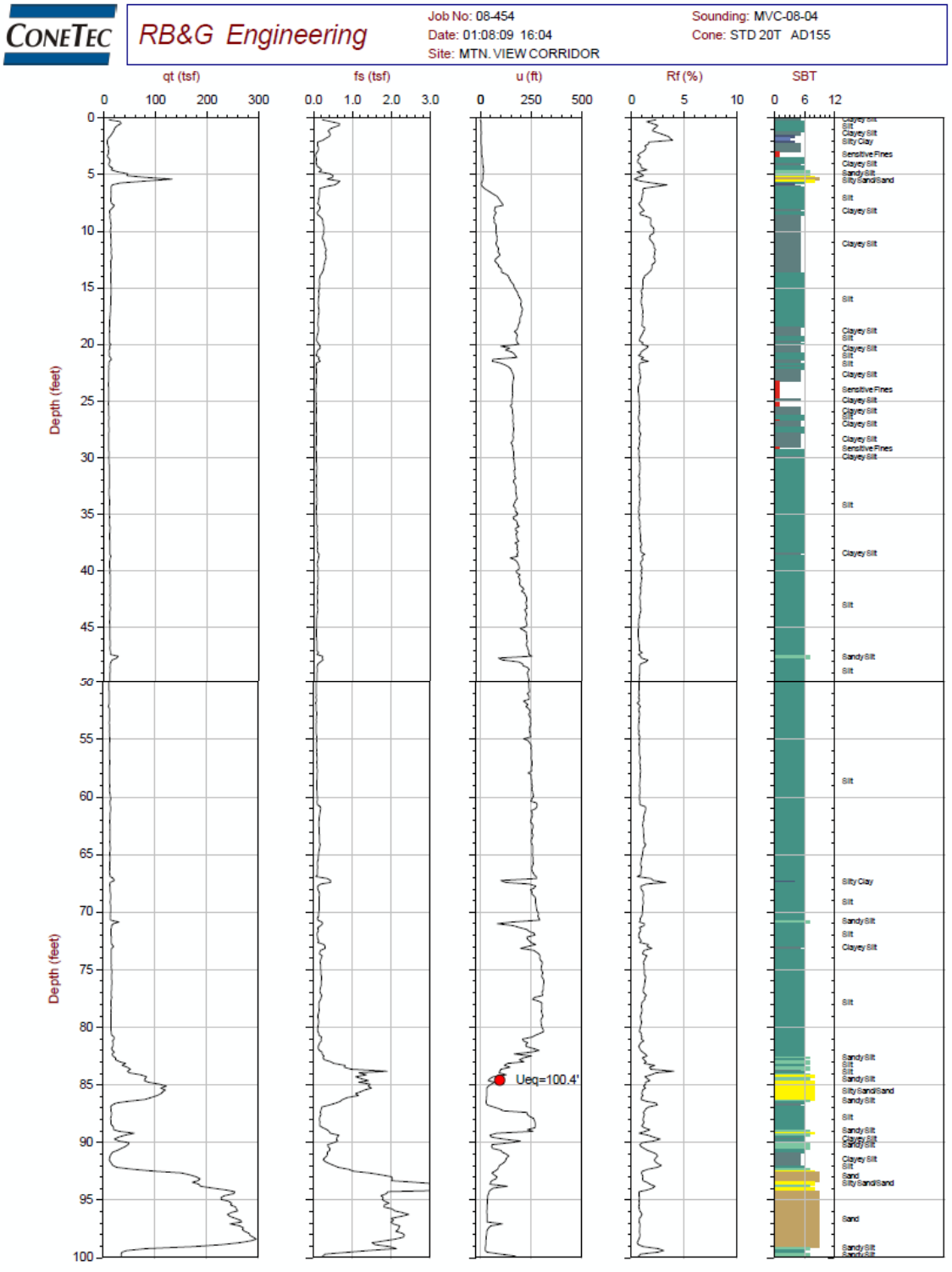

Figure 4-3. Typical CPT Log for the MVC Test Site

As can be seen in the bore hole and CPT logs, the native soil profile below the highway embankment is mainly lean clay (CL) down to a depth of 90 ft beneath the ground surface, with a zone of fat clay (CH) from 64 to 78 ft below the ground surface. The clay layer is bounded at its base by a drainage layer or a silt (ML) and sand (SM).

Along the MVC test site, the top 2 ft of soil was excavated in order to embed the MSE retaining wall, which provided a vertical slope along the outer edge of the embankment. After embedding the wall, one foot of sand was installed to provide a drainage layer for the PV drains, as shown in Figure 4-4. To account for the removal of the 2 ft of clay, the analysis will calculate settlement starting at 2 ft below the natural ground surface.

Figure 4-4. Excavation for Wall Embedment and Drainage Layer

4.1 Soil Properties

The subsurface exploration was conducted to determine the properties of the soils used during the analysis. The in-situ properties provided an understanding of how the soil would behave under loading conditions. Along with the in-situ tests, laboratory tests were performed to classify the soil samples according to the Unified Soil Classification System (USCS). From the field and laboratory results, the properties determined were:

- Natural, or in-situ, moisture content (w_n)
- Moist unit weight (γ_{moist})
- Liquid limit (LL)
- Plastic limit (PL)
- Coefficient of consolidation (C_v)
- Compression index (C_c)
- Re-compression index (C_r)
- Secondary compression index (C_α)
- Overconsolidation ratio (OCR)
- Undrained shear strength (S_u)
- Preconsolidation pressure (σ'_c)

Figure 4-5 presents the moisture content (on the left) and moist unit weights (on the right) versus depth below the native ground surface. These figures show the data from the samples (the markers) with the average values taken at 10 ft intervals (the lines). These figures allowed for the calculation of the estimated existing stress throughout the soil profile.

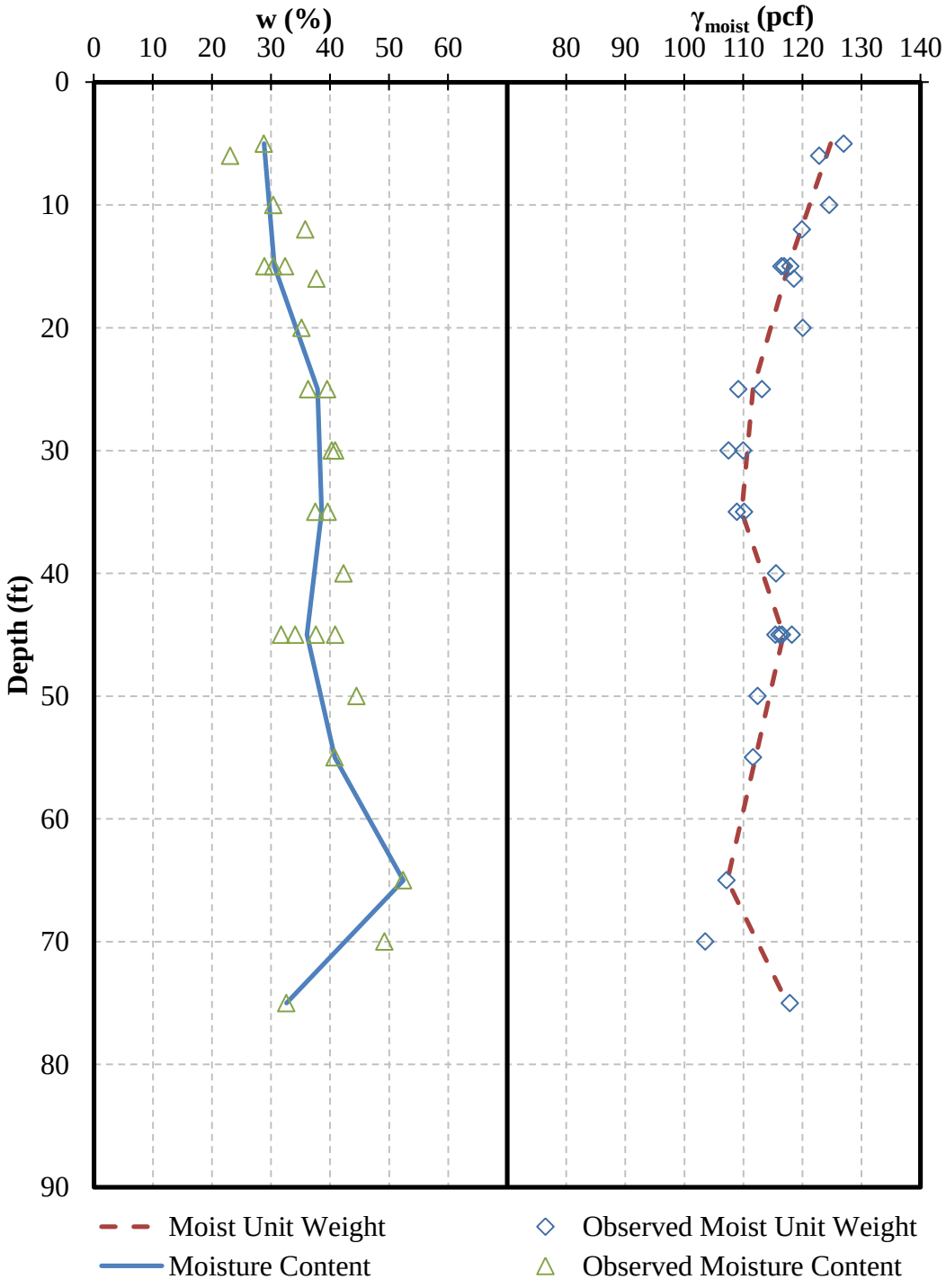

Figure 4-5. Observed and Average Moisture Contents and Moist Unit Weights Versus Depth Below Ground Surface.

Figure 4-6 show the variation of the average PL, LL, and w_n versus depth. Each bore hole log was used to calculate the average PL, LL, and w_n throughout the soil profile and across the entire test section.

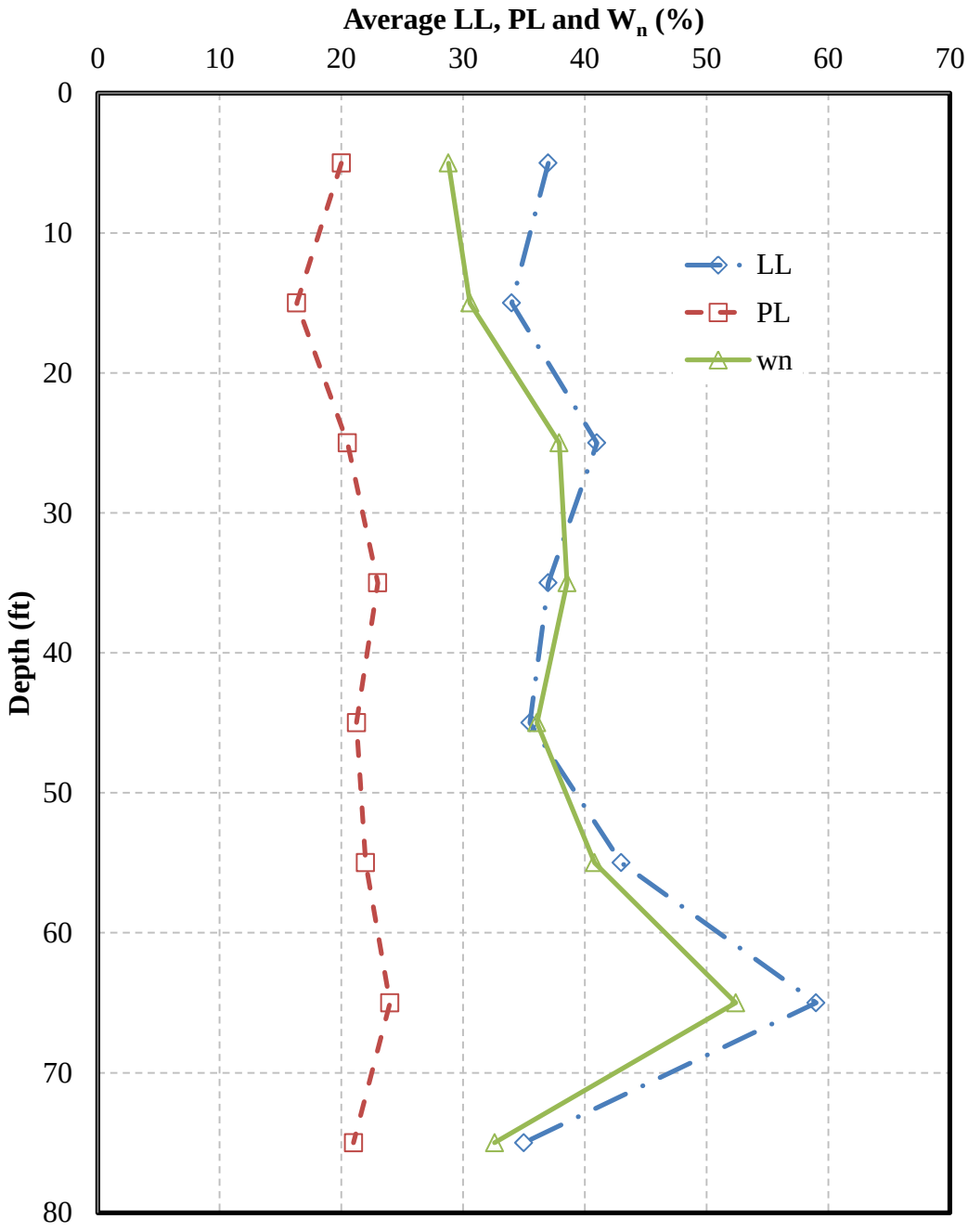

Figure 4-6. Average LL, PL and W_n Based on Bore Hole Logs Versus Depth Below Ground Surface

The Atterberg limits show that the clay layer is quite uniform. The plastic limit is typically around 20%, while the liquid limit is typically 35 to 40% through most of the profile within the lean clay layers, indicating plasticity indices of 15 to 20%. However, the fat clay layer deeper in the profile has an average PI of about 30%.

The plot shows quickly whether the soil is normally consolidated or overconsolidated and sensitive. If the natural water content is between the liquid limit and plastic limit moisture content, the soil is likely overconsolidated. If it is near the liquid limit, it is likely normally consolidated. Finally if it is higher than the liquid limit, it is likely sensitive. The plot shows that the soil is most likely overconsolidated for the first 30 ft beneath the ground. The remaining 50 ft is most likely normally to slightly overconsolidated. There also appears to be a zone of somewhat sensitive soil from a depth of 35 to 45 ft.

From the consolidometer test data, the OCR was able to be calculated and plotted versus depth below the native ground surface, as shown in Figure 4-7. As can be seen from the plot, each marker represents a sample taken from the bore holes. The upper 45 ft of the profile consists of overconsolidated clay, while the remaining 35 ft is slightly overconsolidated.

Figure 4-8 provides a plot of the measured C_v values as a function of depth, along with average values within each 10 ft depth interval. Due to the OCR profile, the upper 30 ft of the profile has a higher C_v value compared to the lower zone, as shown in Figure 4-8. When the clay is overconsolidated, the settlement of the soil is primarily along the recompression curve, where the lower void ratio and reduced compressibility lead to higher C_v values for a given liquid limit value. Figure 4-9 shows the C_v values selected from the idealized profile plotted against curves defining typical C_v values for normally and overconsolidated soil as a function of liquid limit. The measured values are in reasonable agreement with expected values.

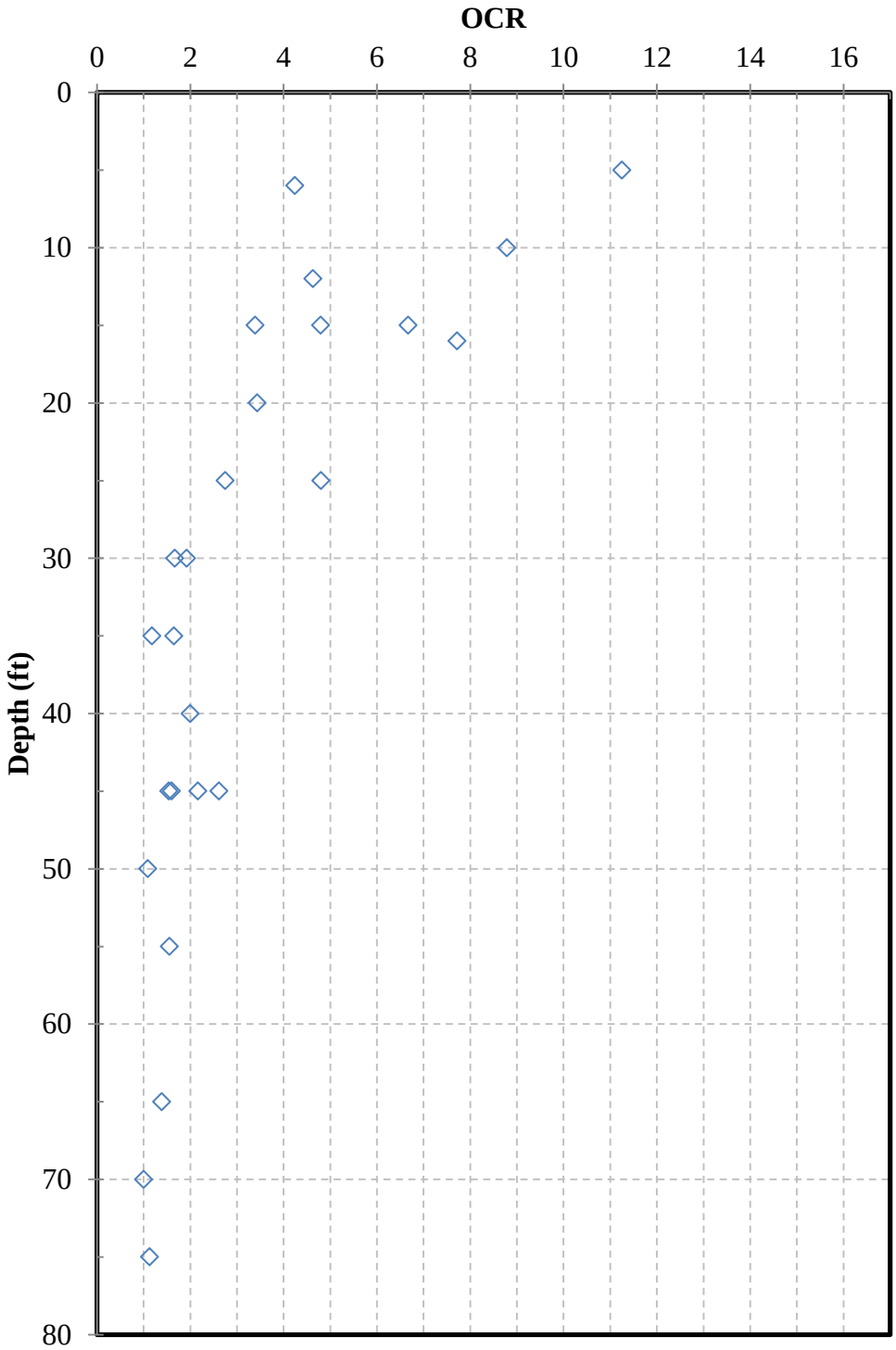

Figure 4-7. OCR Data Collected from Consolidometer Test Plotted Against Depth

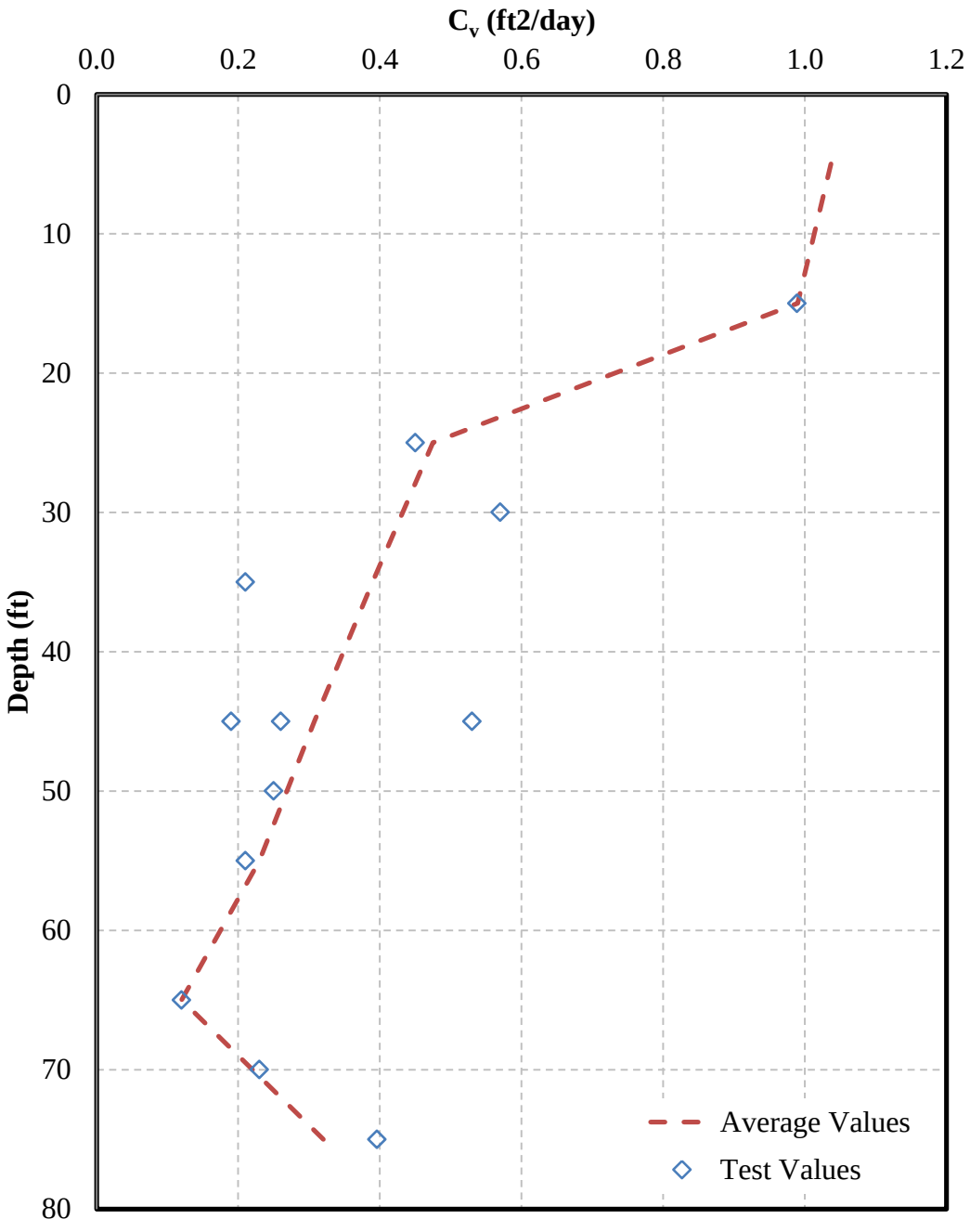

Figure 4-8. C_v Versus Depth Along MVC Test Site Plotted with Average Values Used in Analysis

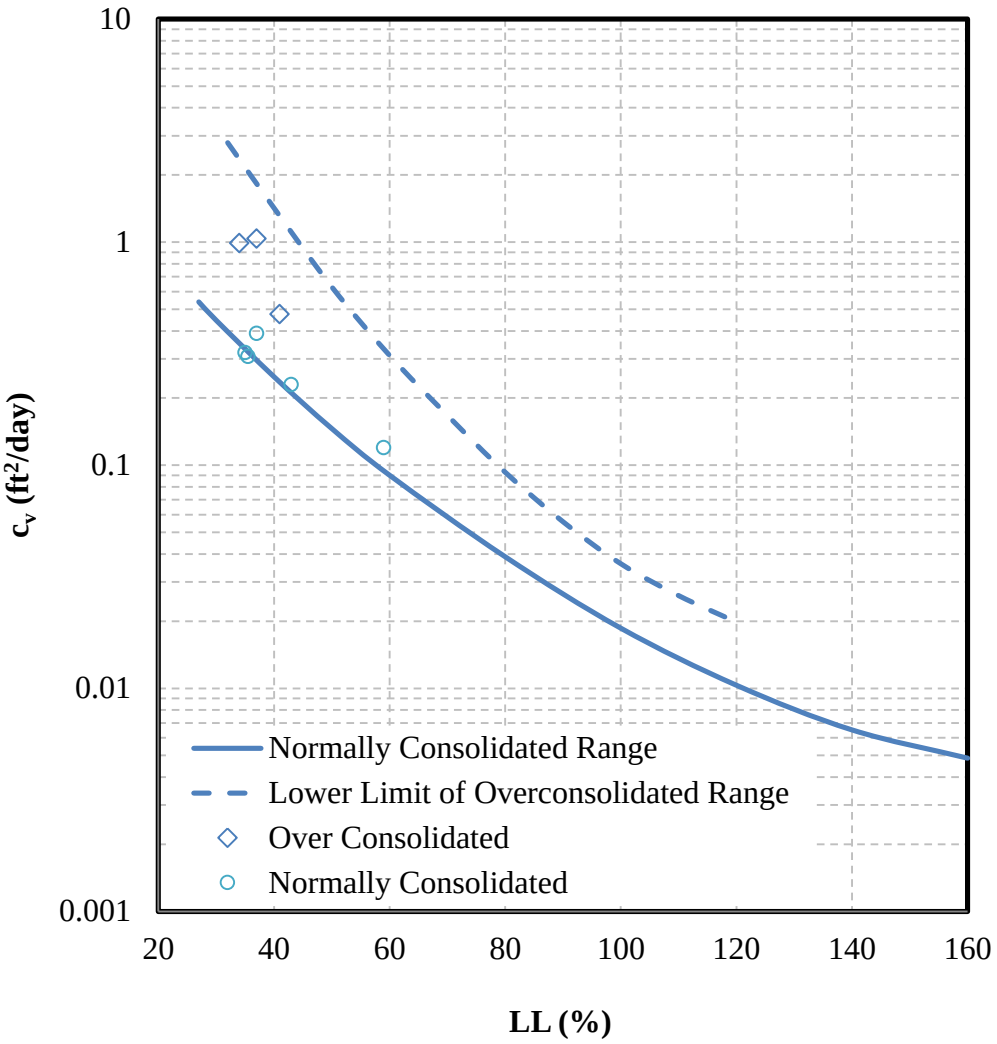

Figure 4-9. Correlation Between C_v and LL for Normally Consolidated and Overconsolidated Clays (After Naval Facilities Engineering Command 1986)

Measured compression and recompression indices are plotted as a function of depth in Figure 4-10. The profile of the compression and recompression indices show that there is a section of fat clay, at a depth of about 60 to 70 ft, which results in the indices being higher in magnitude than in the lean clay zones. In order to check the validity of the recompression and compression indices, the measured indices were compared to the relationship between the indices and plasticity index, as defined by Mayne (1990). The comparison is presented in Figure 4-11.

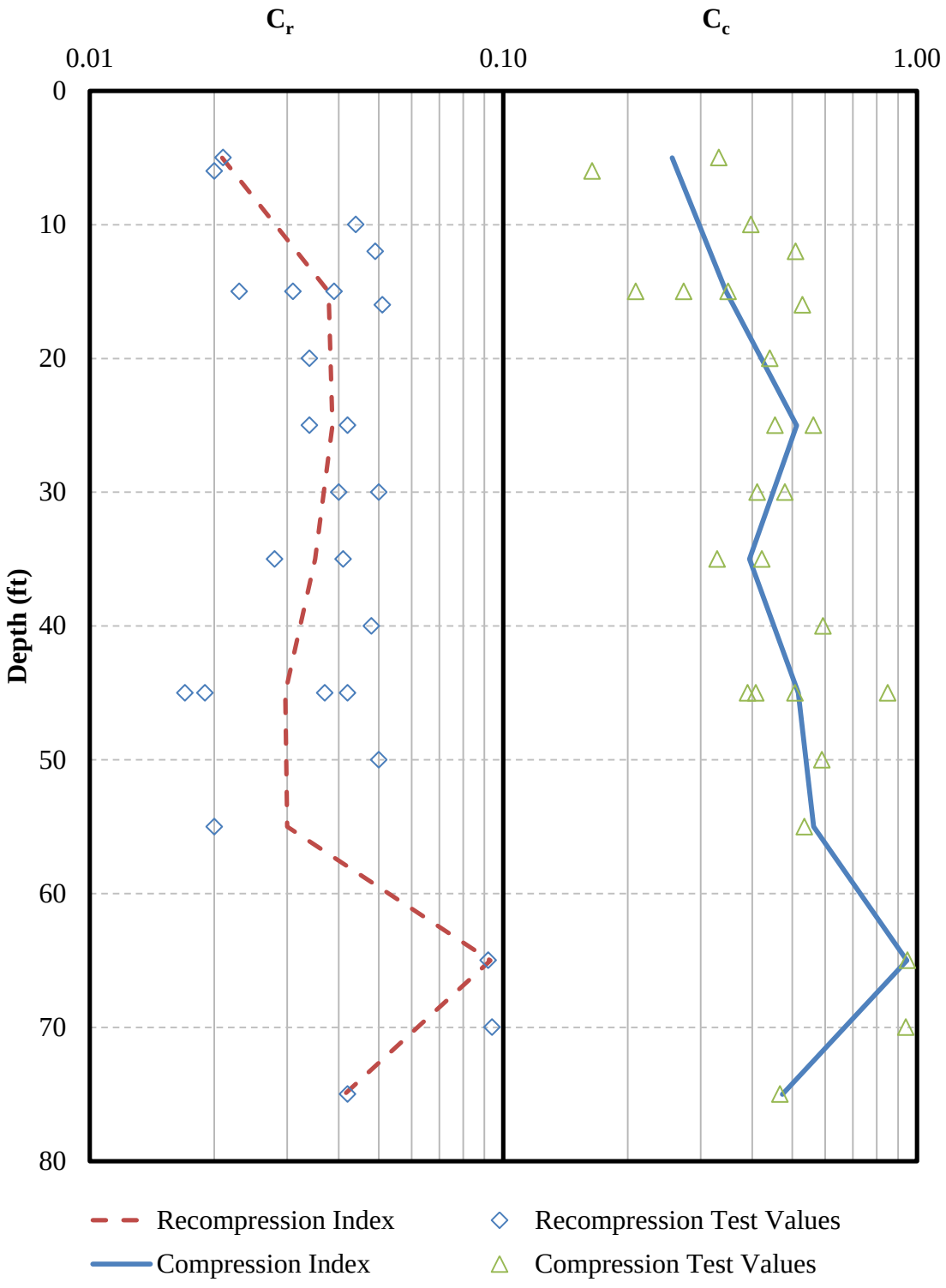

Figure 4-10. Observed and Average C_r and C_c Versus Depth Below Ground Surface

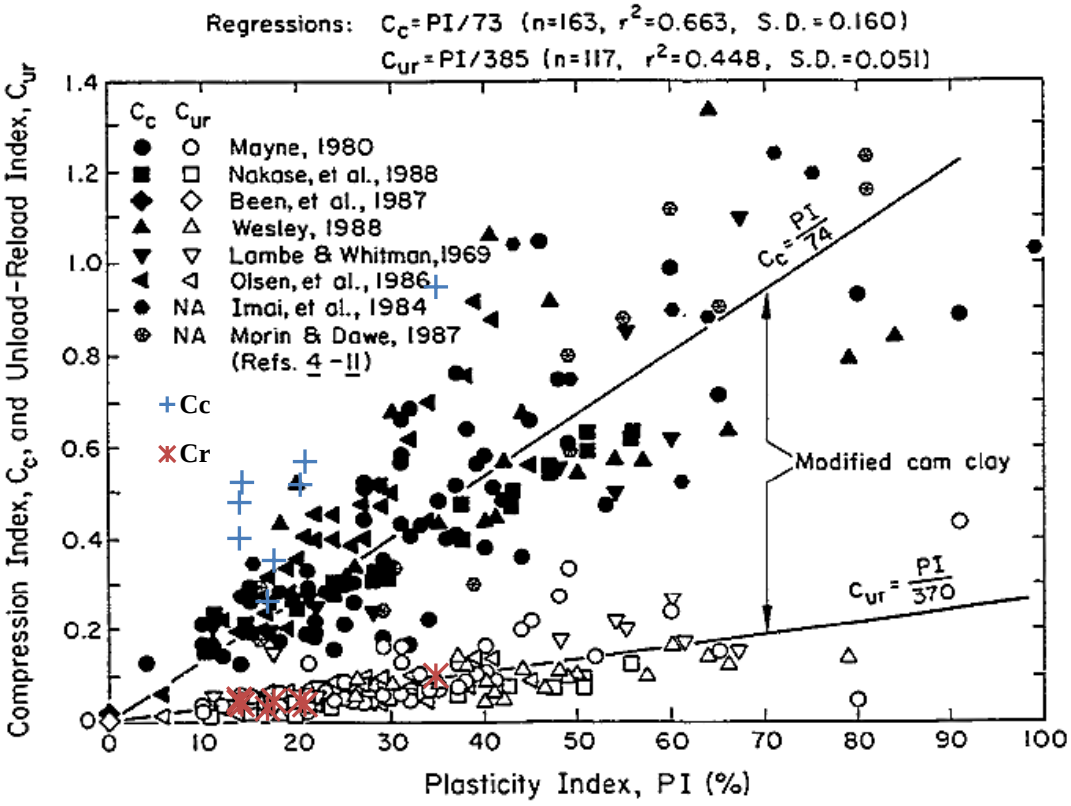

Figure 4-11. Correlation of the Compression Ratio and the Recompression Ratio with the Plasticity Index of the Soil (Kulhawy and Mayne 1990)

As seen in Figure 4-11, the measured recompression index values follow the trend defined by Mayne and are within the general range of the scatter. However, the correlation between the compression index and PI appears to be less robust, and there is extensive scatter along Mayne's compression index trend line. The majority of the MVC compression index data points lie along the upper boundary of the scatter reported by Mayne.

Figure 4-12 provides a plot of the measured secondary compression index (C_α) for samples in the normally consolidated and overconsolidated clay layers. As the clay layer changes from being normally consolidated to overconsolidated, the magnitude of the secondary consolidation, or creep, decreases.

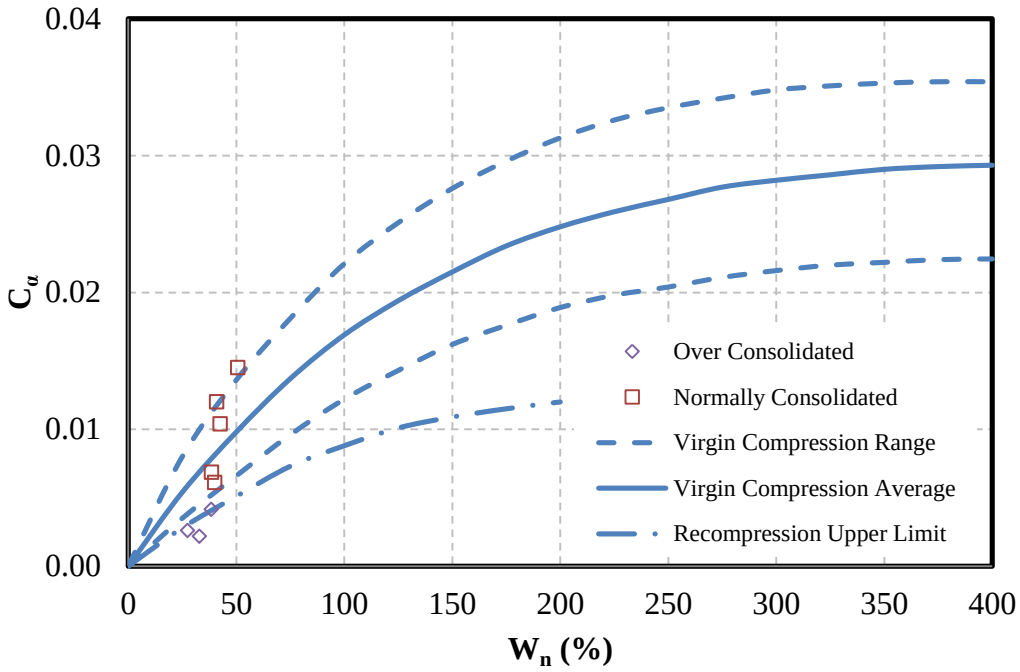

Figure 4-12. Relationship Between the Secondary Compression Index and the Natural Moisture Content of the Soil (After Naval Facilities Engineering Command 1986)

From each of the bore holes and by using torvane testing, the undrained shear strength of the clay at various depths was determined. Figure 4-13 shows the individual data along with the average values.

Figure 4-13 shows that the upper 15 ft is stiff clay (S_u > 1000 psf) while the remaining 65 ft is a medium clay (500 psf < S_u < 1000 psf). On average, the clay profile consists of soft clay; therefore, the undisturbed to disturbed permeability ratios at the MVC test site should agree with those proposed by Rixner et al. (1986). The plot of undrained shear strength versus depth also relates to the OCR profile of the soil profile. The undrained shear strength decreases with depth while the soil is overconsolidated; therefore, the undrained shear strength profile shows that the upper 50 ft is overconsolidated and the remaining 30 ft is normally consolidated, which is shown when the undrained shear strength become fairly constant with depth.

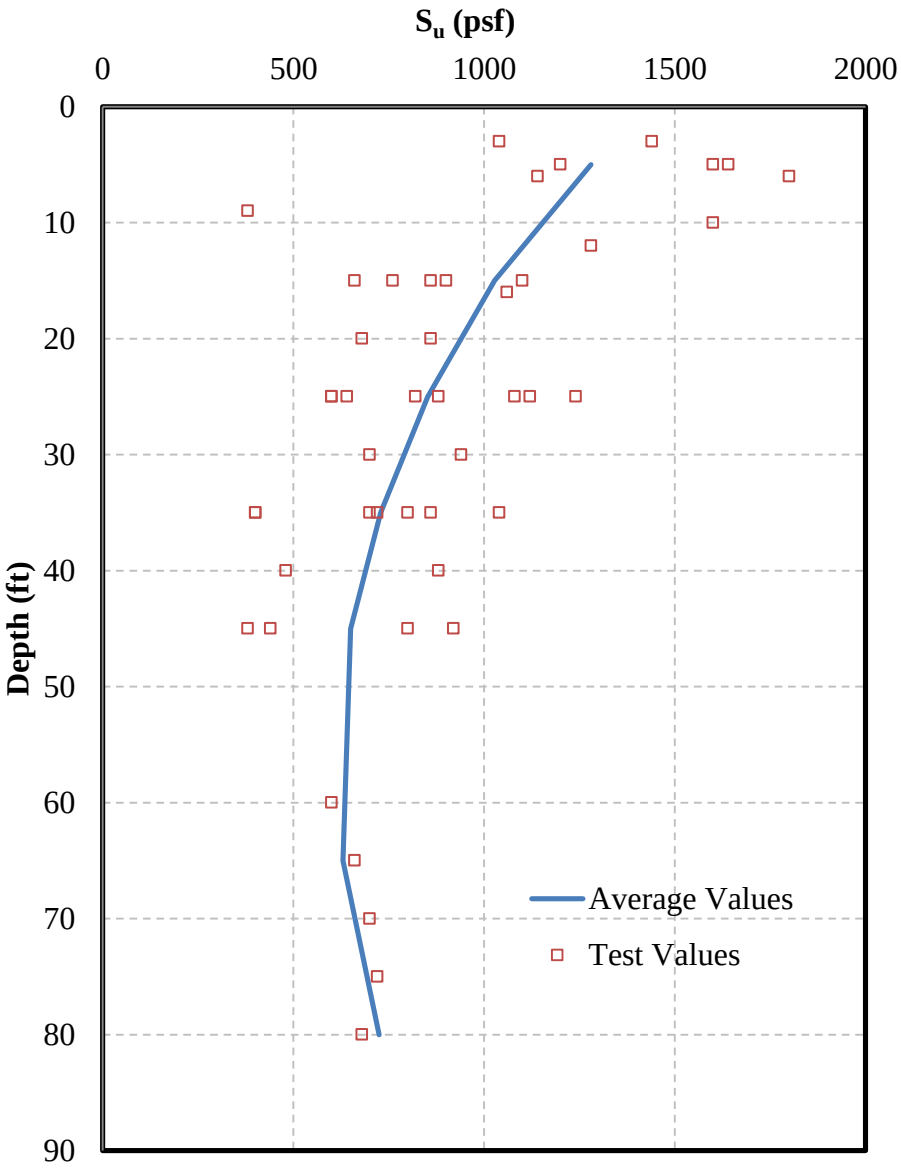

Figure 4-13. Observed and Average Undrained Shear Strength Versus Depth Below Ground Surface

4.2 Idealized Soil Profile

Based on the bore hole and CPT logs, laboratory tests, and accepted correlations of soil properties, an idealized soil profile along the test site was developed. The idealized soil profile is shown in Figure 4-14. The bottom of the clay layer may vary along the test section. The clay at

some locations is bounded by a sand while at others by low-compressibility silt. The low-compressibility silt layer has a low permeability and may be considered impermeable.

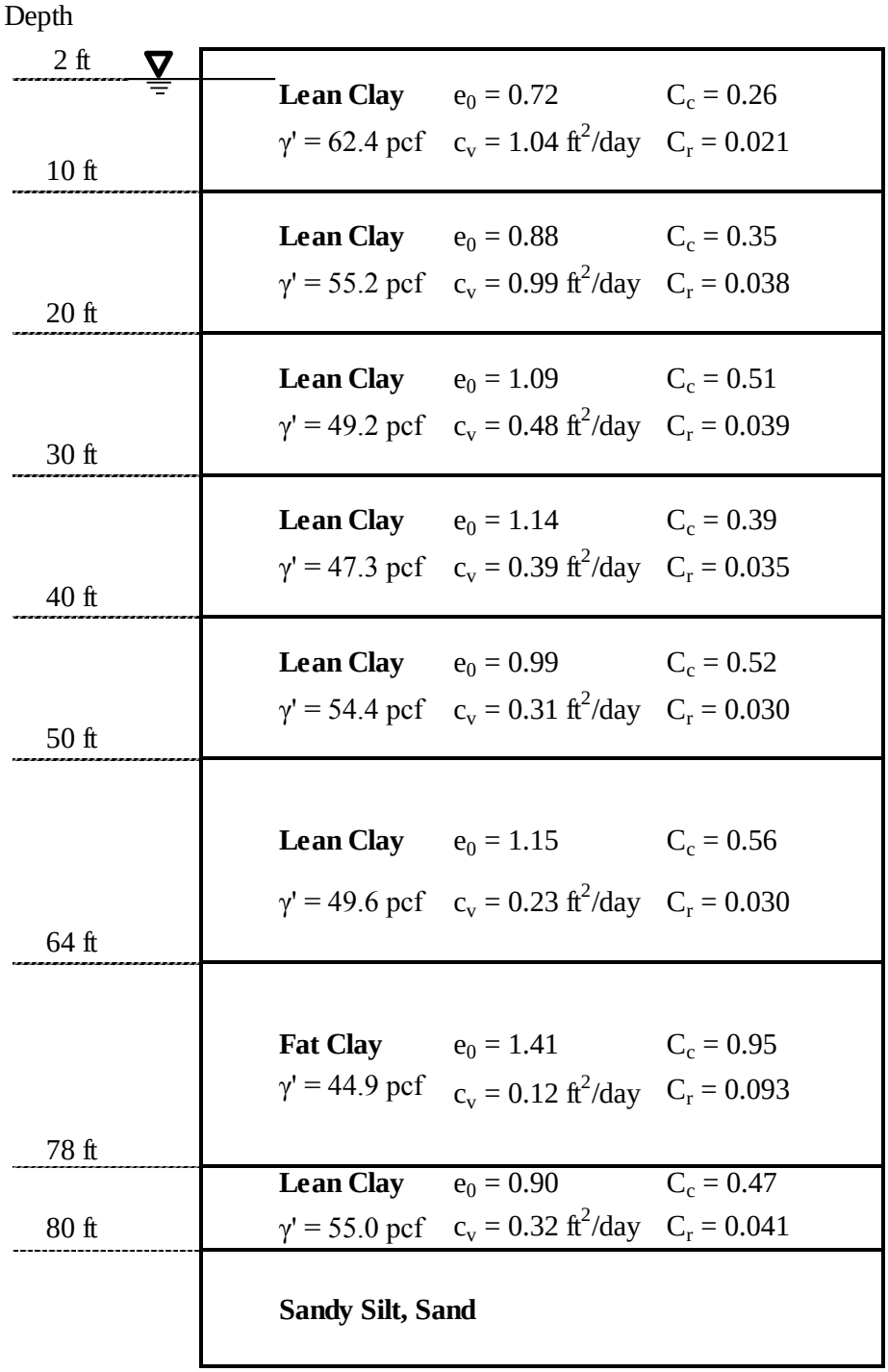

Figure 4-14. Idealized Soil Profile

5 FIELD TEST RESULTS

A key aspect of this research was reducing the collected data to attempt to make preliminary conclusions without extensive analysis. By looking at the raw field data, it became apparent that the observed field test results would be inconclusive without completing more complex analyses. This section explains the process taken to correct erroneous data, develop preliminary conclusions, and come up with an analysis method to be used to verify or correct the preliminary conclusions.

5.1 Data Collection and Reduction

From the MVC test site, each instrument for each spacing and anchor type was monitored, and the data was collected by RB&G engineering. This data were then entered into a spreadsheet, which was received electronically. The initial data evaluation suggested some possible errors and other problems with the collected data.

5.1.1 Errors

The known errors that were easily fixed happened when the manometer settlement systems were flushed with new fluid. When the system was flushed, the data were not adjusted for the new initial reading, which caused a dilative spike to occur in the settlement history, as shown in Figure 5-1. To correct this error, all the data past the day of the system flush were

shifted relative to the day prior to the system flush, in order to account for the new initial reading.

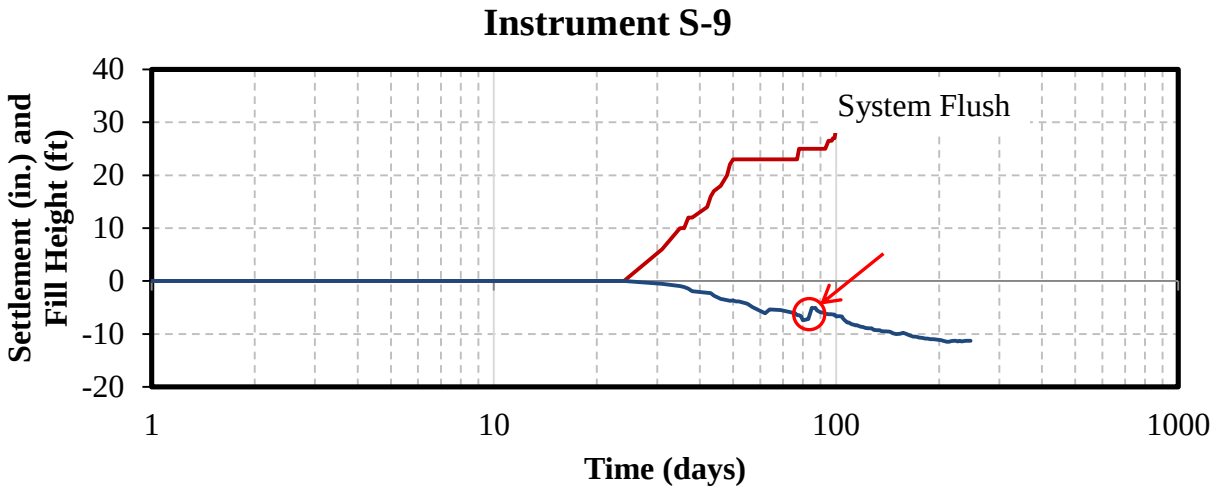

Figure 5-1. Settlement Error Due to System Flush

Other problems in the data, such as oscillating settlement histories as shown in Figure 5-2, may have occurred due to temperature fluctuation throughout the day. A combination of non-consistent times for instrument readings and lack of temperature readings made it impossible to check whether temperature fluctuation was the cause. Another possible error in the settlement versus time curves may have occurred due to the lack of elevation surveys for the measurement boxes. Although elevation surveys were supposed to occur weekly, there were apparently some periods where this did not actually take place. Without elevation surveys being taken, the height of the instrument reading station may have settled or rebounded causing the "measured" settlement under the embankment to decrease or increase, respectively. The oscillating data was corrected by attempting to smooth the time versus settlement curve by filtering the data to the same time interval each day. By using continuous readings and by using the data that was

collected during a set number of hours each day, some oscillation was removed. Continuous readings were only available for the BYU-4 instrument; therefore, only BYU-4 was able to be corrected. Although corrections to BYU-4 were made using the continuous readings, the time versus settlement data still oscillated due to other unknown errors.

Another error in the raw data existed from unrealistic settlement values and patterns. Figure 5-3 and Figure 5-4 show settlement versus time histories for two instruments where the settlement curves were flattening after some time under a constant maximum fill load, which indicates the end of primary consolidation. However, beyond this point, without any change in load, the settlement began to increase substantially as if a new load had been placed. This pattern is unrealistic based upon consolidation theory. Along with contradicting consolidation theory, the time versus settlement data contained measured settlements that were considerably greater than that at the other instrument locations. To adjust for this apparent error in the curve, the point where primary consolidation appeared to end under the maximum fill height was identified, and the data were truncated at that point.

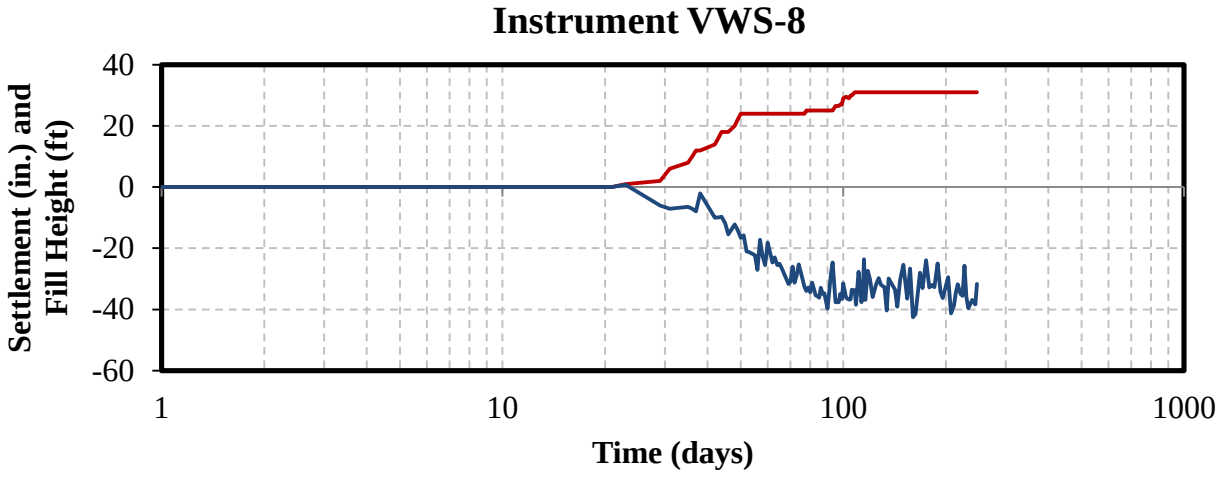

Figure 5-2. Settlement Error Due to Oscillating Data

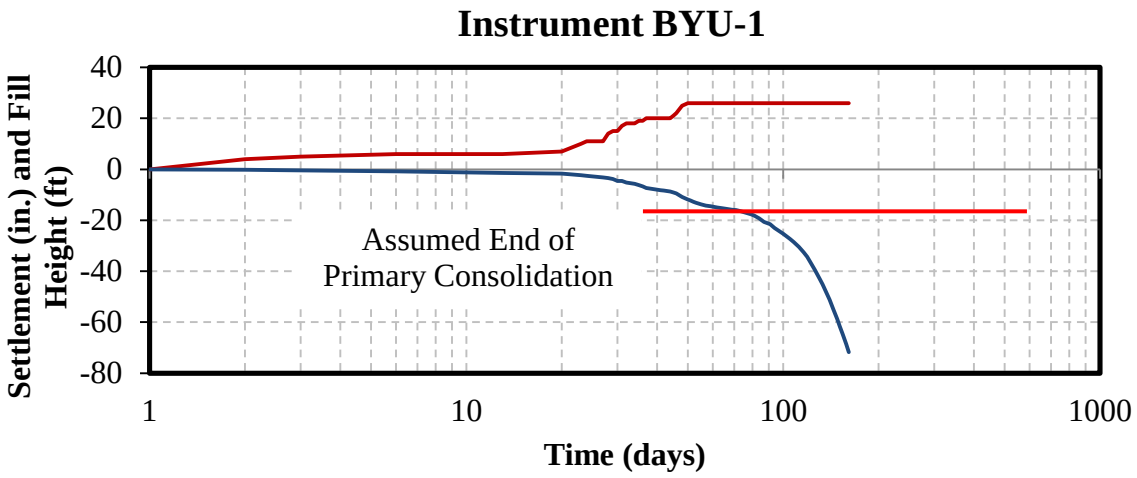

Figure 5-3. Unrealistic Settlement Magnitude

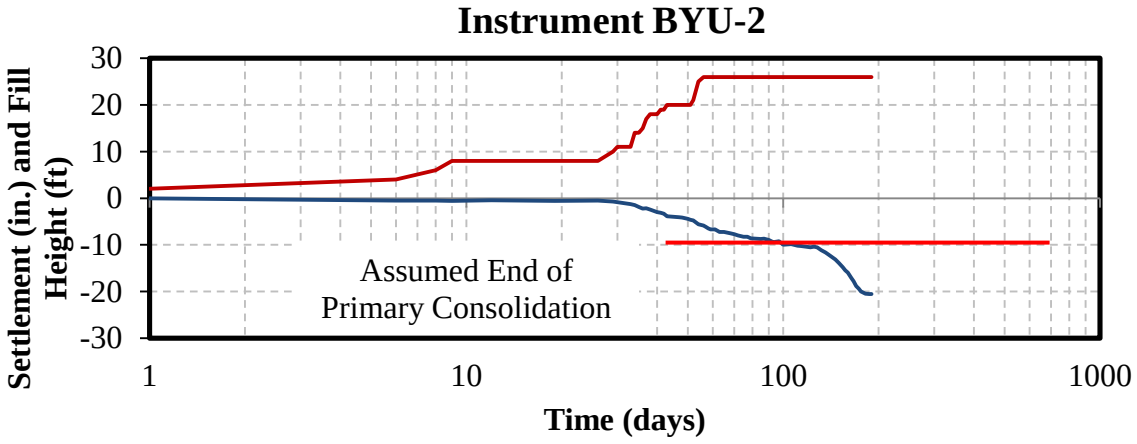

Figure 5-4. Unusual Settlement Curve

5.2 Measured Settlement Curves

From the data collected at the MVC test site, the fill height and amount of settlement was plotted as a function of time. In Figure 5-5 through Figure 5-8, the ordinate shows the settlement magnitude and fill height as negative and positive values, respectively, while the abscissa shows time plotted on a logarithmic scale.

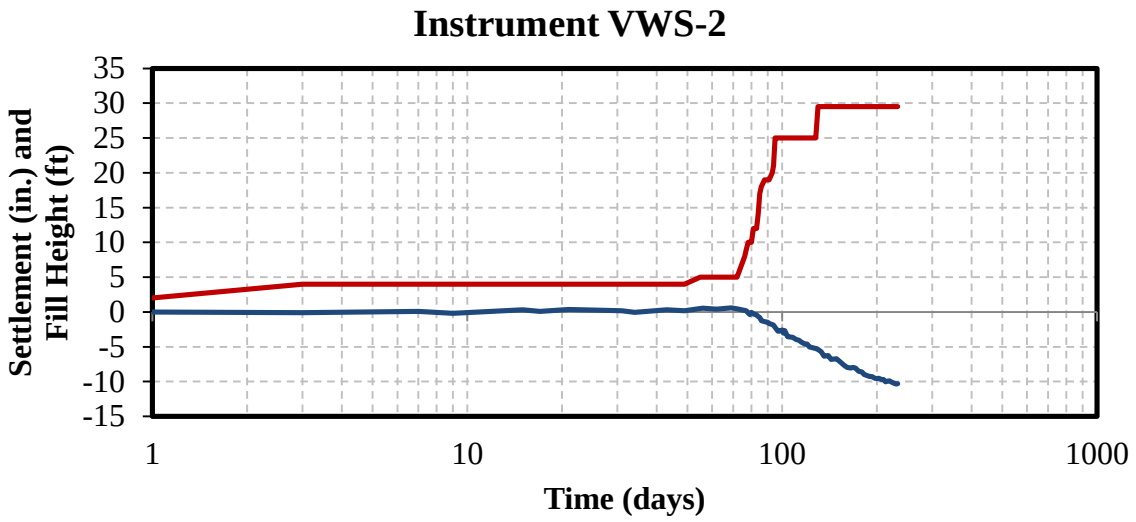

Figure 5-5. Measured Time-Settlement Curve for VWS-2, 5.8 ft Spacing with Plate Anchor from Full-Scale Field Test

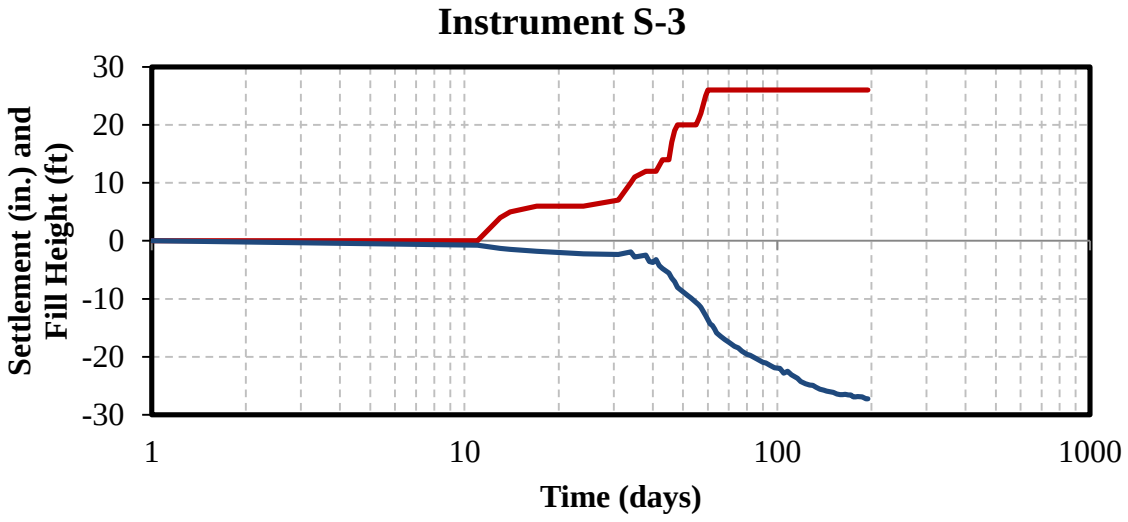

Figure 5-6. Measured Time-Settlement Curve for S-3, 5.8 ft Spacing with Plate Anchor from Full-Scale Field Test

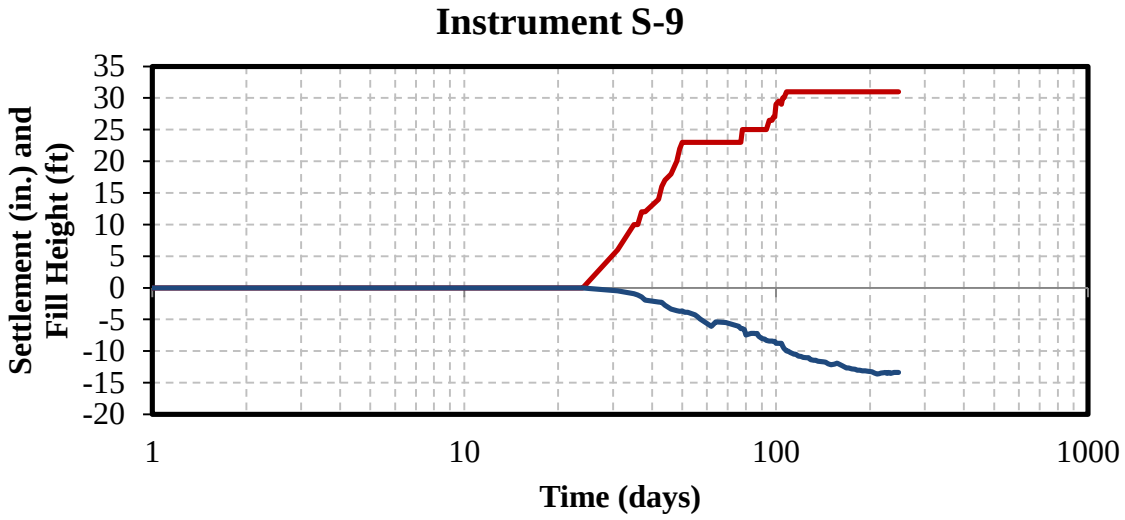

Figure 5-7. Measured Time-Settlement Curve for S-9, 5.8 ft Spacing with Plate Anchor from Full-Scale Field Test

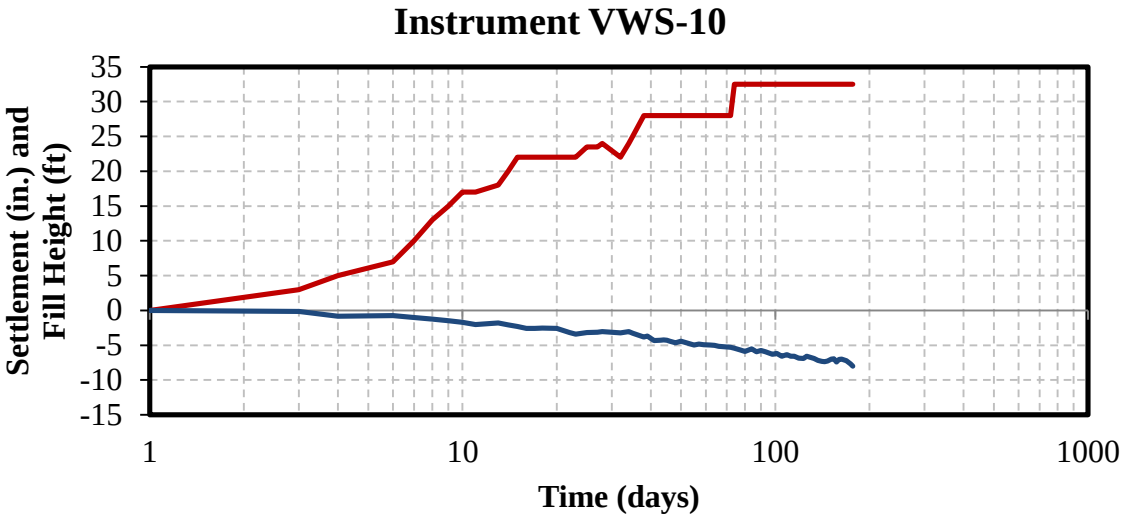

Figure 5-8. Measured Time-Settlement Curve for VWS-10, 5.8 ft Spacing with Plate Anchor from Full-Scale Field Test

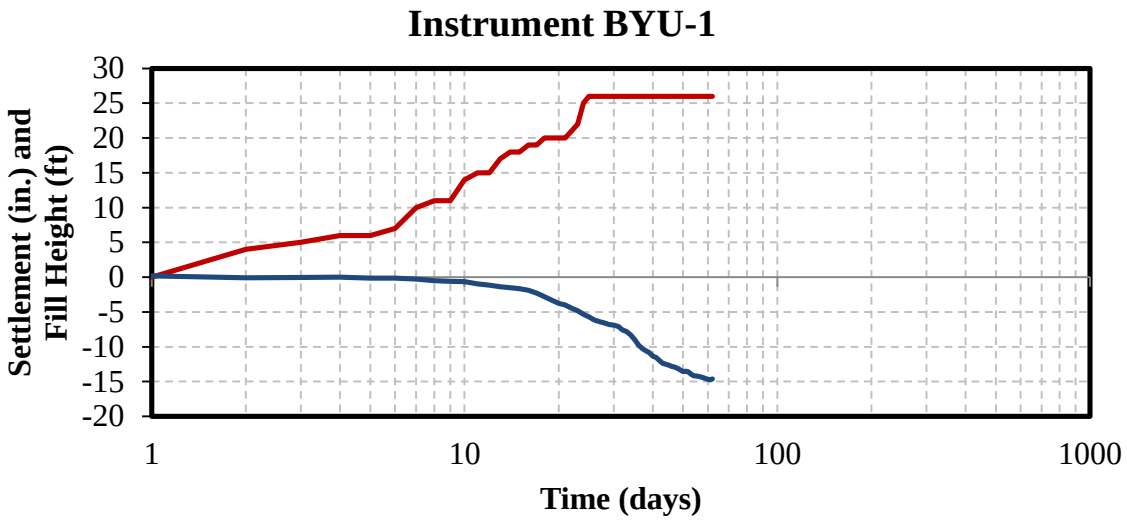

Figure 5-9. Measured Time-Settlement Curve for BYU-1, 5.0 ft Spacing with Plate Anchor from Full-Scale Field Test

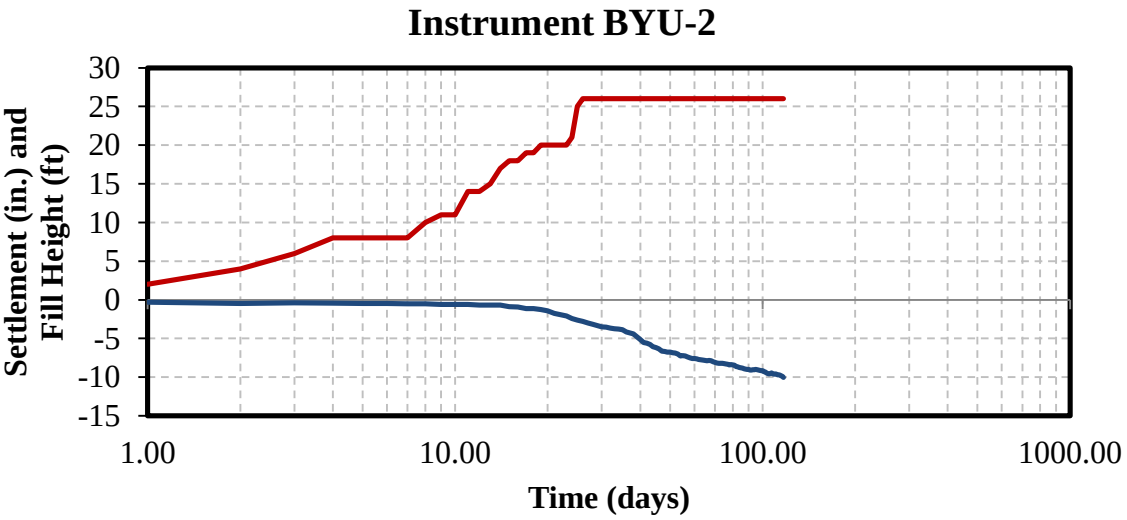

Figure 5-10. Measured Time-Settlement Curve for BYU-2, 5.0 ft Spacing with Plate Anchor from Full-Scale Field Test

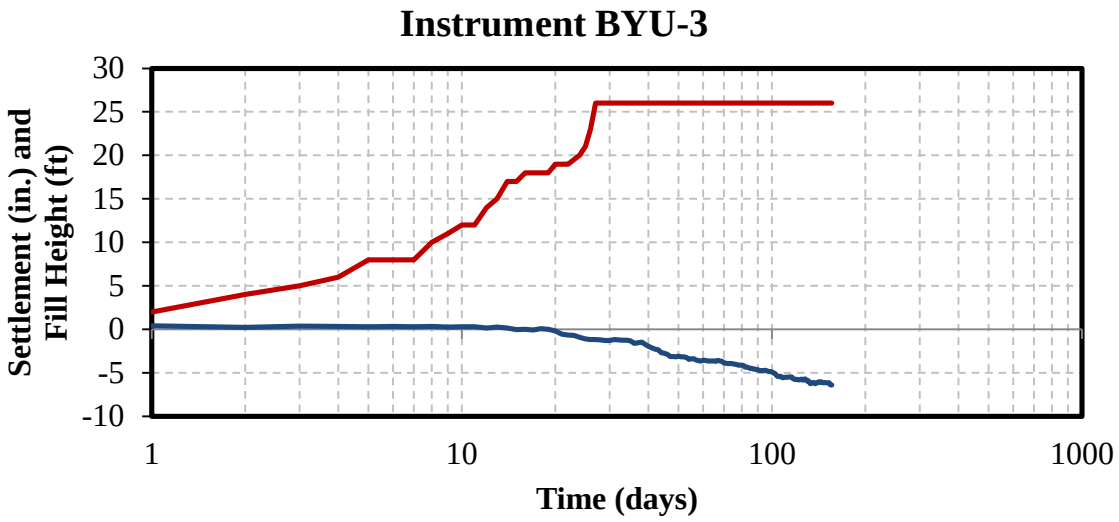

Figure 5-11. Measured Time-Settlement Curve for BYU-3, 4.0 ft Spacing with Plate Anchor from Full-Scale Field Test

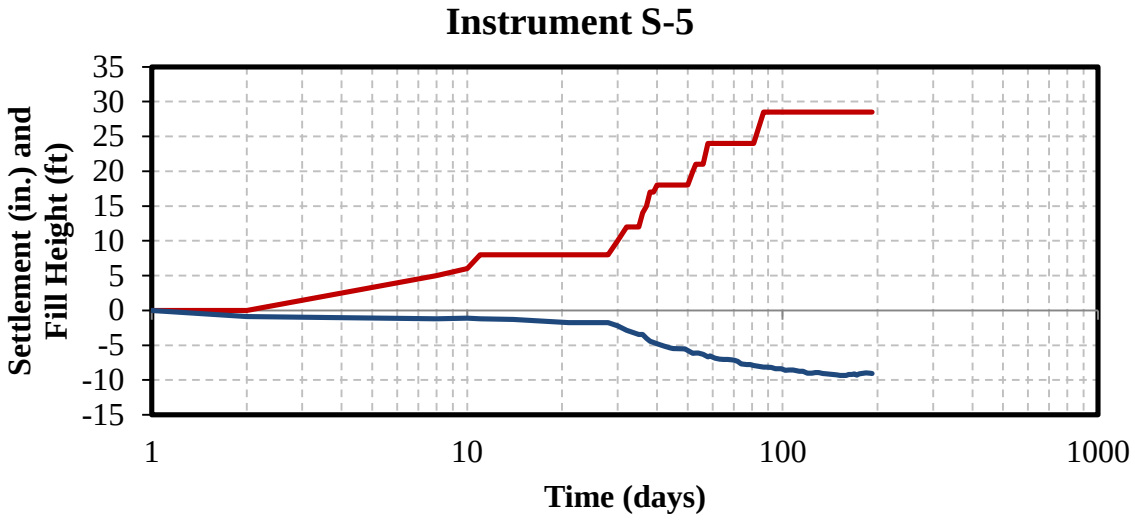

Figure 5-12. Measured Time-Settlement Curve for S-5, 3.0 ft Spacing with Plate Anchor from Full-Scale Field Test

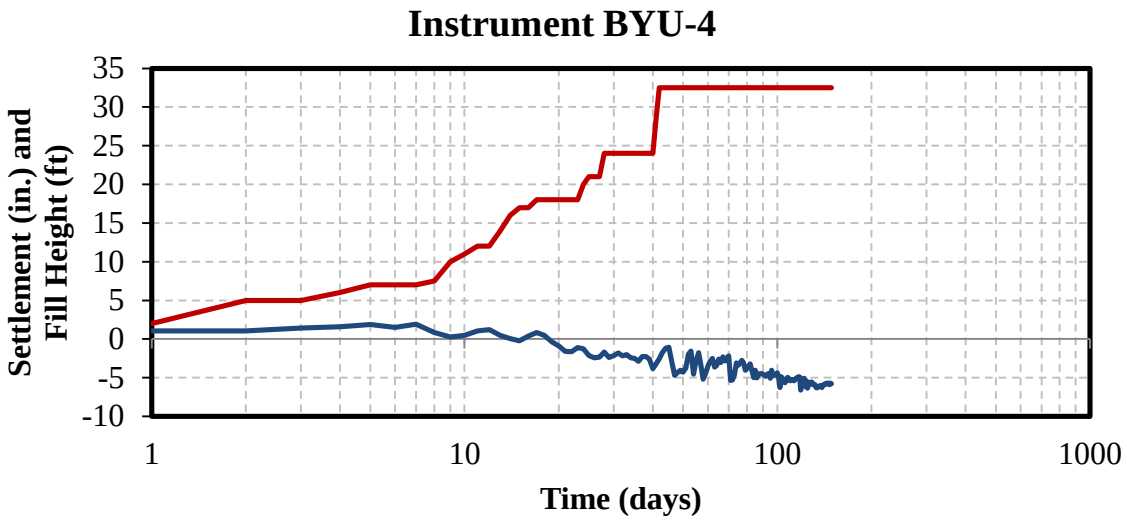

Figure 5-13. Measured Time-Settlement Curve for BYU-4, 3.0 ft Spacing with Plate Anchor from Full-Scale Field Test

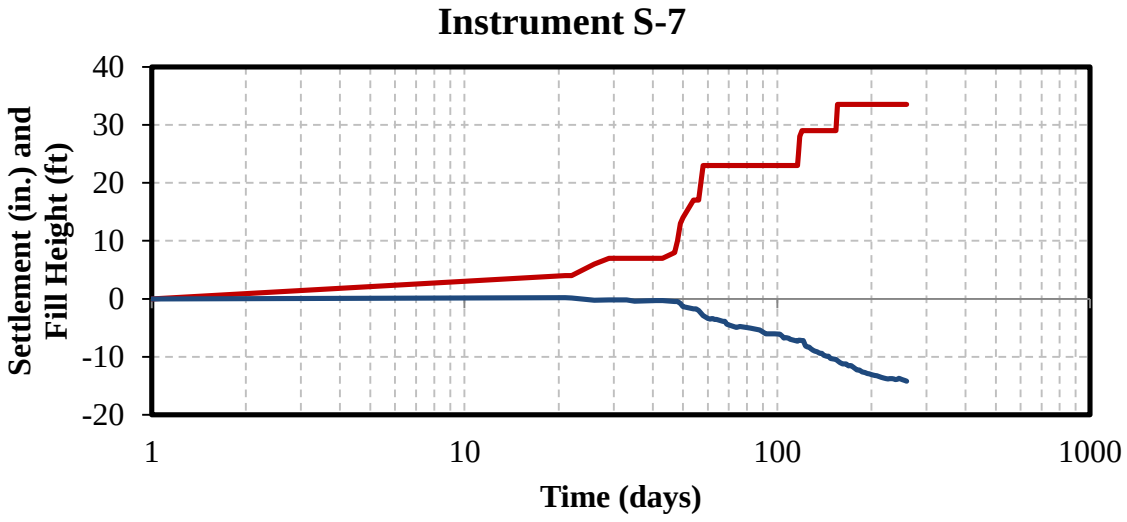

Figure 5-14. Measured Time-Settlement Curve for S-7, 5.8 ft Spacing with Rebar Anchor from Full-Scale Field Test

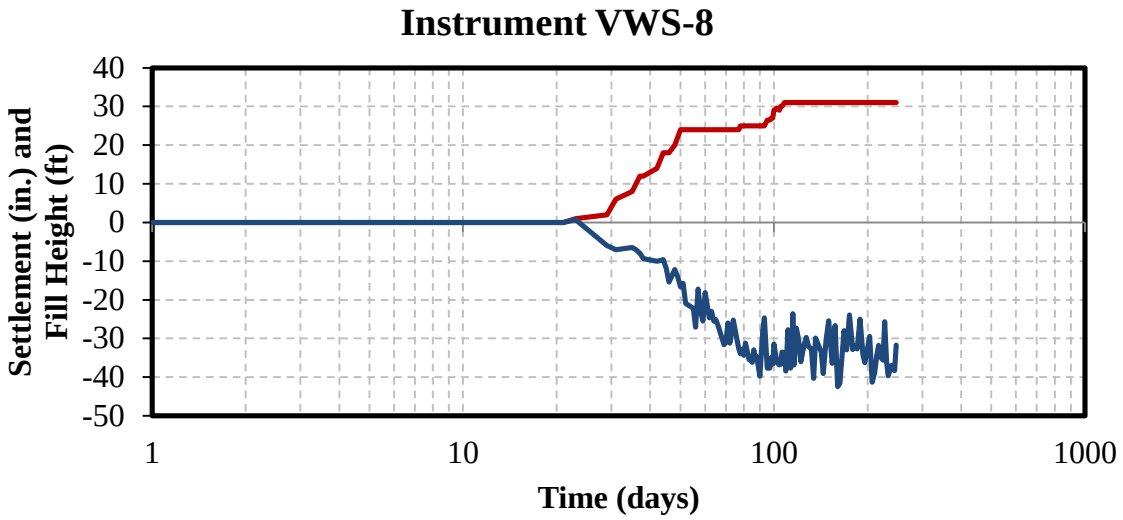

Figure 5-15. Measured Time-Settlement Curve for VWS-8, 5.8 ft Spacing with Rebar Anchor from Full-Scale Field Test

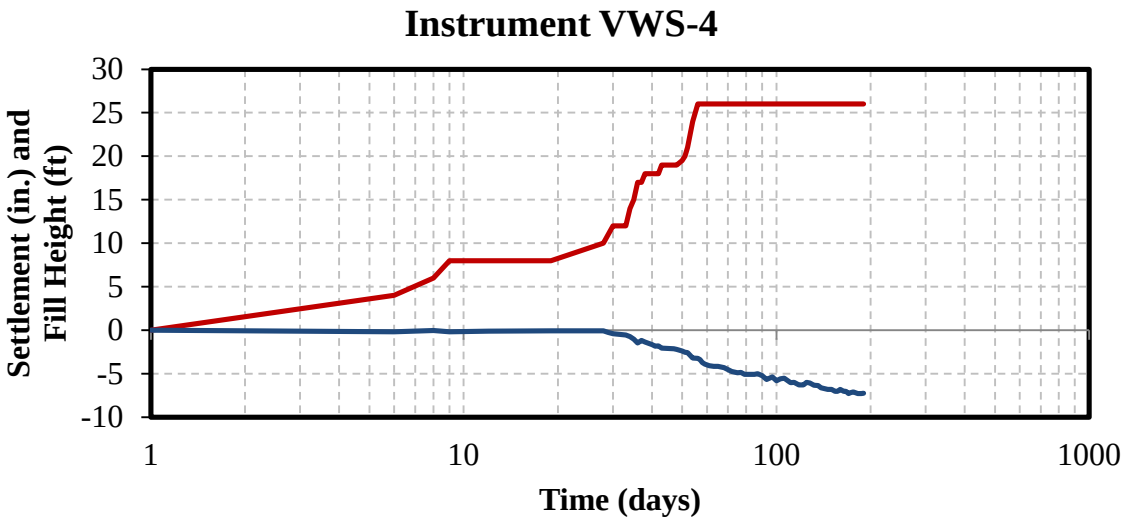

Figure 5-16. Measured Time-Settlement Curve for VWS-4, 4.0 ft Spacing with Rebar Anchor from Full-Scale Field Test

Each of the figures shows the consensus that there was little to no settlement occurring until the fill height exceeded about 5 ft. The figures also show the variability in the magnitude of fill height and in the rate of fill placement, which makes a direct side by side comparison

impossible. At some locations a given fill height was left in place for close to a month before more fill was placed (see Figure 5-5), while other locations had the full fill height built up more quickly (see Figure 5-9). At one of the 5.8 ft plate anchor locations, the fill height was decreased slightly, possibly due to problems with the adjacent wall being built, which caused a slight rebound in settlement as shown in Figure 5-8.

Along with the variation in the timing of fill placement and fill magnitude, the fill height may not have been constant across the individual test segments, which caused a more complex loading scenario. The differential loading led to more complex calculations of the induced stress at depth. Due to these complications, a separate analysis was needed to quantify the effect drain installation had on drain performance.

6 ANALYSIS AND DISCUSSION OF FIELD TEST RESULTS

6.1 Analysis Program

In order to analyze the complicated time-settlement curves arising from the varying load history, the program PVDrain was utilized, which was provided courtesy of Hayward-Baker (Goughnour 2002). This program made it possible to consider variations in soil layers, loading configurations, and loading histories.

6.1.1 Consolidation Theory Assumptions

The analysis program uses the vertical and radial consolidation theories discussed in Chapter 2; however, the analysis is generally performed using finite difference methods. The analysis program does make certain assumptions in using the consolidation equations. In calculating the vertical consolidation, the program assumes that the bottom of the soil profile is impermeable. The program can also take into account the drain discharge capacity; however, the capacity was assumed to be infinite in this study (Goughnour 2002).

A parametric analysis was performed on the assumptions of the infinite drain discharge capacity and soil profile impermeable base. Upon completion, the two assumptions were found to not significantly affect the time rate of consolidation, and, therefore, the assumptions were kept in the model.

6.1.2 Equivalent Step Loading

The PVDrain program allows for up to 10 data points to define the loading history and linearly interpolates between points (Goughnour 2002). However, the actual fill histories consisted of more than 20 points for each instrument site. In the program 10 points that defined the fill history the closest were selected. A few of the plots showing the actual versus equivalent step loadings are shown in Figure 6-1. In these drawings the measured points are shown with diamonds, while the time history used in the program is shown with a solid line. Generally the load versus time history based on 10 points provides a good representation of the actual load versus time history so that the limitation of 10 points was not a problem.

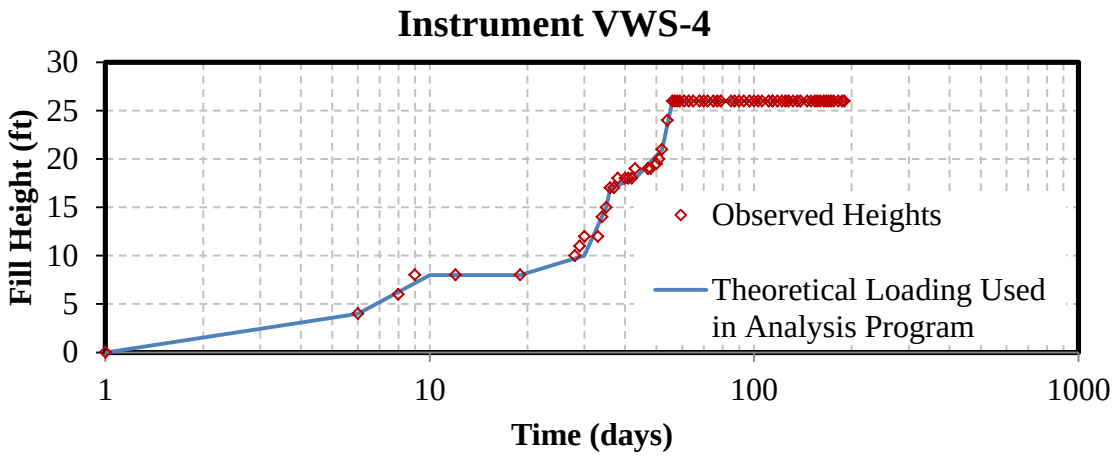

Figure 6-1. Equivalent Step Loadings

6.1.3 Applied Load

The geotechnical design report called for a minimum of 650 psf (RB&G Engineering, Inc., 2009) surcharge load to be placed above the final permanent embankment elevation along the test area. The surcharge was placed on top of the design fill as presented in Chapter 3. In order to simulate the field conditions in the program, two load components were entered. The

first component represented the permanent embankment load while the second component was the actual surcharge load. The construction of the permanent embankment and surcharge loadings were completed in stages. The typical embankment geometry presented earlier shows the end of the final stage of construction. During consolidation, both the west bound and east bound embankment loadings did not co-exist and therefore, the loading was modeled as shown in Figure 6-2.

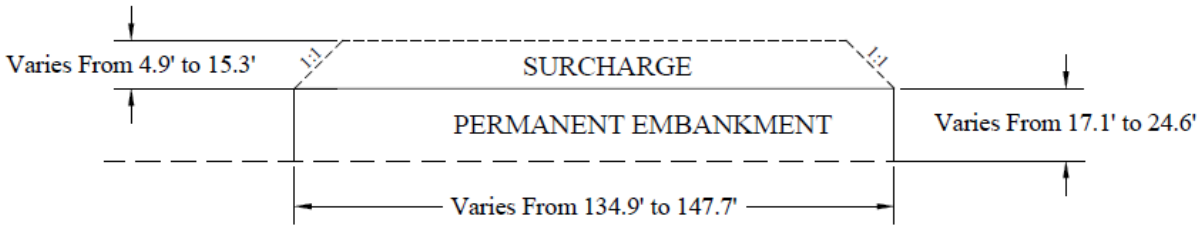

Figure 6-2. Idealized Permanent Embankment and Surcharge Loadings

The permanent embankment load was modeled as a rectangular loaded area due to the MSE retaining wall alongside the fill. The program required the entry of the length and width of the area along with the transverse and longitudinal locations of the instruments, as defined in Figure 6-3. The fill history was entered as a time and a magnitude of the load, with the maximum magnitude equal to the unit weight of the fill multiplied by the wall height at that location.

The surcharge load was modeled as a rectangular embankment load with 3H: 1V side slopes. The program required the entry of the top and bottom lengths and widths along with the transverse and longitudinal locations of the instruments, as defined in Figure 6-4. The load history was entered as a time and a height above the top of the wall.

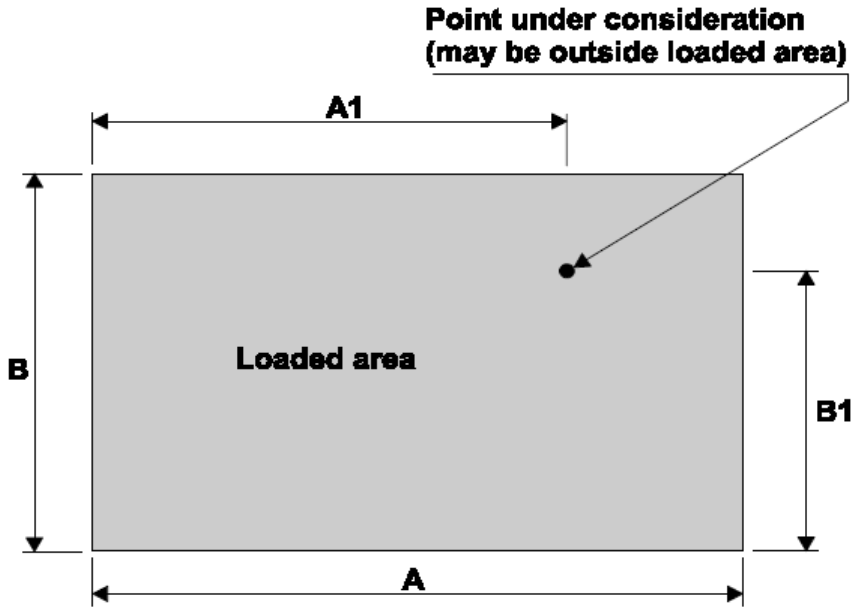

Figure 6-3. Rectangular Loading (Goughnour 2002)

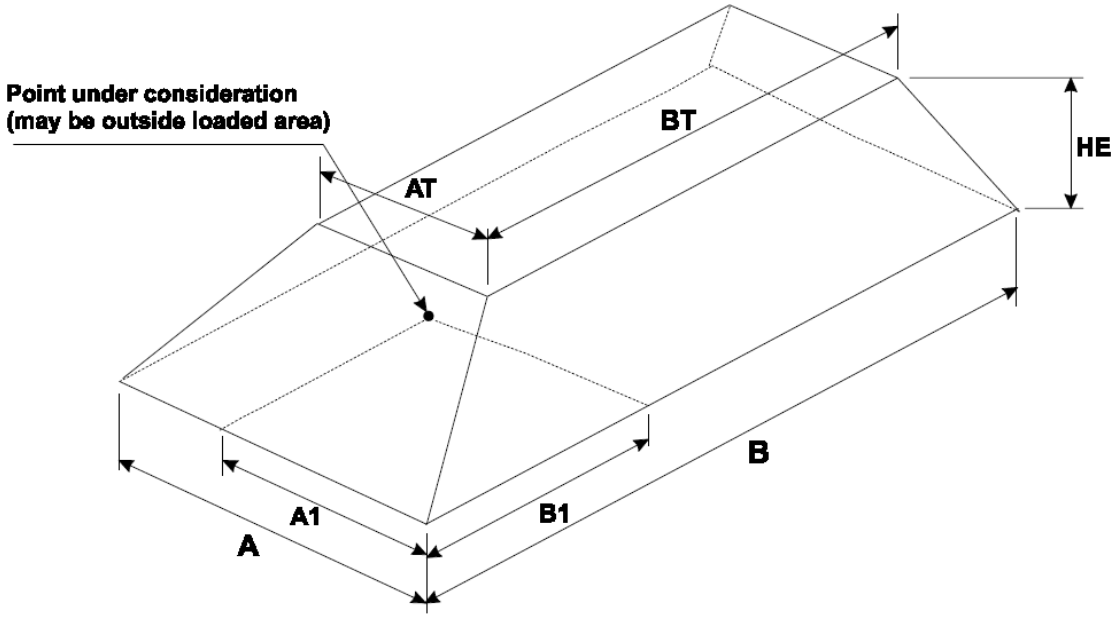

Figure 6-4. Rectangular Embankment Loading (Goughnour 2002)

The dimensions of the permanent embankment and surcharge loads are shown in Table 6-1 and Table 6-2. The lengths of the loadings were taken to be equal to the length of the test section, and the widths were taken to be equal to the limits of the surcharge placement.

Table 6-1. Rectangular Loading Dimensions

Instrument	A (ft)	B (ft)	A1 (ft)	B1 (ft)	H (ft)
VWS-2	897.0	141.0	28.0	70.50	18.5
S-3	884.8	134.9	293.0	67.45	21.1
BYU-1	886.0	135.5	383.0	67.75	20.5
BYU-2	888.6	136.8	513.0	68.40	19.2
VWS-4	889.8	137.4	611.0	68.70	18.6
BYU-3	892.2	138.6	713.0	69.30	17.4
S-5	897.8	141.4	748.0	70.70	17.1
BYU-4	905.6	145.3	803.0	72.65	17.2
S-7	901.4	147.7	26.0	73.85	20.8
VWS-8	888.8	141.4	296.0	70.70	24.6
S-9	891.6	142.8	561.0	71.40	23.2
VWS-10	900.0	147.0	811.0	73.50	20.5

Table 6-2. Rectangular Embankment Loading Dimensions

Instrument	A (ft)	B (ft)	AT (ft)	BT (ft)	A1 (ft)	B1 (ft)	HE (ft)
VWS-2	141	897	119	875	70.5	28	11.0
S-3	134.9	884.8	125.1	875	67.45	293	4.9
BYU-1	135.5	886	124.5	875	67.75	383	5.5
BYU-2	136.8	888.6	123.2	875	68.4	513	6.8
VWS-4	137.4	889.8	122.6	875	68.7	611	7.4
BYU-3	138.6	892.2	121.4	875	69.3	713	8.6
S-5	141.4	897.8	118.6	875	70.7	748	11.4
BYU-4	145.3	905.6	114.7	875	72.65	803	15.3
S-7	147.7	901.4	122.3	876	73.85	26	12.7
VWS-8	141.4	888.8	128.6	876	70.7	296	6.4
S-9	142.8	891.6	127.2	876	71.4	561	7.8
VWS-10	147	900	123	876	73.5	811	12.0

6.1.4 Soil Parameters

The thick clay bed was divided into eight smaller layers. The program uses the strain-based compression and recompression indices instead of the standard void-ratio-based indices. Equations 6-1 and 6-2 were used to calculate the strain-based indices, compression ratio (CR or $C_{c\varepsilon}$) and recompression ratio (RR or $C_{r\varepsilon}$), respectively, from the void-ratio-based indices, compression index (C_c) and recompression index (C_r). Table 6-3 presents the individual layer parameters used in the computer program.

$$CR = \frac{C_c}{1 + e_0} \quad \textbf{(6-1)}$$

$$RR = \frac{C_r}{1 + e_0} \quad \textbf{(6-2)}$$

Table 6-3. Soil Parameters Required by Analysis Program

Layer	Thickness (ft)	γ (kcf)	CR	RR	OCR	C_h (ft^2/day)	C_v (ft^2/day)
1	10.0	0.1248	0.149	0.0121	17.84	1.30	1.04
2	10.0	0.1176	0.184	0.0201	6.33	1.24	0.99
3	10.0	0.1116	0.245	0.0185	3.85	0.59	0.48
4	10.0	0.1097	0.184	0.0164	2.76	0.49	0.39
5	10.0	0.1168	0.26	0.015	2.16	0.38	0.31
6	14.0	0.1120	0.262	0.014	1.71	0.29	0.23
7	14.0	0.1073	0.392	0.0385	1.37	0.15	0.12
8	2.0	0.1174	0.249	0.0218	1.23	0.40	0.32

Based on the unit weights in Table 6-3, the initial vertical effective stress and preconsolidation pressures were calculated as a function of depth as shown in Figure 6-5. By plotting these pressures together, it becomes clear that the complete soil profile is overconsolidated for the in-situ or geostatic stress conditions prior to embankment loading. By

using the geometry of the fill and surcharge, the induced stresses were also calculated according to the Boussinesq theory. Adding the induced stress to the initial vertical effective stress produces the final vertical stress, which is also plotted in Figure 6-5. The range accounts for variations in fill height along the length of the test section. The final vertical stress is still lower than the pre-consolidation pressure in the top 35 ft of the profile; however, in the lower 45 ft of the soil profile, the induced stress would produce virgin compression because the final stress would increase beyond the preconsolidation pressures.

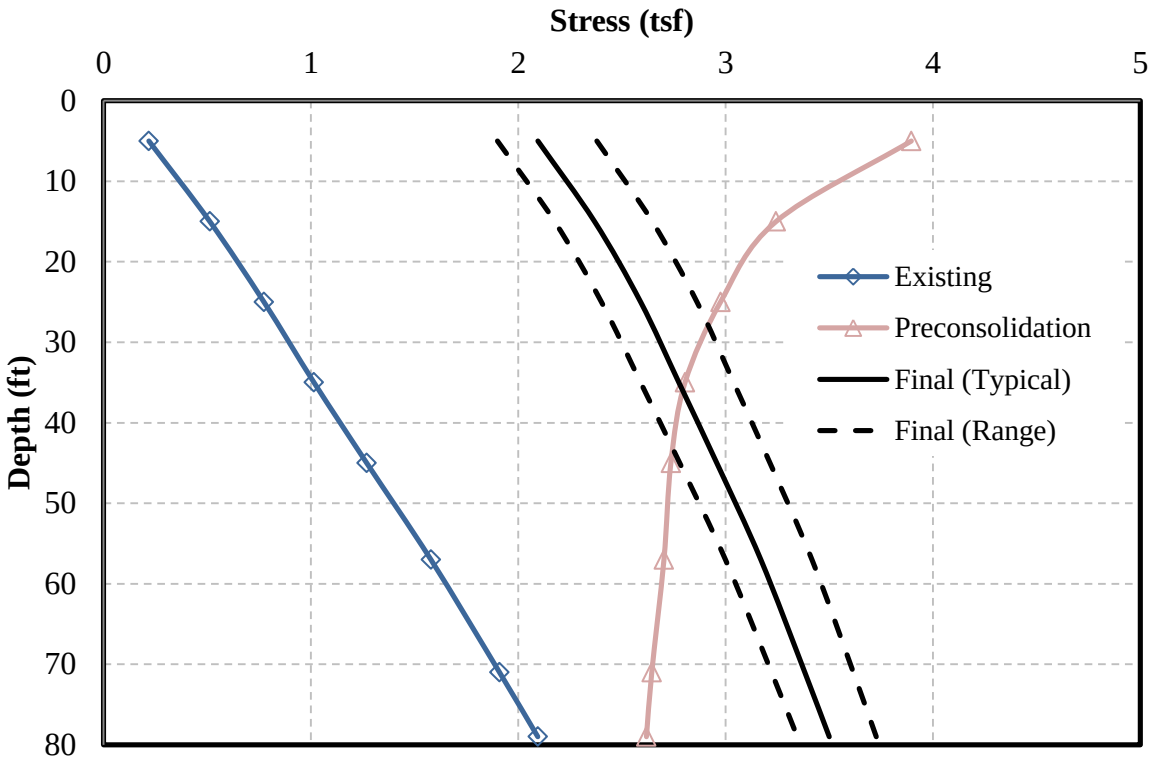

Figure 6-5. Typical Existing, Preconsolidation and Final Stresses

6.2 Analysis of Total Settlement

6.2.1 Model Calibration

Using the program, the maximum settlement was calculated with the initial estimates of soil parameters for each instrument location and compared with the measured settlement. The calculated settlement magnitudes were typically higher than the observed magnitudes. To obtain magnitudes that would be comparable with the measured values, the model needed to be calibrated. The calibration process initially consisted of changing the overconsolidation ratio (OCR) profile for the soil profile because the other parameters (C_r, C_c, etc.) appeared to be reasonable based on correlations with Atterberg limits and verification from laboratory consolidometer tests, as discussed previously. Initially a best-fit logarithmic equation, with the minimum value limited to 1.0, was used as shown in Figure 6-6 to define the variation of OCR with depth. However, the resulting equation led to an overestimation of almost all of the measured settlement.

To provide a more accurate estimate of the average settlement, the OCR profile was increased relative to the best-fit curve. As the OCR profile changed, the magnitudes of settlement began to converge with the observed magnitudes. The final OCR profile used in the program is shown in Figure 6-6. Figure 6-7 shows the deviation between the observed and calculated magnitudes.

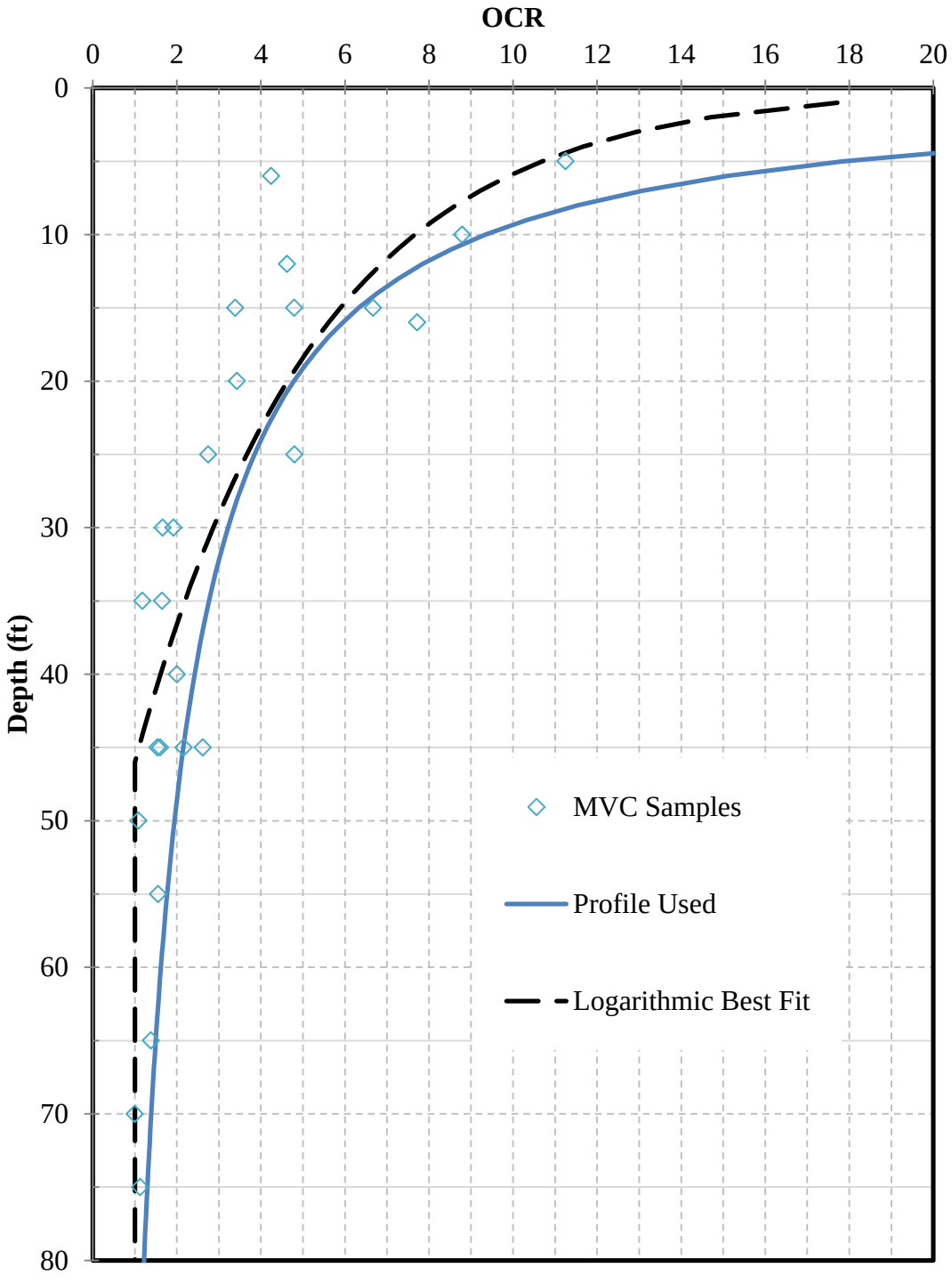

Figure 6-6. OCR Versus Depth Profile Containing Sample Data, Logarithmic Best-Fit, and Idealized Curves Based on Calibration

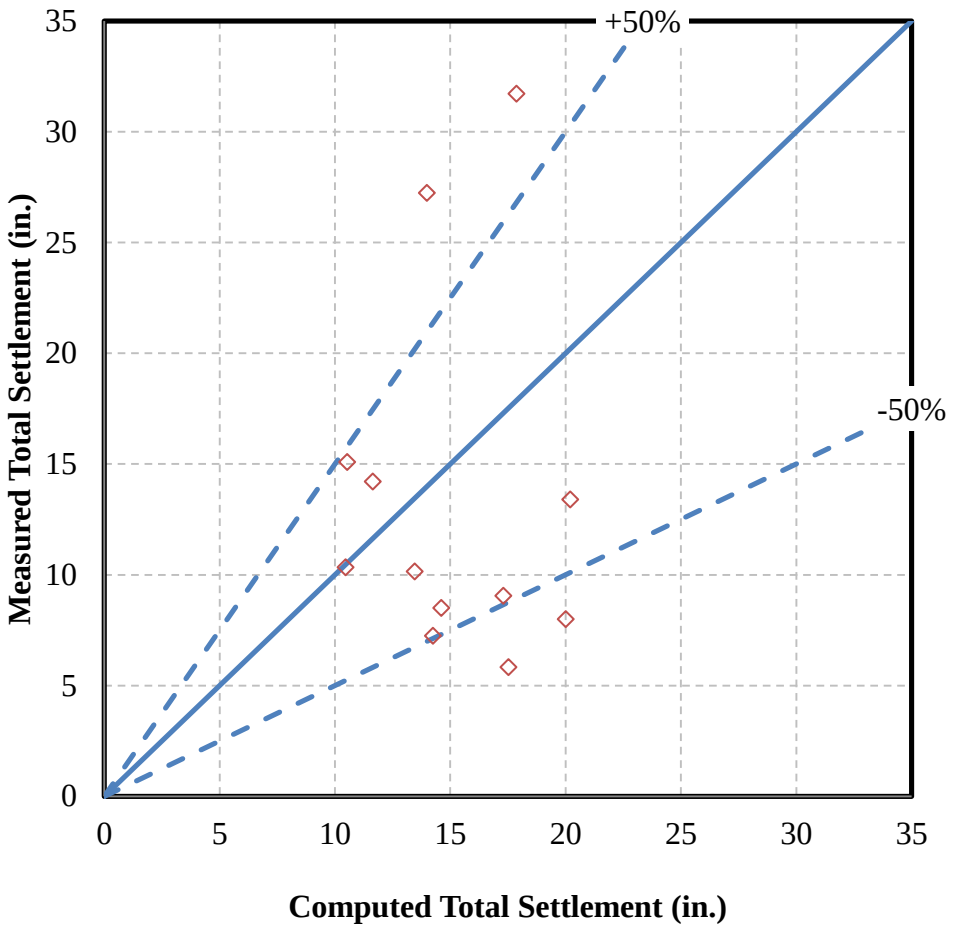

Figure 6-7. Measured Versus Computed Settlement Magnitudes Using C_c from Consolidometer Tests

In Figure 6-7, the solid line represents the condition where the computed total settlement is equal to the measured total settlement. The acceptable range of scatter is typically within 25 to 30% of the solid line (Duncan 2000); however, the data for the MVC test site lie outside of the typical range. The higher variation of settlement magnitudes may be attributed to the fact that the C_c values were around two times higher than those found from the correlation between PI and C_c, as defined by Mayne (1990). By utilizing the C_c values based on Mayne's correlation instead of the values based on consolidometer tests, the variation between measured and computed total settlement decreases, and the scatter about the exact match line decreases. Although use of the C_c values based on Mayne's correlation to PI caused a decrease in

variability, the C_c values based on the consolidometer tests were kept in the model since no evidence was found to invalidate the values.

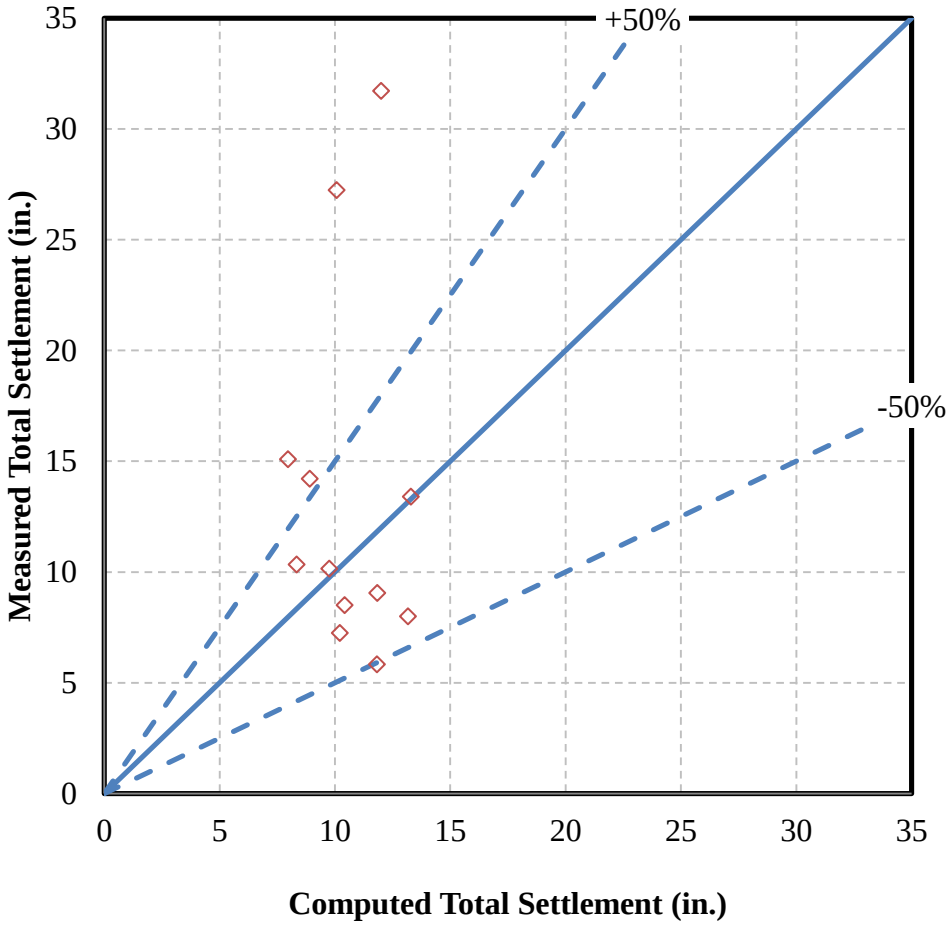

Figure 6-8. Measured Versus Computed Settlement Magnitudes Using C_c = PI/74

Even by decreasing the C_c values to fit the Mayne correlation with PI, the variation was still greater than 50% from the line of equality. Other possible explanations for this scatter could be that a single model was used across the entire MVC test site when there is inherent variability in the soil profile. According to Duncan (2000), the C_c and preconsolidation pressure parameters have a coefficient of variation of 10 to 37% and 10 to 35%, respectively. Since there is this

inherent variability in these two parameters, upon which magnitude of settlement is dependent, the soil properties may be different at some locations along the MVC test site than those used in the model. The spatial variation in either the C_c or preconsolidation pressure would cause the data points to be adjusted independently and could lead to a better fit along the solid line in Figure 6-8.

6.3 Analysis of Time-Settlement Curves

With the plate and rebar anchor models calibrated to the observed settlement magnitude, the models were calibrated against the time rate of settlement. First, the smear zone approach was used to match the calculated time-settlement curves to the observed data and then the back-calculated C_h/C_v approach, as proposed by Saye (2002), was used.

6.3.1 Analysis with Smear Zone Approach

The objective of the analysis assuming a smear zone around the PV drain was to determine if one constant and consistent set of soil parameters could be used to provide reasonable agreement with the measured time-settlement histories at each drain spacing and for each anchor type. In addition to the average C_v values, which had already been determined as a function of depth, it was necessary to determine a number of other key soil parameters. These parameters were (1) the diameter of the smear zone, (2) the C_h/C_v ratio in the undisturbed zone, and (3) the ratio of permeability in the undisturbed zone to the permeability in the smear zone.

Based on CSSM and the tables published by Ghandeharioon (2010), the smear zone diameter was defined as 3.07 times equivalent mandrel/anchor diameter, d_m. For the bar anchor, this led to a diameter of 2.24 ft while for the plate anchor this led to a diameter of 1.94 ft. In

addition, the C_h/C_v ratio in the undisturbed soil was defined to be 1.25 because the CPT logs clearly showed the clay layers in the profile to be thickly bedded with relatively little variation in soil type or tip resistance with depth. Goughnour (2002) and Rixner et al. (1986) indicates that this C_h/C_v is applicable for thickly bedded clay layers.

The only parameter that was not previously defined was the ratio of undisturbed permeability to disturbed permeability (k_u/k_s) for the smear zone. The time-settlement histories for the rebar (instrument S-7) and plate (instrument S-3) anchors at 5.8-ft spacing were used to calibrate the model. Through trial and error, a k_u/k_s ratio of 2.20 produced very good agreement with the measured settlement time history for the PV drain at 5.8-ft spacing with a rebar anchor (see Figure 6-20). In contrast, a k_u/k_s ratio of only 1.20 produced very good agreement with the measured time history for the PV drain at 5.8-ft spacing with a plate anchor (see Figure 6-12). The fact that a higher ratio was obtained for the rebar anchor than for the plate anchor indicates that the rebar anchor produced more disturbance to the soil within the smear zone. This is consistent with the fact that the equivalent mandrel/anchor diameter was also larger for the rebar anchor than for the plate anchor (2.24 ft versus 1.94 ft). In addition, the plate anchor is somewhat flexible and would tend to wrap around the mandrel thereby reducing the potential for smear, while the anchor bar is quite rigid.

Figure 6-9 and Figure 6-10 provide drawings that summarize the calibrated parameters used in the analyses for the plate anchor and rebar anchor cases, respectively. For subsequent smear zone method analyses, these ratios, along with all the other parameters for each anchor type, were held constant as the PV drain spacing decreased from 5.8 ft to 5.0, 4.0, and 3.0 ft.

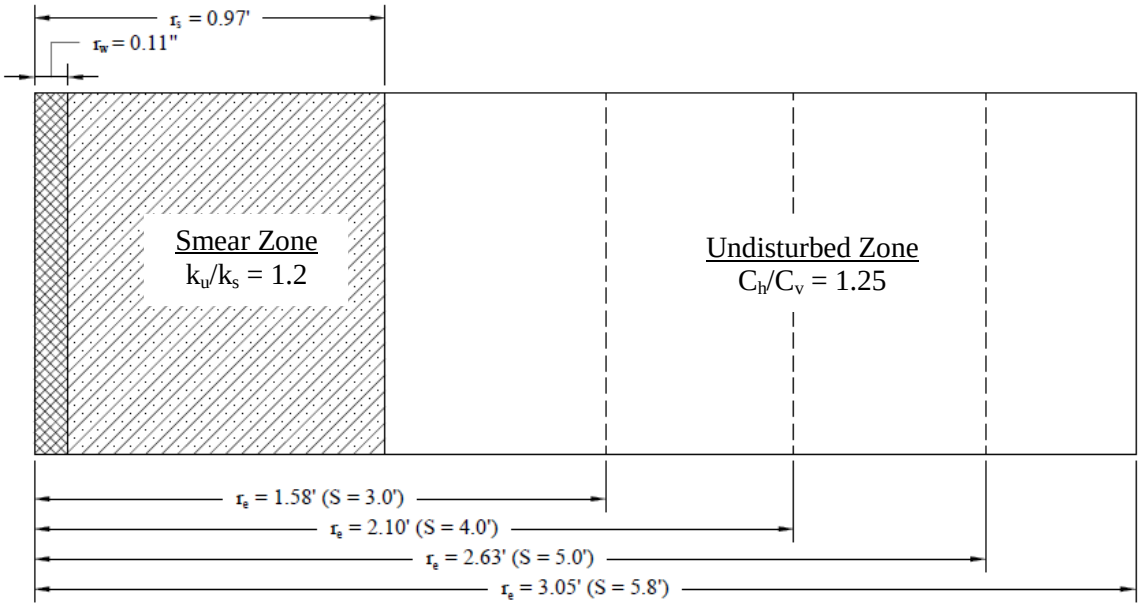

Figure 6-9. Model Using Smear Zone Approach Using Plate Anchor Showing C_h/C_v, Permeability Ratios and Wick, Smear and Effective Drain Radii

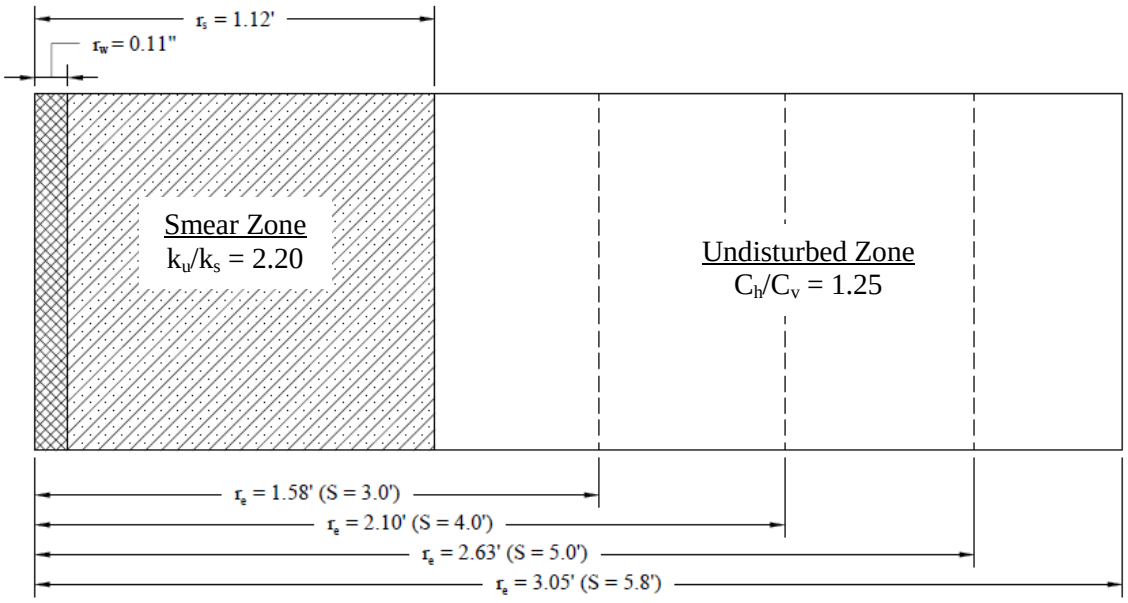

Figure 6-10. Model Using Smear Zone Approach Using Rebar Anchor Showing C_h/C_v, Permeability Ratios and Wick, Smear and Effective Drain Radii

By using this analysis method, time-settlement curves were generated for each of the observation locations that were reasonably close to the measured curves. The time-settlement curves with the plate anchors are shown in Figure 6-11 through Figure 6-19. The normalized settlement was calculated by dividing the calculated settlement at a given time by the maximum calculated settlement occurring during the time period being analyzed, which is equal to the last day of the observed data. The time-settlement curves for the spacings with the rebar anchor are presented in Figure 6-20 through Figure 6-22. To facilitate comparisons from site to site and to focus on the rate of settlement, the settlement at each sensor location was normalized by the maximum measured settlement at that location.

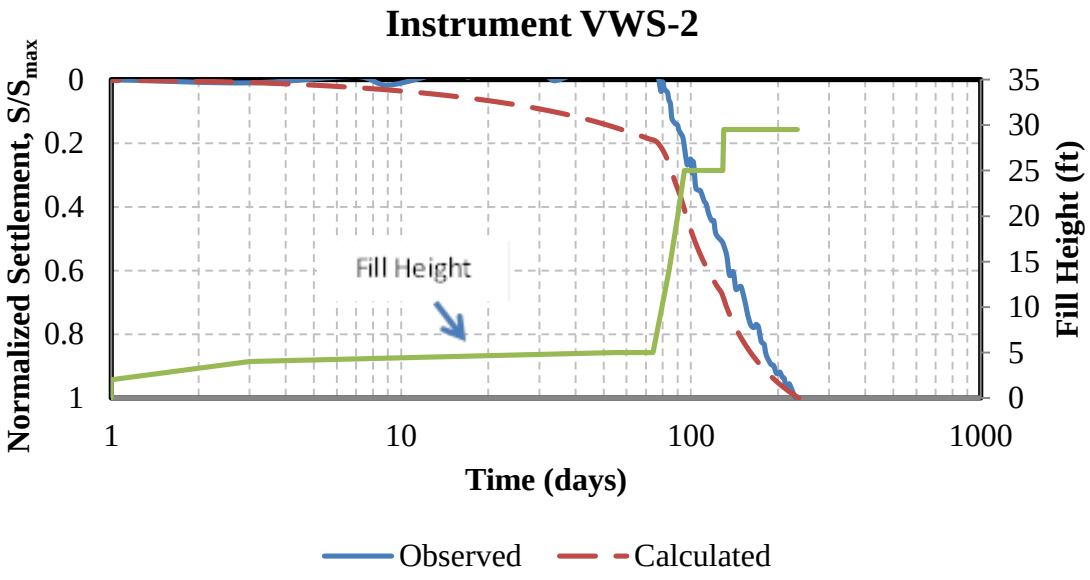

Figure 6-11. Calculated and Observed Time-Settlement Curve for VWS-2, 5.8 ft Spacing with Plate Anchor Using Smear Zone Approach

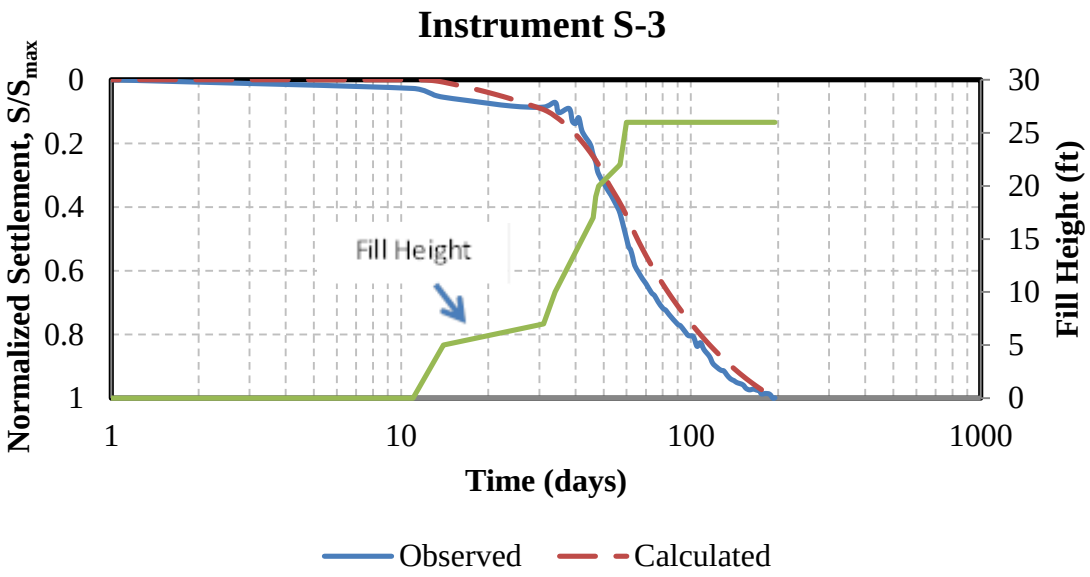

Figure 6-12. Calculated and Observed Time-Settlement Curve for S-3, 5.8 ft Spacing with Plate Anchor Using Smear Zone Approach

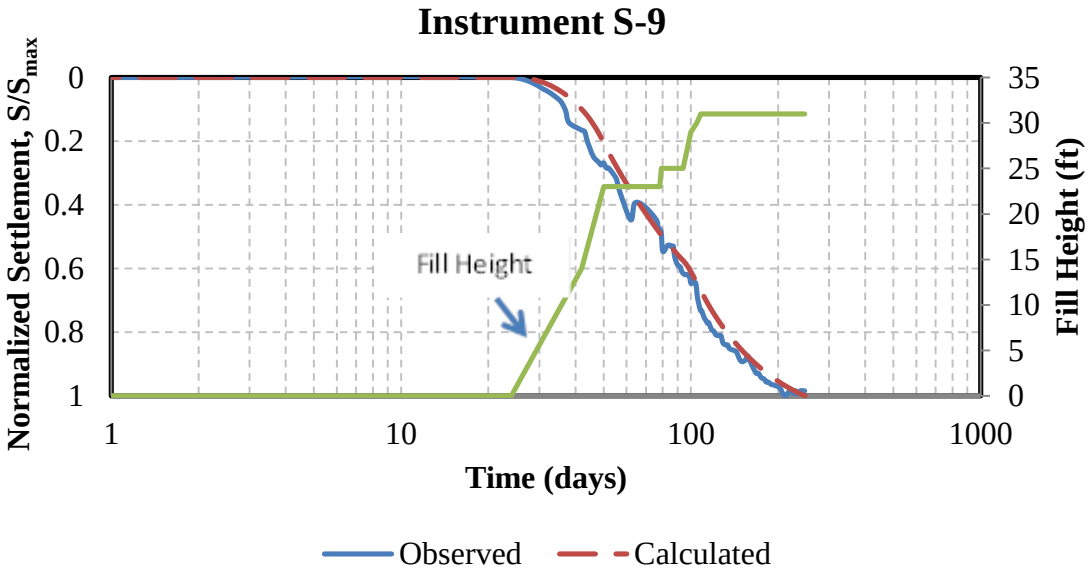

Figure 6-13. Calculated and Observed Time-Settlement Curve for S-9, 5.8 ft Spacing with Plate Anchor Using Smear Zone Approach

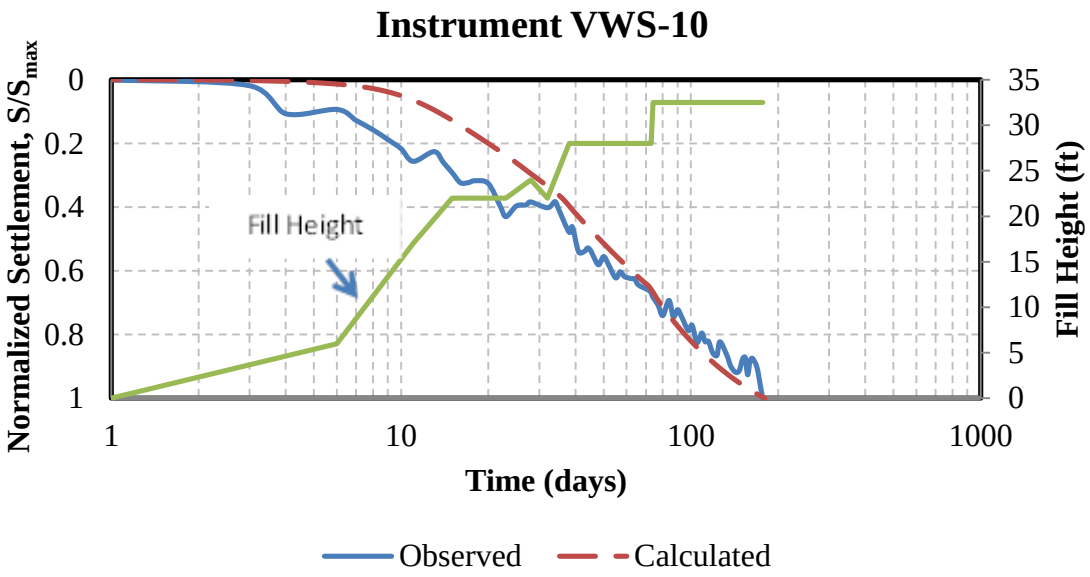

Figure 6-14. Calculated and Observed Time-Settlement Curve for VWS-10, 5.8 ft Spacing with Plate Anchor Using Smear Zone Approach

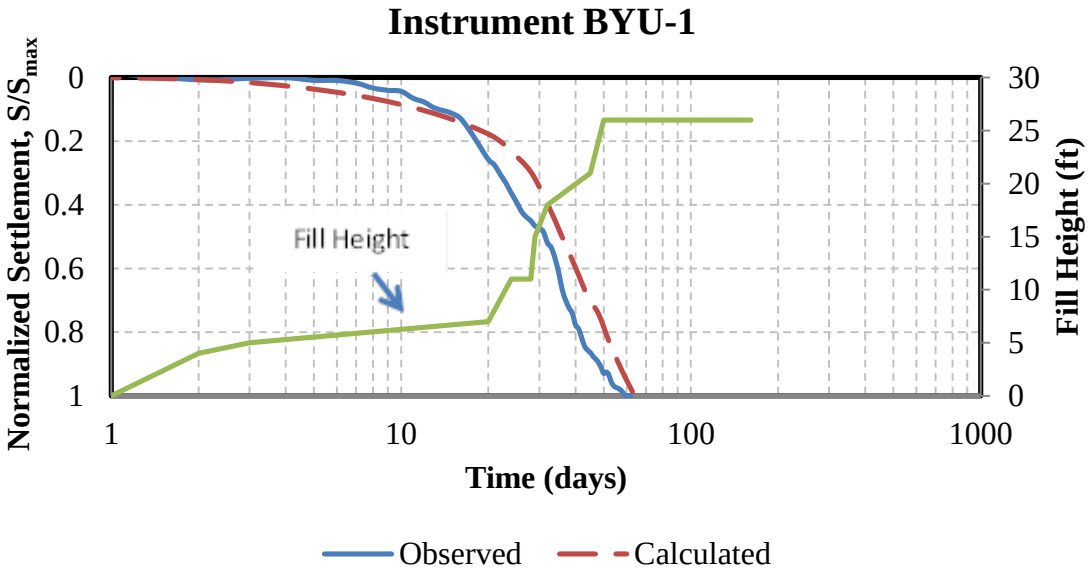

Figure 6-15. Calculated and Observed Time-Settlement Curve for BYU-1, 5.0 ft Spacing with Plate Anchor Using Smear Zone Approach

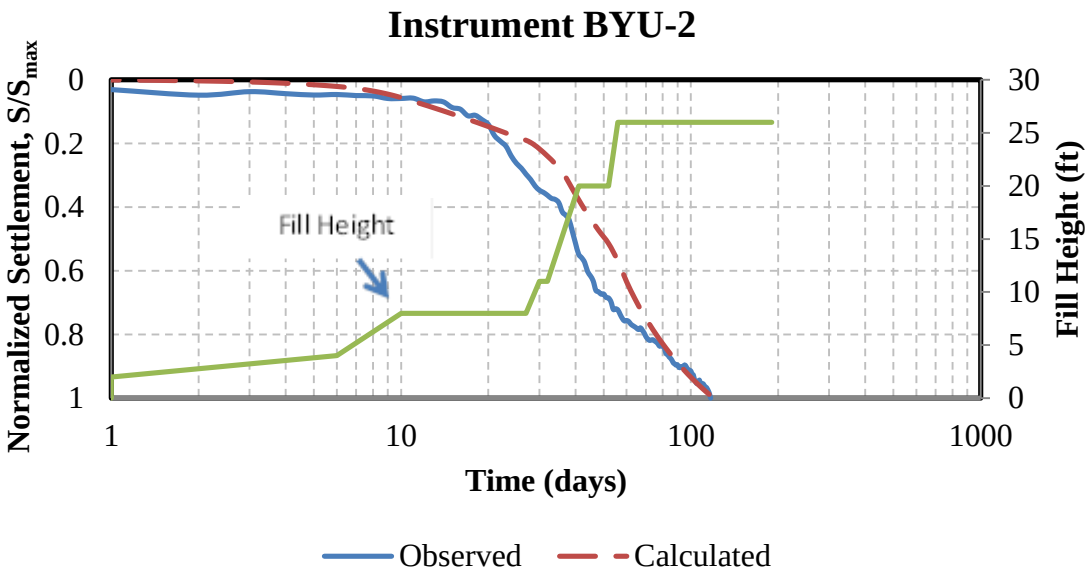

Figure 6-16. Calculated and Observed Time-Settlement Curve for BYU-2, 5.0 ft Spacing with Plate Anchor Using Smear Zone Approach

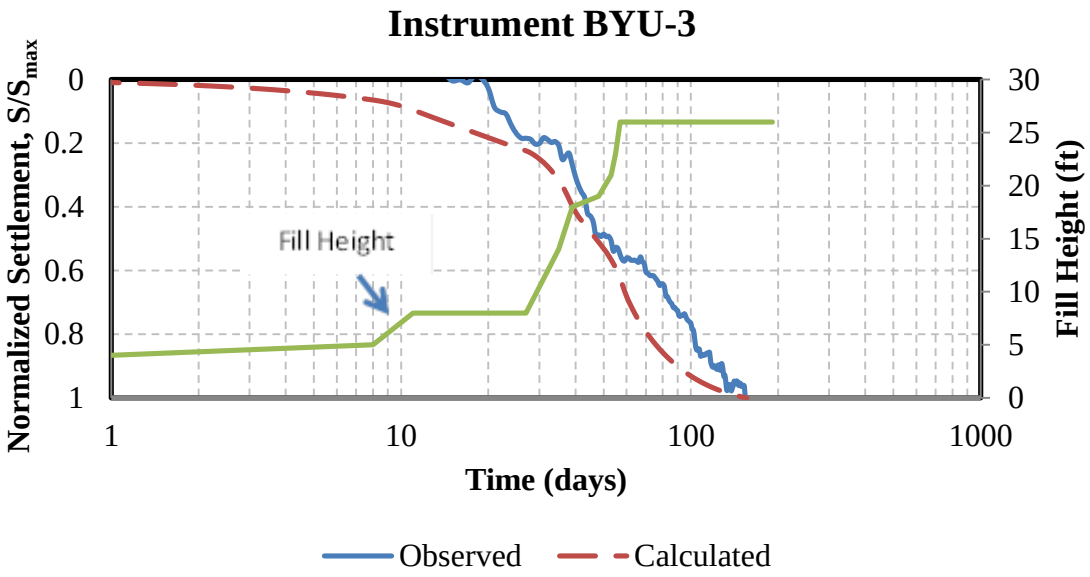

Figure 6-17. Calculated and Observed Time-Settlement Curve for BYU-3, 4.0 ft Spacing with Plate Anchor Using Smear Zone Approach

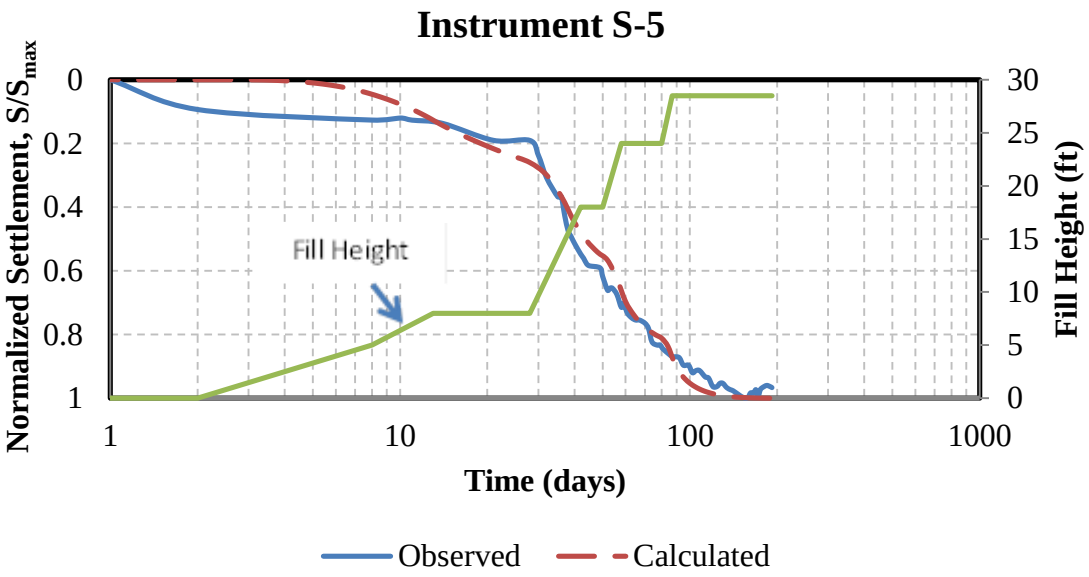

Figure 6-18. Calculated and Observed Time-Settlement Curve for S-5, 3.0 ft Spacing with Plate Anchor Using Smear Zone Approach

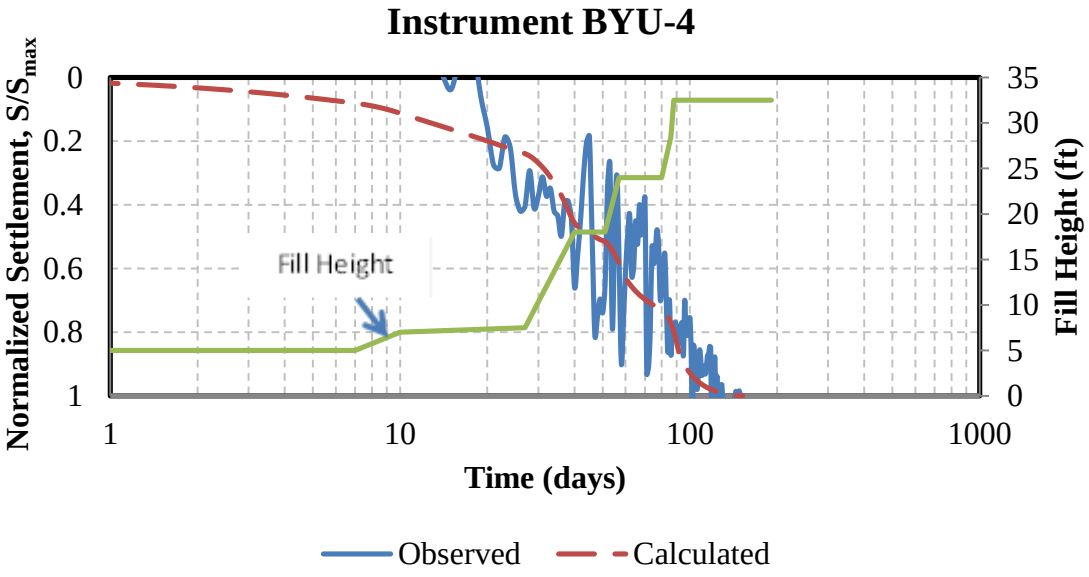

Figure 6-19. Calculated and Observed Time-Settlement Curve for BYU-4, 3.0 ft Spacing with Plate Anchor Using Smear Zone Approach

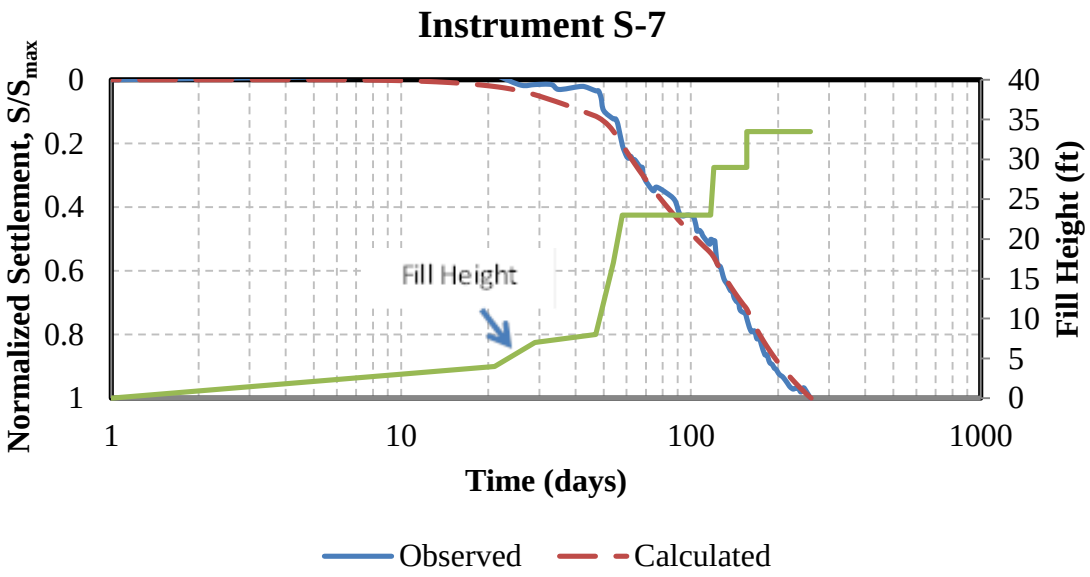

Figure 6-20. Calculated and Observed Time-Settlement Curve for S-7, 5.8 ft Spacing with Rebar Anchor Using Smear Zone Approach

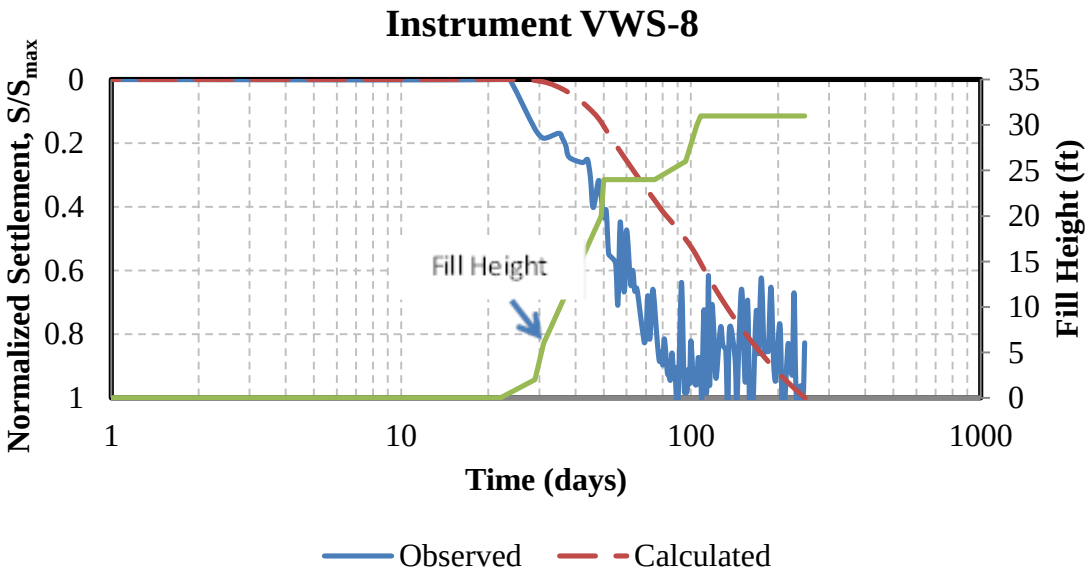

Figure 6-21. Calculated and Observed Time-Settlement Curve for VWS-8, 5.8 ft Spacing with Rebar Anchor Using Smear Zone Approach

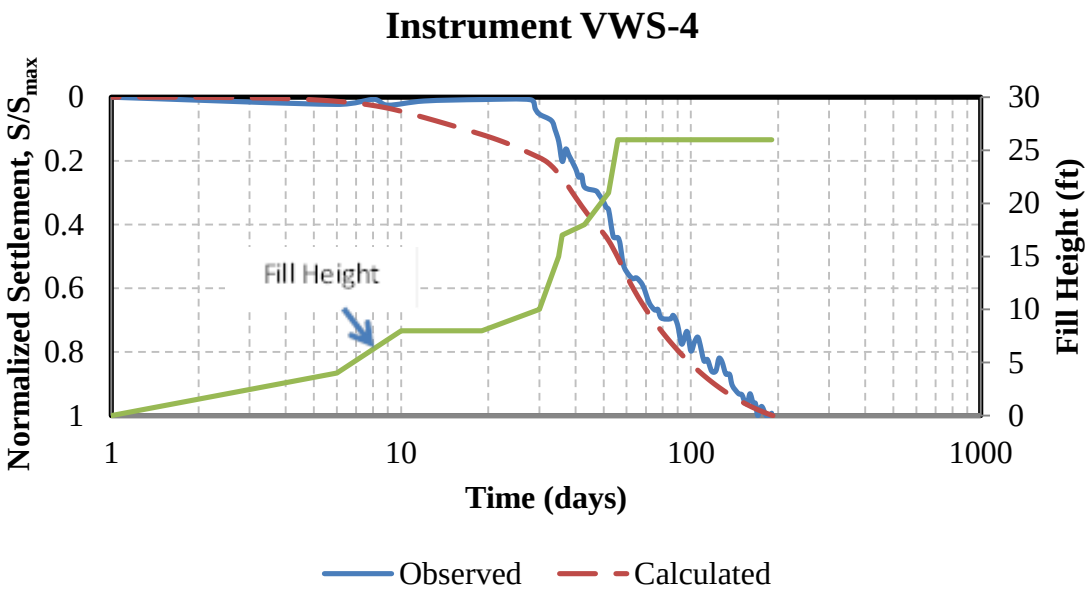

Figure 6-22. Calculated and Observed Time-Settlement Curve for VWS-4, 4.0 ft Spacing with Rebar Anchor Using Smear Zone Approach

The agreement between the observed and calculated normalized time-settlement curves varies from location to location. The curves for S-3 (see Figure 6-12) and S-7 (see Figure 6-20) were used to calibrate the plate and rebar anchor models and result in better fits, while the curves for VWS-2 (see Figure 6-11) have disagreement that may be caused by the selection of model parameters. The disagreements may be attributed to the single C_v value chosen for each location. If the in-situ C_v value is lower than the idealized model value, the calculated time rate of settlement will be faster than the observed.

The agreement between the calculated and observed curves is also not as good for BYU-4 and VWS-8, which contain oscillating data (see Figure 6-19 and Figure 6-21). BYU-4 exhibits a better fit than VWS-8 since continuous readings were made at BYU-4, resulting in the ability to decrease the oscillation slightly. VWS-8 did not have any continuous readings and could not be corrected or smoothed; therefore, the validity of the VWS-8 data cannot be confirmed.

6.3.2 Analysis with Back-Calculated C_h/C_v Ratio

The method proposed by Saye (2002) simplifies the settlement analysis by only considering radial drainage and accounts for smear effects by reducing the effective C_h/C_v ratio for the entire layer. Therefore, the analysis program was changed to only calculate the radial component of the consolidation in computing the degree of consolidation.

The same model parameters calibrated for the smear zone approach were used, but, unlike the smear zone approach, the ratio of the undisturbed permeability to the disturbed permeability was set to unity. By changing to model, the C_h/C_v ratio governed how quickly the soil would settle. A schematic drawing of the model, which shows the wick radius along with the various effective radii from the various spacings, is provided in Figure 6-23.

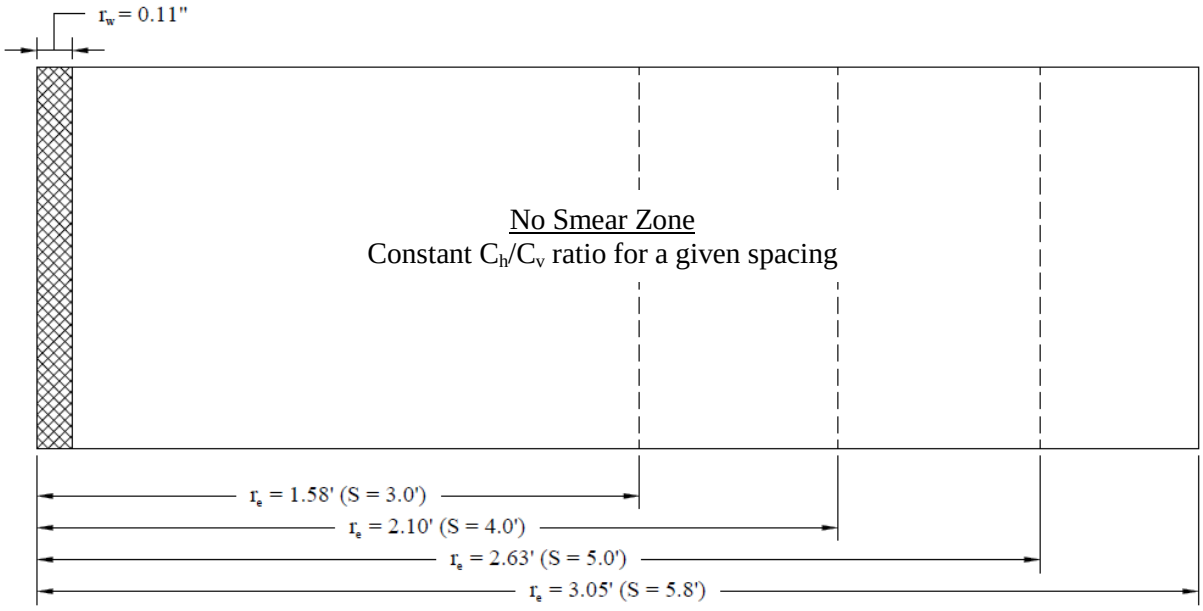

Figure 6-23. Model Using Back-Calculated C_h/C_v Ratio Approach Using Plate or Rebar Anchor Showing C_h/C_v, and Wick and Effective Drain Radii

By changing the C_h/C_v ratio through trial and error, an effective C_h/C_v ratio was determined for each instrument location individually. The C_h/C_v ratio was changed until the

time-settlement plots for the individual locations converged with the time-settlement plots calculated using the smear zone approach. The C_h/C_v ratio would account for any disturbance caused from the installation of the PV drains at the various spacings without defining a smear zone. Back-calculated C_h/C_v ratios for the MVC test areas are plotted against the modified spacing ratio in Figure 6-24 along with the data from other test sites.

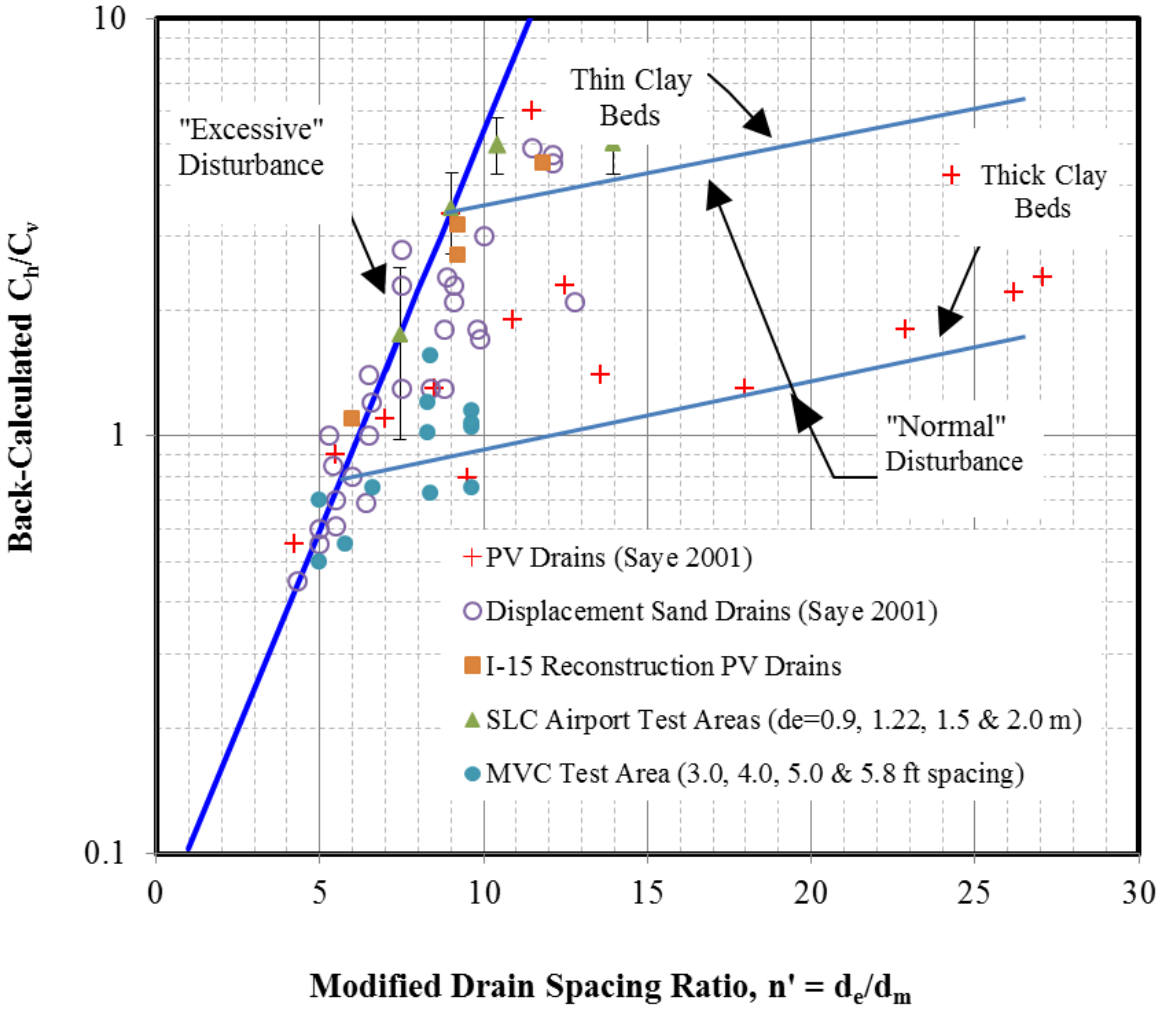

Figure 6-24. Final Back-Calculated C_h/C_v Ratios for Various Tests

As shown in Figure 6-24, back-calculated C_h/C_v values for the thick, fairly uniform soil profile along the MVC test site fit the Saye model quite well. The data points plot along the

lower boundary line associated with thickly bedded clay layers for "normal disturbance" and trend downward with the excessive disturbance line for modified spacing ratios less than about six as predicted by Saye.

The comparison between the MVC data and the previous I-15 or SLC airport data illustrates that the PV drain spacing is dependent upon the soil profile in which the drains are being installed. A thick, fairly uniform clay profile will have an in-situ C_h/C_v ratio of 1 to 2 while a thinly bedded clay profile might have an in-situ ratio of 4 to 6. The in-situ C_h/C_v ratio is dependent on the layered structure of the soil profile and, based on the Saye model, will also govern how closely drains can be installed.

The soil profiles at the SLC airport and I-15 had thinly bedded clay layers for which excessive disturbance occurred at higher modified spacing ratios than for the thickly bedded profile at MVC as shown in Figure 6-24. If the in-situ C_h/C_v ratio is incorrectly chosen to be higher than what actually exists (e.g. by incorrectly assuming a thin, interbedded clay profile), PV drains may be spaced farther apart than the actual critical spacing, leading to an unnecessarily long t_{95} for the site. In contrast, if the in-situ C_h/C_v ratio is incorrectly chosen to be lower than what actually exists (e.g. by incorrectly assuming a thick clay profile), drains may be installed at a spacing that is closer than the critical spacing, leading to a higher cost due to the installation of more drains that are of no benefit in reducing the t_{95}. Therefore, it becomes particularly important to accurately assess the layering of the profile in selecting an appropriate C_h/C_v ratio and the modified spacing ratio where significant disturbance will begin to occur. CPT soundings, which provide continuous profiles, are particularly helpful in this regard.

Figure 6-25 through Figure 6-33 provide comparisons between the measured and computed settlement time histories using the effective C_h/C_v ratio approach for the plate

anchored spacings, while the rebar anchored spacings are shown in Figure 6-34 through Figure 6-36.

Again, the normalized settlement was calculated by dividing the calculated settlement at a given time by the maximum calculated settlement occurring during the time period being analyzed. The time period of analysis is equal to the period of time for which observed data had been collected at the MVC test location. The agreement between measured and computed values is generally quite good. For a given anchor type, the C_h/C_v value typically decreased as the spacing decreased, indicating increasing disturbance effects from drain installation.

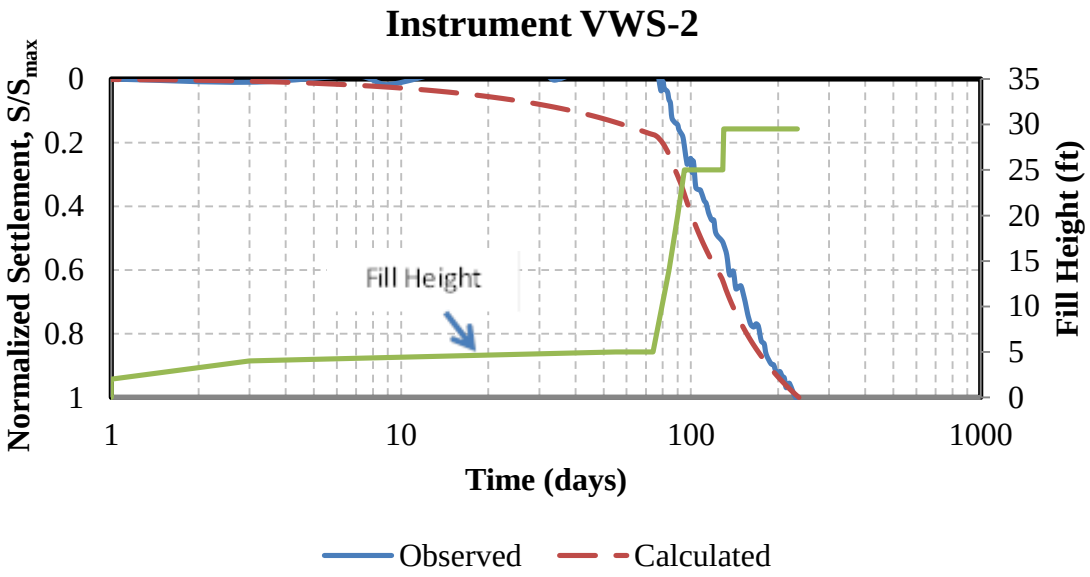

Figure 6-25. Calculated and Observed Time-Settlement Curve for VWS-2, 5.8 ft Spacing with Plate Anchor Using Back-Calculated C_h/C_v Approach

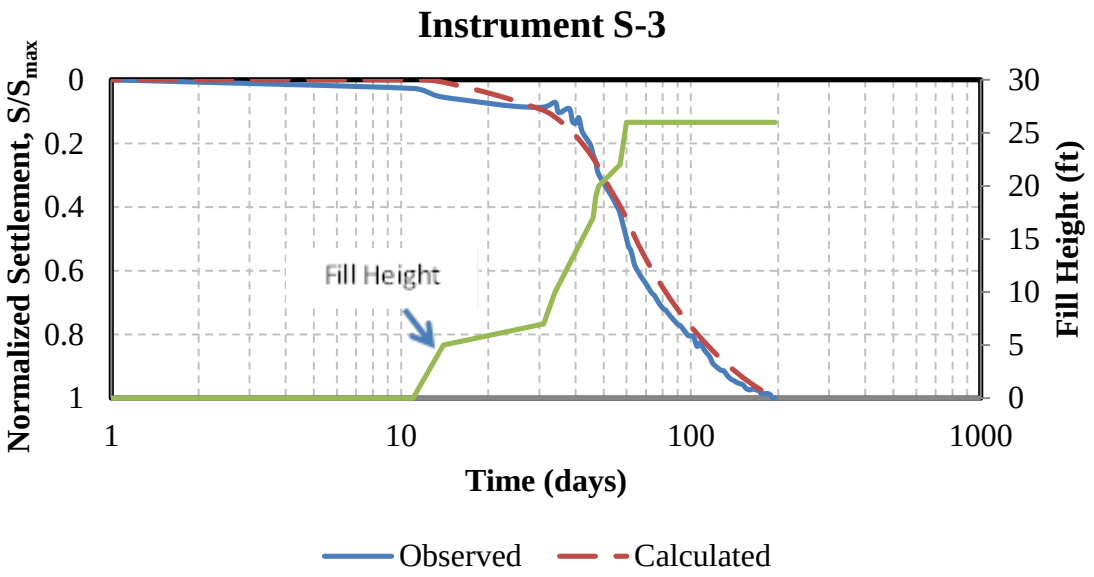

Figure 6-26. Calculated and Observed Time-Settlement Curve for S-3, 5.8 ft Spacing with Plate Anchor Using Back-Calculated C_h/C_v Approach

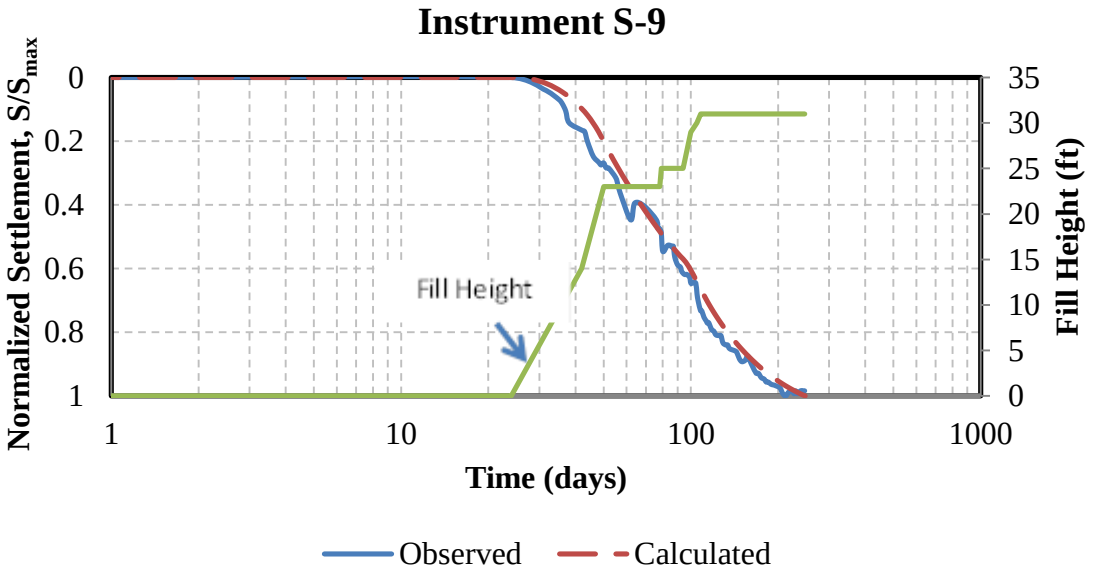

Figure 6-27. Calculated and Observed Time-Settlement Curve for S-9, 5.8 ft Spacing with Plate Anchor Using Back-Calculated C_h/C_v Approach

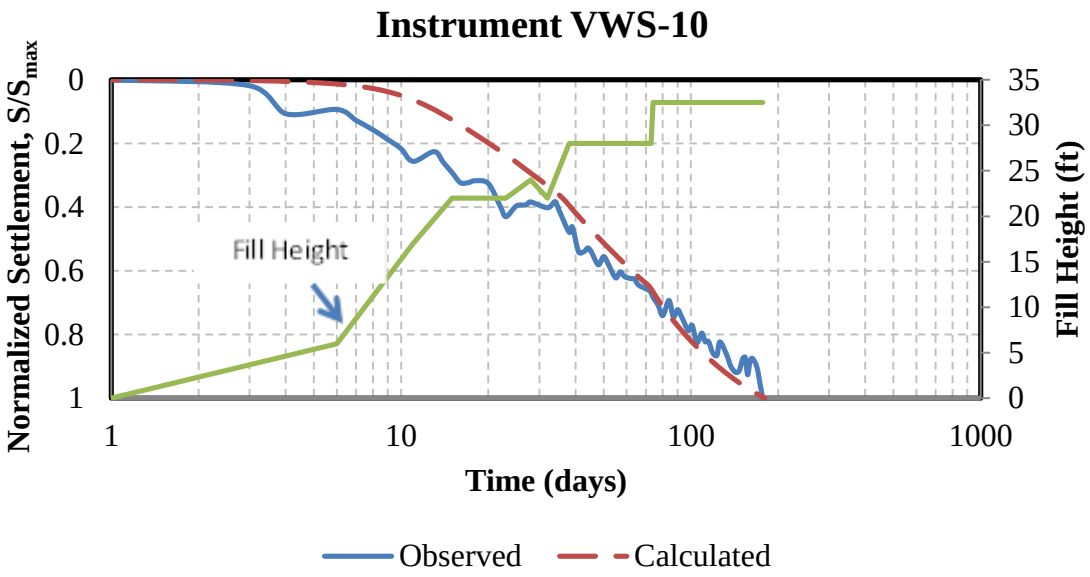

Figure 6-28. Calculated and Observed Time-Settlement Curve for VWS-10, 5.8 ft Spacing with Plate Anchor Using Back-Calculated C_h/C_v Approach

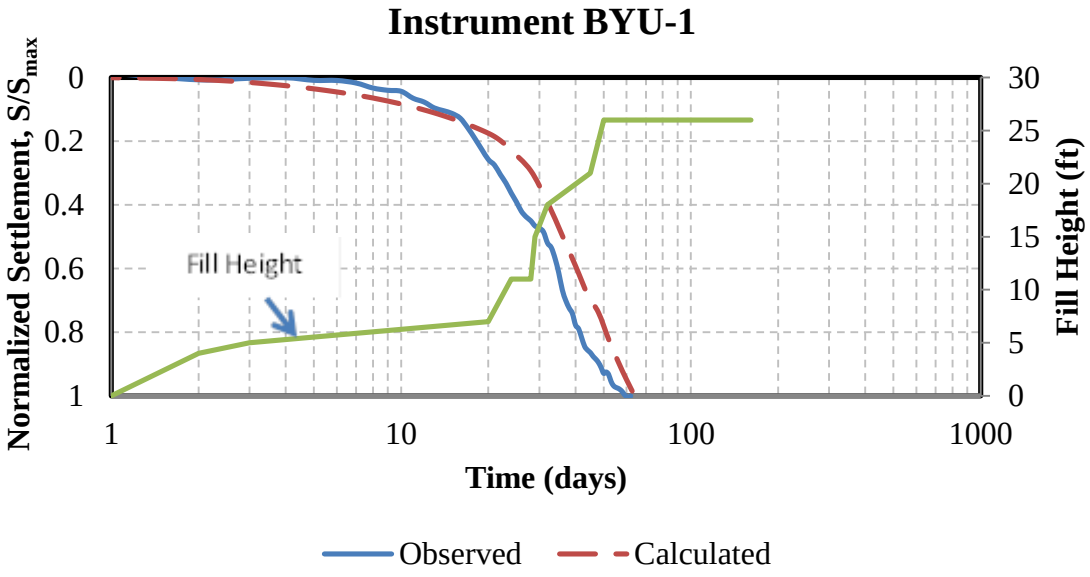

Figure 6-29. Calculated and Observed Time-Settlement Curve for BYU-1, 5.0 ft Spacing with Plate Anchor Using Back-Calculated C_h/C_v Approach

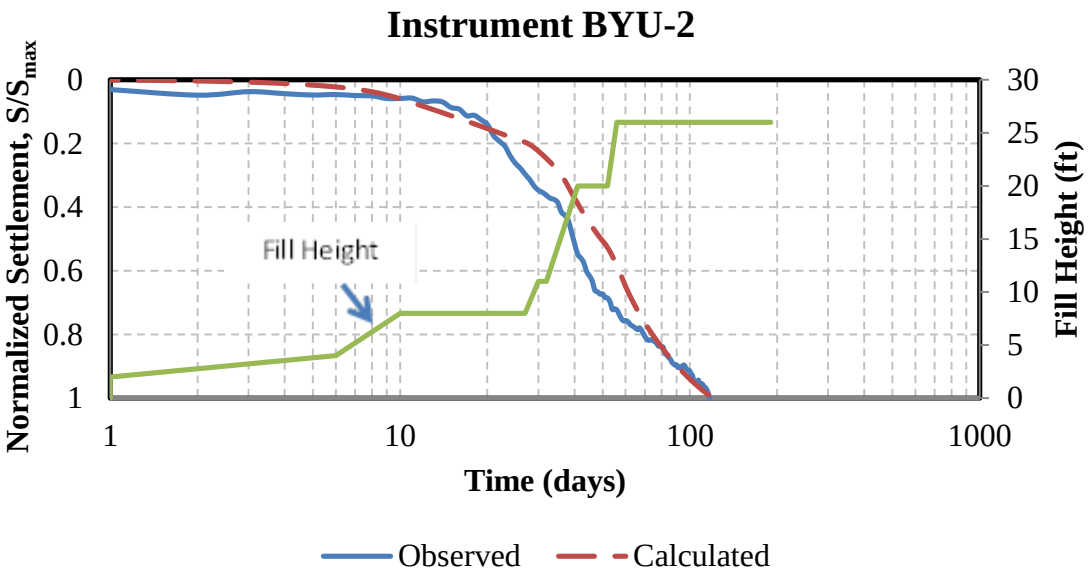

Figure 6-30. Calculated and Observed Time-Settlement Curve for BYU-2, 5.0 ft Spacing with Plate Anchor Using Back-Calculated C_h/C_v Approach

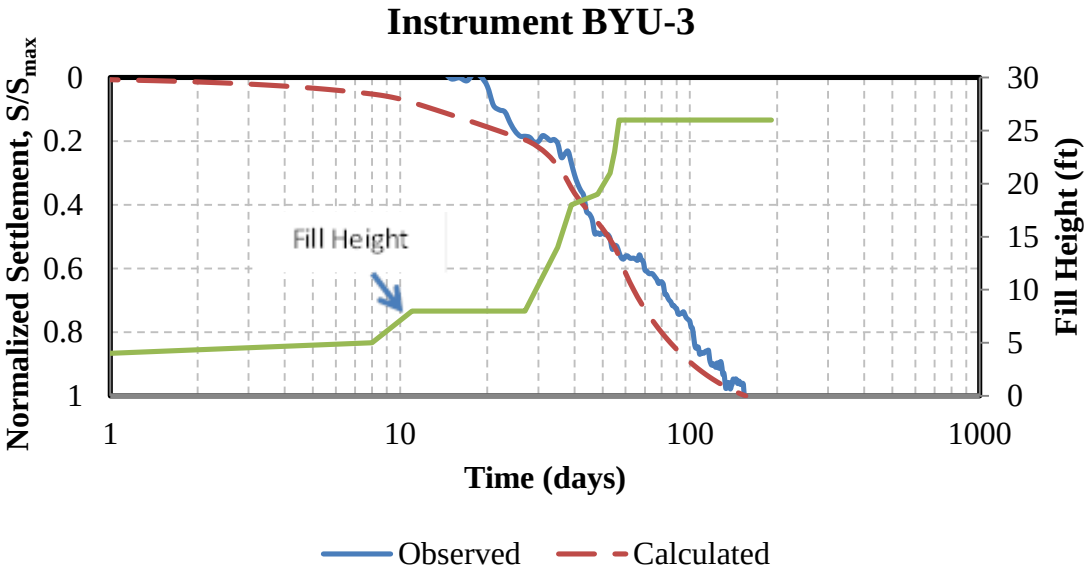

Figure 6-31. Calculated and Observed Time-Settlement Curve for BYU-3, 4.0 ft Spacing with Plate Anchor Using Back-Calculated C_h/C_v Approach

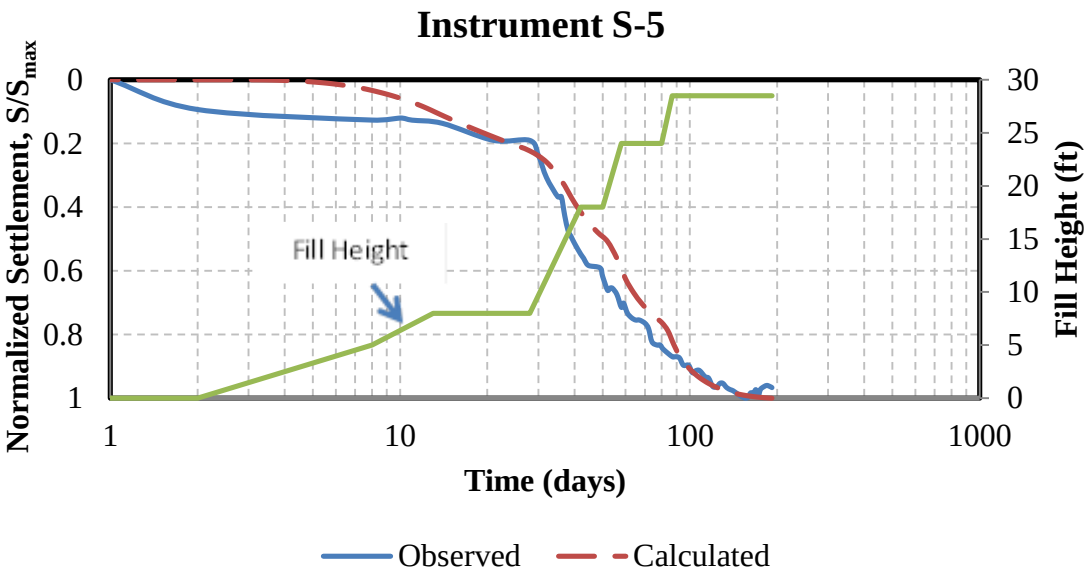

Figure 6-32. Calculated and Observed Time-Settlement Curve for S-5, 3.0 ft Spacing with Plate Anchor Using Back-Calculated C_h/C_v Approach

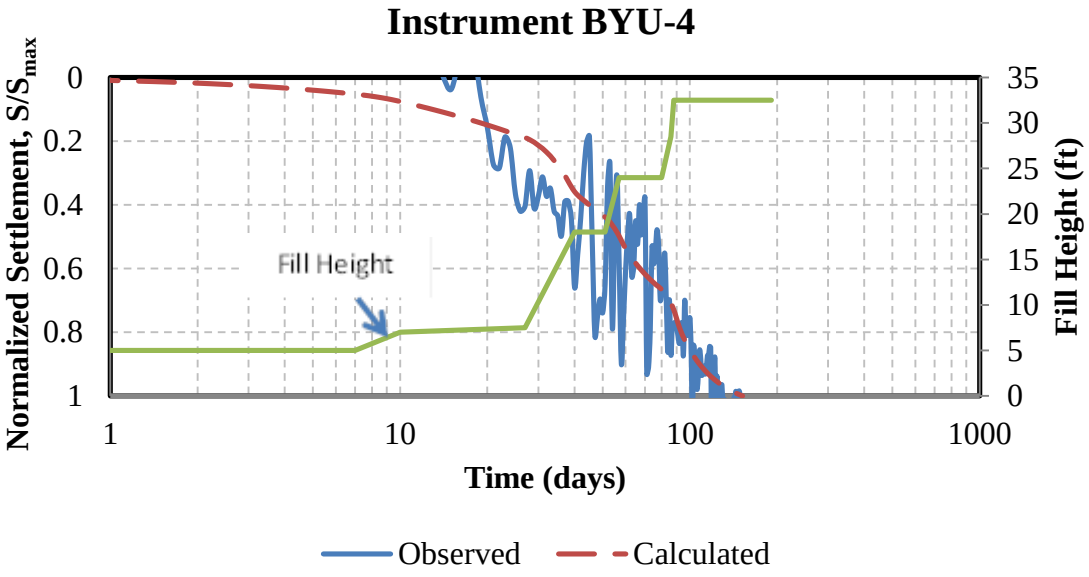

Figure 6-33. Calculated and Observed Time-Settlement Curve for BYU-4, 3.0 ft Spacing with Plate Anchor Using Back-Calculated C_h/C_v Approach

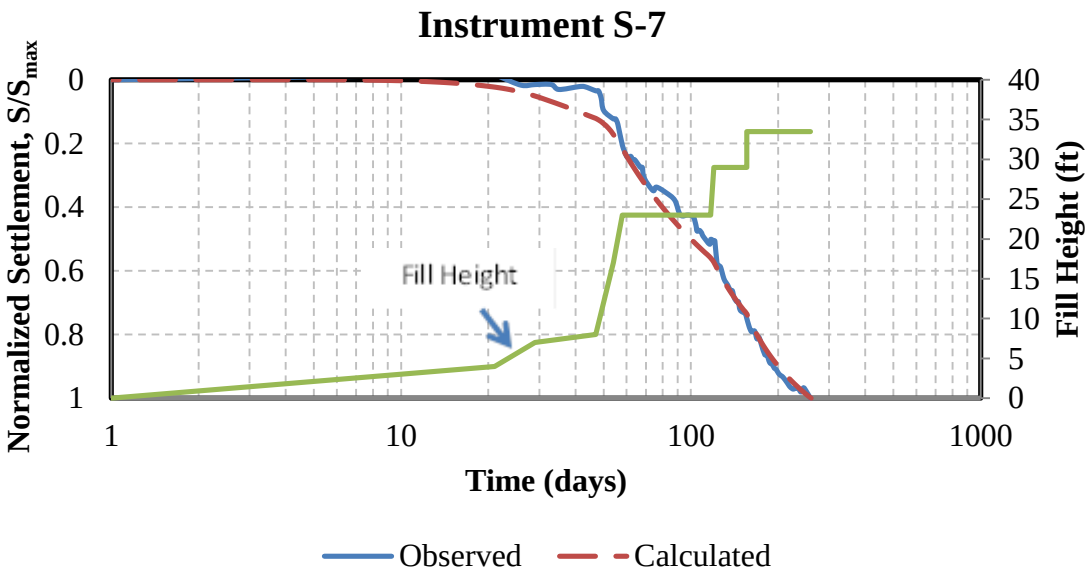

Figure 6-34. Calculated and Observed Time-Settlement Curve for S-7, 5.8 ft Spacing with Rebar Anchor Using Back-Calculated C_h/C_v Approach

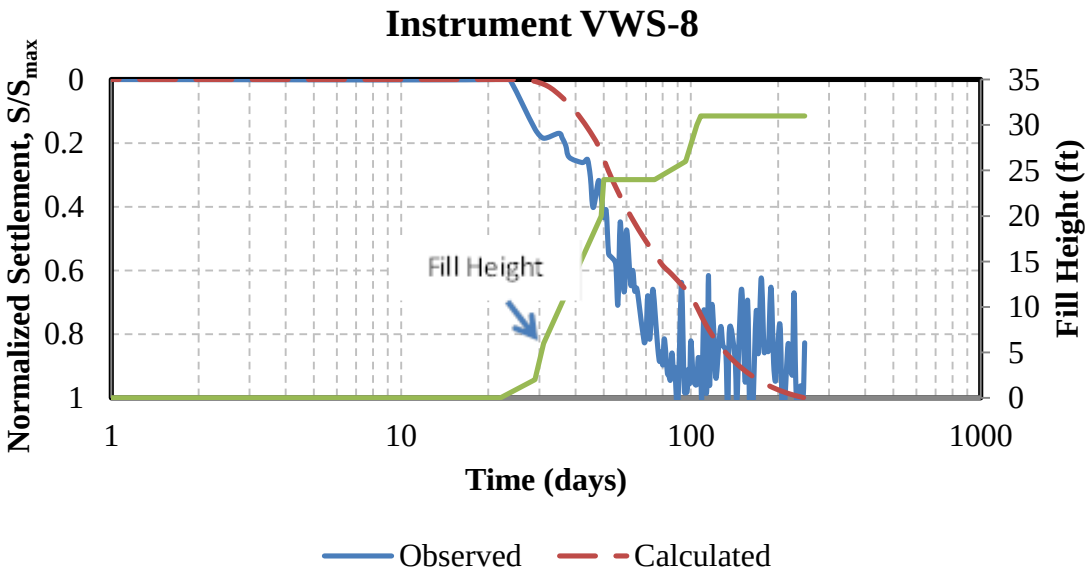

Figure 6-35. Calculated and Observed Time-Settlement Curve for VWS-8, 5.8 ft Spacing with Rebar Anchor Using Back-Calculated C_h/C_v Approach

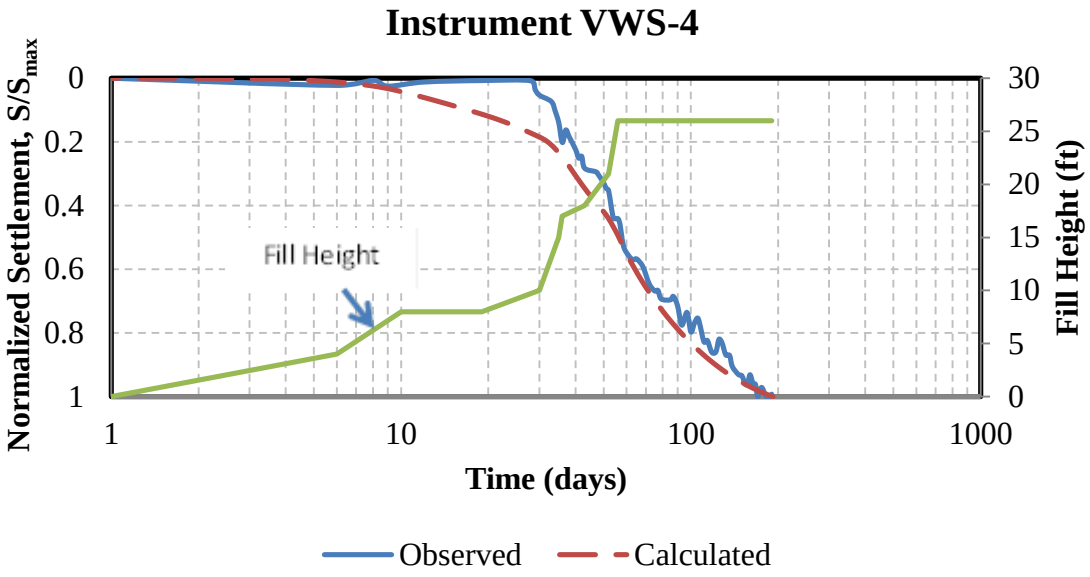

Figure 6-36. Calculated and Observed Time-Settlement Curve for VWS-4, 4.0 ft Spacing with Rebar Anchor Using Back-Calculated C_h/C_v Approach

The back-calculated C_h/C_v ratio method of analysis provided a better agreement between observed and calculated time-settlement curves than the smear zone method. In the C_h/C_v method, each site was calibrated independently by changing the C_h/C_v ratio by trial and error. By independently changing this ratio at each location, a fairly good agreement was able to be achieved for each site. Some disagreement existed at a few locations (VWS-2, VWS-8, BYU-3 and BYU-4) due to the abnormal shape of the observed time-settlement curves. The oscillation of data also presented problems when matching calculated curves to the observed curves. Oscillation in the data requires subjective interpretation, which leads to possible error when trying to find the best fit between calculated and observed data. The final C_h/C_v ratios for each instrument location are shown in Table 6-4, with the associated spacing and anchor type.

Table 6-4. Summary of Instrument Names, Spacings, Anchor Types and C_h/C_v Ratios

Instrument	Spacing (ft)	Anchor Type	C_h/C_v
VWS-2	5.8	Plate	0.75
S-3	5.8	Plate	1.15
BYU-1	5.0	Plate	1.10
BYU-2	5.0	Plate	1.20
VWS-4	4.0	Rebar	0.55
BYU-3	4.0	Plate	0.75
S-5	3.0	Plate	0.70
BYU-4	3.0	Plate	0.50
S-7	5.8	Rebar	0.73
VWS-8	5.8	Rebar	1.56
S-9	5.8	Plate	1.05
VWS-10	5.8	Plate	1.07

6.3.3 Analysis with Consistent Loading

The major complication encountered, neglecting the errors discussed previously, was that each instrument location experienced a different loading rate and magnitude. For example, Figure 6-37 shows the variation in fill-time histories for several measurement sites, and there is considerable variation. Since the fill history resulted in various step loadings, a direct side-by-side comparison of the observed settlement rate curves was not possible. Some instruments were loaded to the maximum height much quicker than others, causing settlement to occur more rapidly. As a result, the measured t_{95} would be lower compared to t_{95} values at sites where the loading occurred much slower. The effect of spacing would appear to increase or decrease the PV drain effectiveness, when in reality the loading history was the cause.

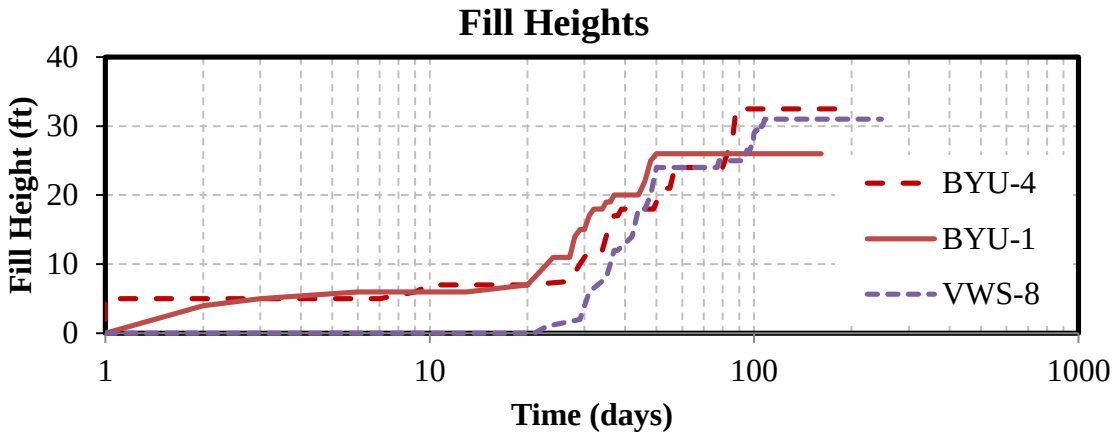

Figure 6-37. Variation Between Fill Histories

To properly assess the spacing effects, a consistent ramp loading, as defined in Figure 6-38, was input into the calibrated model. This ramp load assumed a constant rate of loading to the maximum fill height in 26 days, followed by a constant load thereafter. With the single ramp load, the spacing would be the only variable at each site. The results from the program could then be used to determine how spacing affects the PV drain performance.

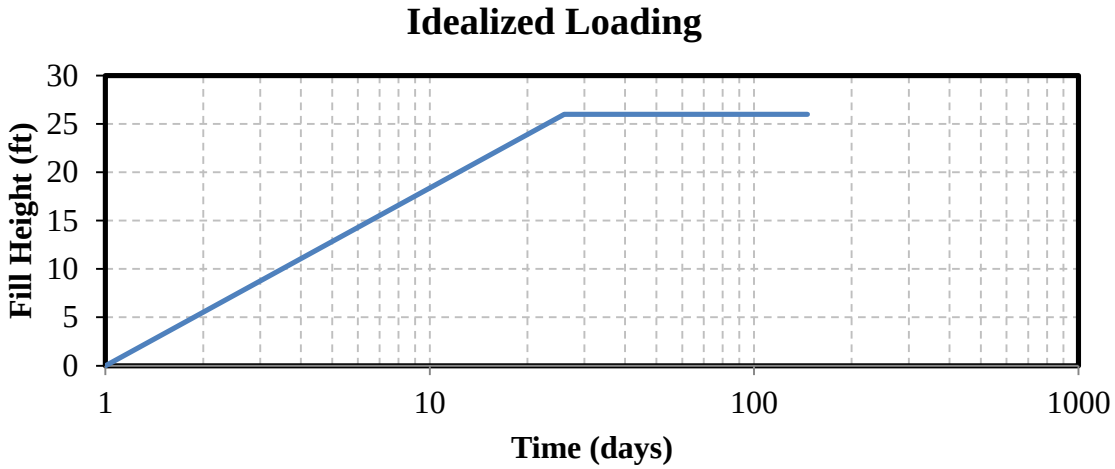

Figure 6-38. Idealized Loading Scenario

By changing the loading history for all twelve observation locations in the smear zone model developed previously and keeping all other parameters the same as before, time-settlement curves were developed for a given anchor type with various spacings and for a given spacing with the two anchor types. The time-settlement curves for all the plate-anchored drains are shown in Figure 6-39. The time-settlement curves for all the rebar-anchored drains are shown in Figure 6-40. Figure 6-41 and Figure 6-42 show the time-settlement curves for the 5.8-ft and 4.0-ft spacings, respectively. In each plot, the 95% consolidation line is shown along with the time-settlement curve. The point of intersection of the time-settlement curve and 95% consolidation line results in the t_{95} for that instrument location.

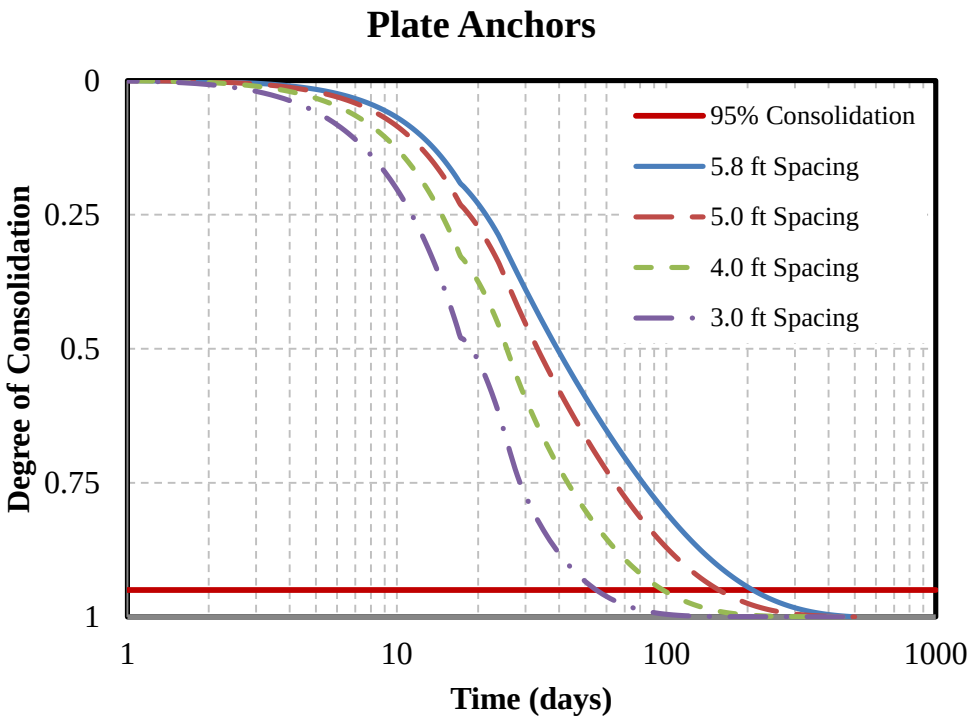

Figure 6-39. Average Time-Settlement Curves for Plate Anchors with Varying Spacings

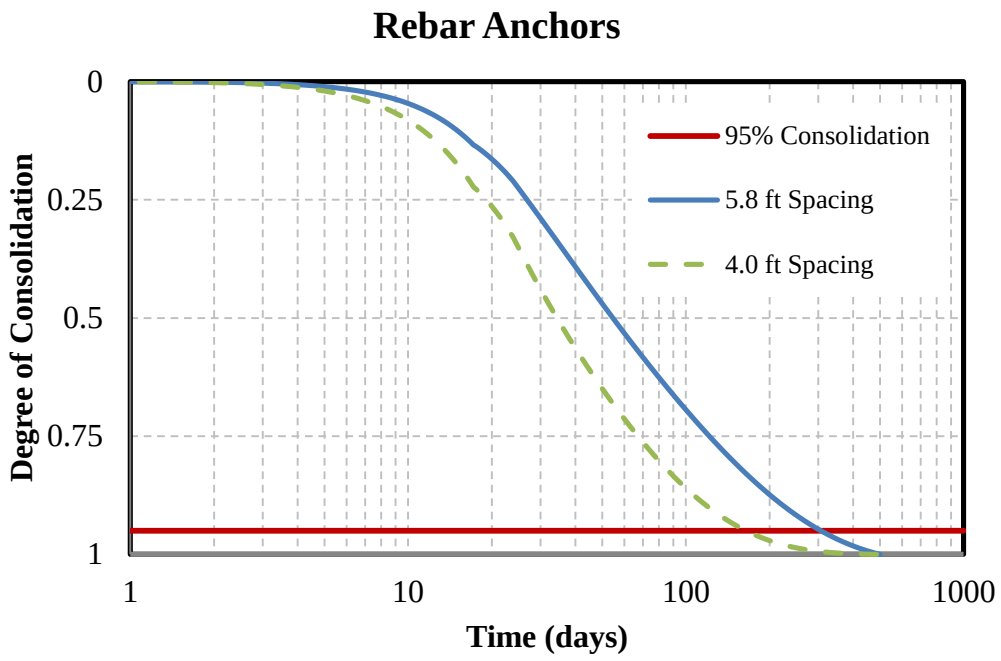

Figure 6-40. Time-Settlement Curves for Rebar Anchors with Varying Spacings

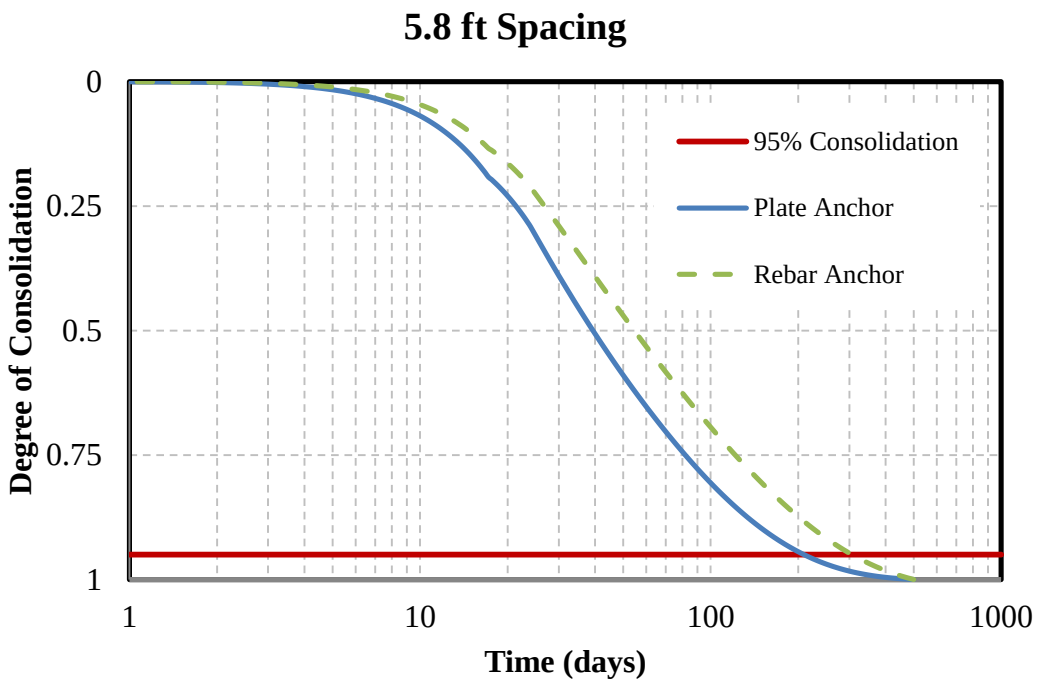

Figure 6-41. Time-Settlement Curves for 5.8 ft Spacing with Plate and Rebar Anchors

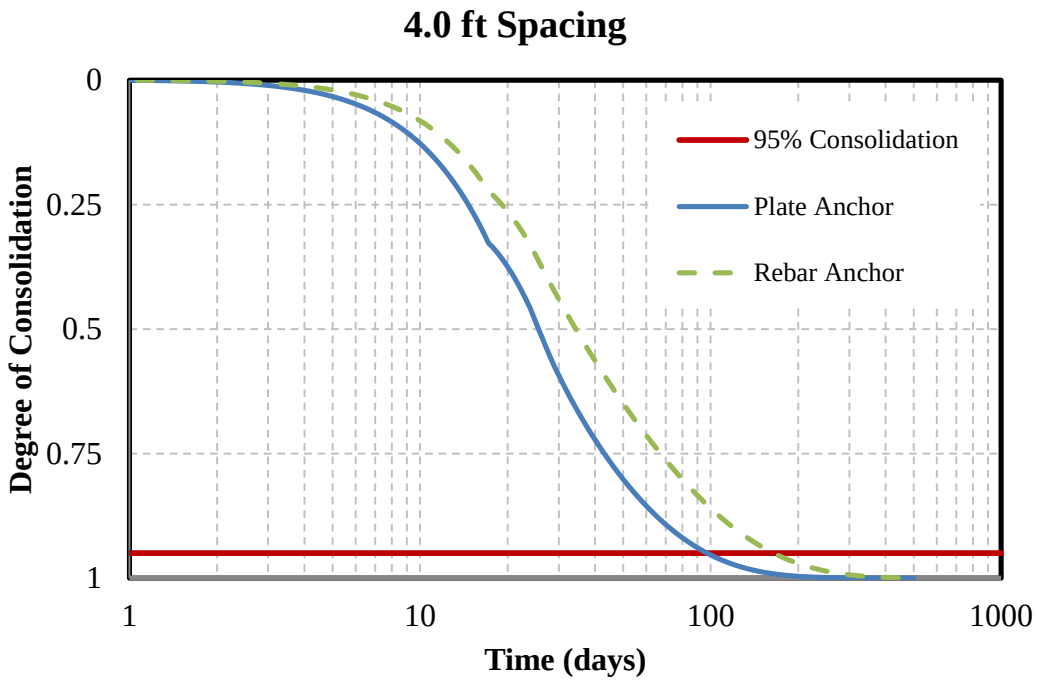

Figure 6-42. Time-Settlement Curves for 4.0 ft Spacing with Plate and Rebar Anchors

All the data show a slight to abrupt change in slope, as noted in Figure 6-43. This change is more prominent in the plate-anchored drains and corresponds to the point in time where the loading changed from the permanent embankment to surcharge loading.

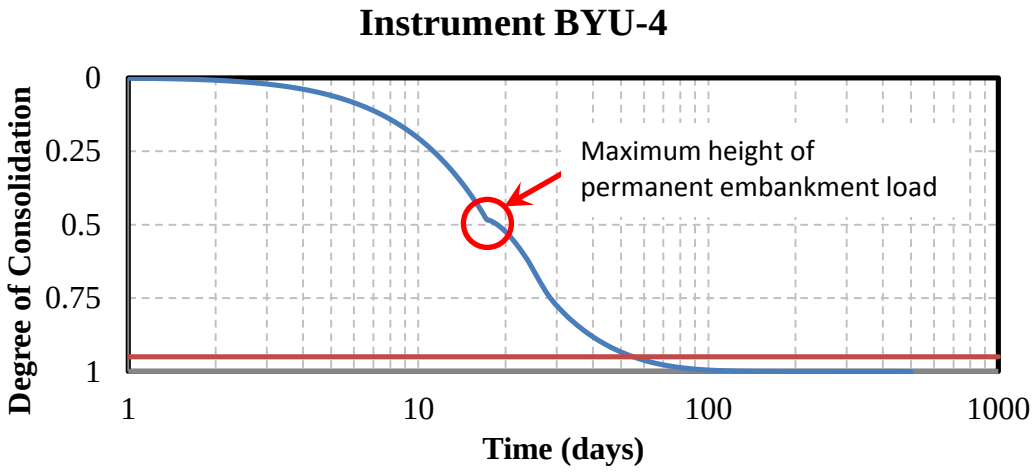

Figure 6-43. Change in Time-Settlement Curve Slope Due to Change in Loading

Table 6-5. Tabulated Average t_{95} from Each of the Spacings and Anchor Types

Spacing (ft)	Anchor Type	Number of Instruments	Average t_{95} (days)
5.8	Plate	4	151.9
	Rebar	2	255.7
5.0	Plate	2	115.6
	Rebar	0	-
4.0	Plate	1	72.6
	Rebar	1	139.6
3.0	Plate	2	42.7
	Rebar	0	-

The average t_{95} for each spacing and anchor type, taken from each of the 12 locations, are tabulated in Table 6-5. The values from Table 6-5 have been plotted in Figure 6-44, with t_{95} along the ordinate and drain spacing along the abscissa. The two different anchor types are shown, as well as the best-fit power trend line through the plate-anchored data points. A trend line was not developed for the rebar anchors because of the smaller number of data points.

The results in Table 6-5 and Figure 6-44 clearly show that greater t_{95} values are predicted for the rebar anchors than for the plate anchors based on the calibrated model. For conditions at this site, t_{95} values were 50 to 100% higher with the rebar anchor in comparison to the plate anchor. As discussed previously, this is likely attributable to the larger anchor/mandrel diameter and the rigidity of the rebar relative to a flexible anchor plate that may bend upward around the mandrel during insertion.

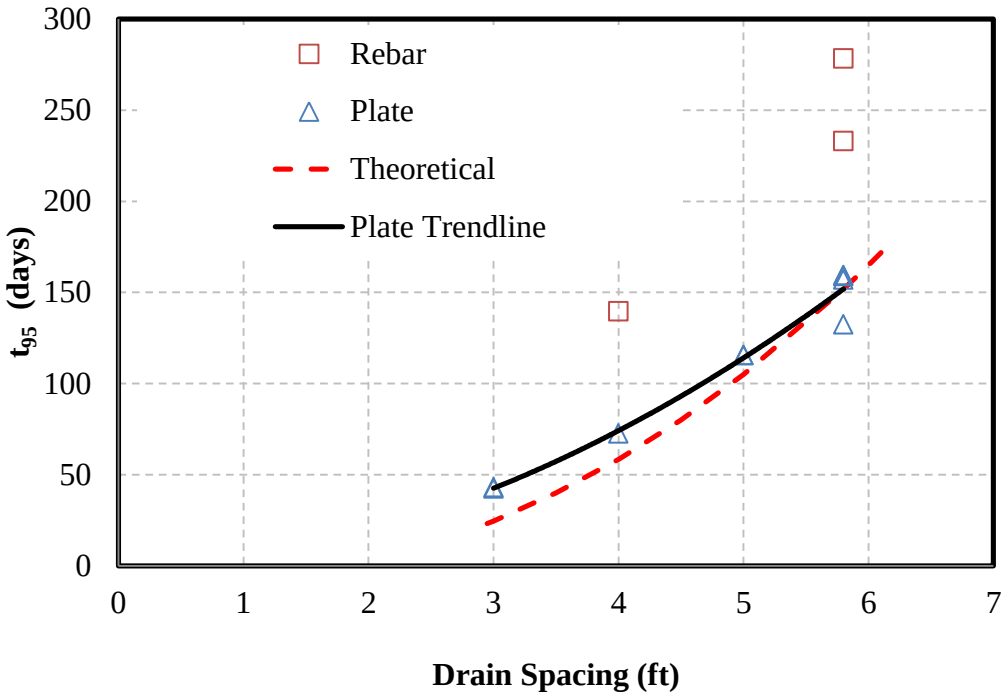

Figure 6-44. Each Anchor Type and Spacing t_{95} Plotted Against Drain Spacing with Best-fit Trend Line and Theoretical Line for C_h = 0.27 ft^2/day

Figure 6-44 also shows that a critical drain spacing was not reached. The critical drain spacing is the point where the decrease in spacing no longer causes a decrease in t_{95} due to the smear zone effect. For this test site with thick uniform clay layers, the drain spacing can be closer than the critical spacing suggested for other I-15 studies and projects. The change in the critical drain spacing can be attributed to differences in soil profiles between the MVC site and other sites in Salt Lake City. Along the MVC, the consistency of the tip stress found from the CPT logs indicates almost no macrolayering in the soil profile, while other sites had significant variation in tip stresses, indicating a profile with interbedded clay and sand or sandy silt layers. The presence of more permeable layers, such as silty sand and sandy silt, intermixed with the clay layers cause the smear zone to greatly affect the drain performance. When the profile consists of a thickly bedded clay layer, the permeability and therefore the coefficient of

consolidation in the vertical and horizontal directions are approximately the same. With approximately the same permeability throughout the profile, the smearing caused from the installation cannot excessively decrease the permeability; however, when interbedded layers with higher permeability are present, the smearing produced by the mandrel insertion causes the lower permeability clay to smear across the higher permeability sand layers, resulting in a significant decrease in horizontal permeability in that layer.

7 CONCLUSIONS

The research was completed by using full-scale testing along the MVC project, located at 2100 North in Lehi, Utah. This test section was divided into segments that contained either rebar or plate anchors and had the PV drains spaced at 5.8, 5.0, 4.0 or 3.0 ft. Each of the segments contained either a vibrating wire or manometer settlement system that measured settlement as a function of time. As the testing proceeded, surveys were made to determine the elevation of the instrument and the amount of surcharge that was placed. All data pertaining to settlement was compiled into a spreadsheet.

By using the PVDrain program alongside the observed settlement data, computer models were developed to match calculated time-settlement curves to those observed in the field. These computer models were then used to analyze the effectiveness of the PV drains. The effectiveness was determined through the use of two models. The first model used a smear zone approach, and the second used a back-calculated C_h/C_v ratio to account for the smear effects that installation of the PV drains had on the radial drainage.

The purpose of the research study conducted along the MVC test site was to determine how the installation of the PV drains affected the performance of the drains and to evaluate analysis methods that account for these effects. Based on the results of the field testing and analysis of the data, the following conclusion can be made:

1. For thickly bedded, relatively uniform clay layers, such as those at the MVC test site, the C_h/C_v ratios can be expected to be slightly higher than 1.0, perhaps 1.2 to 1.5 and smear

effects will be less important for these profiles. In contrast, C_h/C_v ratios may typically be 3 to 5 for profiles with thin clay layers interbedded with higher permeability soils (silts, silty sand), such as those at the SLC airport and I-15 in Salt Lake Valley. Disturbance from drain installation will also be much more significant for these profiles because smear effects can substantially reduce the C_h/C_v ratio.

2. PV drains can be installed at closer spacings without excessive smear effects when thick, uniform clay beds are present as compared to interbedded clay and sand layers. For the MVC test site, where relatively little layering was present, decreasing the drain spacing from 5.8 to 3.0 ft led to progressively smaller t_{95} values. In contrast, for thin interbedded clays in Salt Lake Valley, t_{95} values did not decrease after drain spacing decreased below about 5 ft.
3. Rebar anchors cause more disturbance to the soil during installation than plate anchors. This increased disturbance causes a decrease in drain performance and an increase in t_{95} values due to greater disturbance and remolding of the clay layers. The installation of the rebar caused the diameter of the remolded zone to extend further (2.24 ft versus 1.94 ft) due to the difference in the perimeter-based equivalent mandrel diameter. In addition, the ratio of the undisturbed permeability to the disturbed permeability for the rebar anchor was more than two times that of the plate anchor (2.2 versus 1.0).
4. For the MVC site, the effect of smearing from PV drain installation could be computed with reasonable accuracy using a model with a smear zone having a diameter about 3 times the equivalent mandrel/anchor diameter with allowance for reduction in permeability in the smear zone. However, the selection of the various parameters

involved in the model makes this method somewhat problematic from a practical standpoint.

5. The C_h/C_v versus normalized drain spacing chart developed by Saye (2002) provides a reasonable approach for evaluating the effect of drain spacing, mandrel-anchor diameter, and soil layering on the reduction in C_h due to smear effects from PV drain installation. Based on this chart, significant disturbance occurs at normalized drain spacings of about 9 and 6 for thin interbedded clay layers and thick uniform clay layers, respectively.
6. CPT soundings are particularly helpful in determining the degree of layering within a given profile so that appropriate C_h/C_v ratios can be determined along with the spacing ratio where excessive disturbance may occur.

7.1 Future Study Recommendations

1. Conducting consolidation tests to determine in-situ C_h/C_v ratios along with full-scale field testing of wick drains will provide a better calibration of the model. By finding the in-situ C_h/C_v ratio, the Saye method of back-calculating C_h/C_v ratios will become a more robust design method. Knowing the in-situ C_h/C_v ratio may provide a maximum value for the Saye method.
2. The limited data dealing with rebar-anchored PV drains show an increase in soil disturbance compared to plate anchors; however, more data and testing are required to be able to define the relationship between rebar anchor spacing and PV drain performance. Conducting full-scale field tests with rebar anchors installed at closer spacings will provide more data that can be used to better define the spacing effects on PV drain performance for rebar anchors.

3. Full-scale tests rely on instrumentation accuracy to properly monitor and analyze consolidation settlement. The accuracy of measurements is dependent on conducting regular elevation surveys to determine the settlement relative to the instrument readout box. To eliminate potential human error in the surveys and calculation of settlement, elevations of the settlement monitoring instruments should be monitored via high resolution GPS.

REFERENCES

Barron, R. A. (1948). Consolidation of Fine-Grained Soils by Drain Wells. *Trans. ASCE, 113*, 718.

Bergado, D. T. (1999). Asian Experiences on the Use of Prefabricated Vertical Drains (PVD) in Soft Bangkok Clay. *34th Annual Symposium on Engineering Geology and Geotechnical Engineering.*

Bergado, D. T., Asakami, H., Alfaro, M. C., & Balasubramaniam, A. S. (1991, October). Smear Effects of Vertical Drains on Soft Bangkok Clay. *Journal of Geotechnical Engineering, 117*(10), 1509-1530.

Bo, M. W., Chu, J., Low, B. K., & Choa, V. (2003). *Soil Improvement: Prefabricated Vertical Drain Techniques.* Thomson Learning.

Carrillo, N. (1942). Simple Two and Three Dimensional Cases in the Theory of Consolidation of Soils. *Journal of Mathematics and Physics, 21*(1), 1-5.

Chai, J.-C., & Miura, N. (1999, March). Investigation of Factors Affecting Vertical Drain Behavior. *Journal of Geotechnical and Geoenvironmental Engineering, 125*(3), 216-226.

Das, B. (2011). Principles of Foundation Engineering. Cenage Learning.

Duncan, J. M. (2000, April). Factors of Safety and Reliability in Geotechnical Engineering. *Journal of Geotechnical and Geoenvironmental Engineering, 126*(4), 307-316.

Geokon, Inc. (2010). *Instruction Manual: Model 4650 VW Settlement Sensor.*

Ghandeharioon, A., Indraratna, B., & Rujikiatkamjorn, C. (2010). Analysis of Soil Disturbance Associated with Mandrel-Driven Prefabricated Vertical Drains Using an Elliptical Cavity Expansion Theory. *International Journal of Geomechanics, 10*(2), 53-64.

Goughnour, R. R. (2002). *PVDrain: A Computer Program for Analysis of Consolidation Settlement of Soft Ground Treated by Prefabricated Vertical Drains.*

Hansbo, S. (1979). Consolidation of Clay by Band Shaped Prefabricated Drains. *Ground Engineering, 12*(5), 21-25.

Hansbo, S. (1981). Consolidation of fine-grained soils by prefabricated drains. *Paper 12/22: Proc, 10th International Conference on Soil Mechancics and Foundation Engineering.*

Hansbo, S. (1987). Design Aspects of Vertical Drains and Lime Column Installation. *9th Southeast Asian Geotechnical Conference*, (pp. 8-1-8-12).

Hird, C. C., & Moseley, V. J. (2000). Model Study of Seepage in Smear Zones Around Vertical Drains in Layered Soil. *Geotechnique, 50*(1), 89-97.

Indraratna, B., & Redana, I. W. (1998). Laboratory Determination of Smear Zone due to Vertical Drain Installation. *Journal of Geotechnical and Geoenvironmental Engineering, 124*(2), 474-478.

Kulhawy, F. H., & Mayne, P. W. (1990). Section 6: Time-Dependent Deformability. In *Manual on Estimating Soil Properties for Foundation Design* (pp. Section 6: 1-19).

Naval Facilities Engineering Command. (1986). Chapter 3. Laboratory Testing. In *Soil Mechanics: Design Manual 7.01* (pp. 7.1-117-7.1-144).

RB&G Engineering, Inc. (2009). *Mountain View Corridor 2100 North; Redwood Road to I-15.* Geotechnical Investigation.

Rixner, J. J., Kraemer, S. R., & Smith, A. D. (1986). *Prefabricated Vertical Drains: Vol. I Engineering Guidelines.* Report No. FHWA DR-86/168, FHWA, Washington, D.C.

Sathananthan, I., & Indraratna, B. (2006). Laboratory Evaluation of Smear Zone and Correlation Between Permeability and Moisture Content. *Journal of Geotechnical and Geoenvironmental Engineering, 132*(7), 942-945.

Saye, S. R. (2002). Assessment of Soil Disturbance by the Installation of Displacement Sand Drains and Prefabricated Vertical Drains. *Soil Behavior and Soft Ground Construction, GSP 119*, pp. 325-362.

Saye, S. R., & Ladd, C. C. (2004). Analysis of Geotechnical Instrumentation to Assess Foundation Performance of I-15. *Geotechnical Engineering for Transportation Projects, GSP 126*, pp. 2103-2114.

Saye, S. R., Ladd, C. C., Gerhart, P. C., Pilz, J., & Volk, J. C. (2001). Embankment Construction in an Urban Environment: the Interstate 15 Experience. *Foundations and Ground Improvement, GSP 113*, pp. 842-857.

Sharm, J. S., & Xiao, D. (2000). Characterization of a Smear Zone Around Vertical Drains by Large-Scale Laboratory Tests. *Canadian Geotechnical Journal, 37*(6), 1261-1271.

Smith, A., & Rollins, K. (2007). *Wick Drain Effectiveness as a Function of Spacing Based on Full-Scale Tests at the Salt Lake International Airport.* MS Project, Brigham Young University, Department of Civil and Environmental Engineering, Provo.

Smith, A., & Rollins, K. (2009). Minimum Effective PV Drain Spacing From Embankment Field Tests in Soft Clay. *Proceedings of the 17th International Conference on Soil Mechanics and Geotechnical Engineering (ICSMGE 2009),* (pp. 2184-2187).

Walker, R., & Indraratna, B. (2006, July). Vertical Drain Consolidation with Parabolic Distribution of Permeability in Smear Zone. *Journal of Geotechnical and Geoenvironmental Engineering, 132*(7), 937-341.

Zhu, G., & Yin, J. (2000). Finite Element Analysis of Consolidation of Soils with Vertical Drain. *International Journal for Numerical and Analytical Methods in Geomechanics, 24*(4), 337-366.